Al-Farabi Kazakh National University

UDC 536:621.557(043)

YELNAR YERDESH BAKYTKHANULY

Thermodynamic optimization of ground source heat pump systems with four thermal reservoirs

8D05403 – Mechanics

Dissertation submitted in fulfillment of the requirements for the degree of Doctor of Philosophy (PhD)

Scientific supervisor:
Yerzhan Belyayev,
PhD, Assoc. Prof., Professor-Researcher,
Al-Farabi KazNU, Almaty

Foreign scientific supervisor:
Professor Huasheng Wang,
PhD, FHEA, MInstR,
Queen Mary University of London, UK

Republic of Kazakhstan
Almaty, 2025

CONTENTS

NORMATIVE REFERENCES

The following standards are referenced in this dissertation:

GOSO RK 5.04.034-2011: State compulsory educational standard of the Republic of Kazakhstan. Higher postgraduate education. Doctoral studies. Basic provisions (as amended on August 23, 2012, No. 1080);

GOST 7.32-2001. Research report. Structure and rules for formatting;

GOST 7.1-2003. Bibliographic record. Bibliographic description. General requirements and rules for compilation.

DESIGNATIONS AND ABBREVIATIONS

$\dot{E}$	Exergy rate (W)
e	Specific exergy (J/kg)
E	Energy consumption per annum (kWh)
$\dot{c}$	Heat capacity rate (W/K)
c	Non-dimensional heat capacity rate (-)
c_p	Specific heat capacity (J/kg·K)
COP	Coefficient of Performance (-)
I	Irreversibility ratio (-)
h	Specific enthalpy (kJ/kg)
L	Leakage rate per year (%/year)
$\dot{m}$	Mass flow rate (kg/s)
m	Refrigerant charge (kg)
n	System operating life (year)
P	Pressure (Pa)
$\dot{Q}$	Heat transfer rate /Heat capacity (W)
q	Non-dimensional heat rate (-)
RE	Relative Exergy (-)
$\dot{S}$	Entropy production rate (W/K)
s	Non-dimensional entropy production rate (-)
T	Temperature (°C/K)
$TEWI$	Total Equivalent Warming Impact (kg eq. CO_2)
$\dot{V}$	Volume flow rate (m^3/h)
VRC	Volumetric Refrigeration Capacity (kJ/m^3)
$\dot{W}$	Power consumption (W)
w	Non-dimensional power consumption (-)
α'	Composite heat transfer parameter (K/W)
α	Composite heat transfer parameter (-)
β	Indirect CO_2 emission factor (kg/kWh)
ε	Heat exchanger effectiveness (-)
η	Efficiency (-)
ρ	Density (kg/m^3)
τ	Non-dimensional temperature (-)

Subscripts

CAP	Condenser Approach
$cond$	Condenser
$comp$	Compressor
EAP	Evaporator Approach
elec	Electrical
$evap$	Evaporator
g	Ground side/HX
$g0$	Imposed heat extraction

in Inlet
isen Isentropic
out Outlet
p Production (delivery) side/HX
$p0$ Imposed heat production
$pump$ Pump
s Source (soil)
source Heat source
$sink$ Heat sink (user side)
SC Subcooling
SH Superheating
t Total
TEV Thermostatic expansion valve
ref Refrigerant

Superscripts
alt Alternative
dest Destruction
ex Exergetic
in Inlet
out Outlet

Abbreviations
BHE Borehole Heat Exchanger
COP Coefficient of Performance
FTT Finite-Time Thermodynamics
GHE Ground Heat Exchanger
GSHP Ground Source Heat Pump
GWP Global Warming Potential
HFC Hydrofluorocarbons
HFO Hydrofluoroolefin
HP Heat Pump
HTF Heat Transfer Fluid
HX Heat Exchanger
TRT Thermal Response Test

INTRODUCTION

Global energy and environmental context.

Heating for buildings is one of the most energy- and carbon-intensive final uses, so decarbonizing space and water heating is a central element of global climate policy. This challenge is particularly acute in countries with long, cold winters such as Kazakhstan, where a strongly continental climate leads to extended heating seasons, high peak thermal loads, and a continued dependence on coal- and gas-fired boilers. These systems not only generate substantial CO_2 emissions, but also worsen local air quality in large cities. Under such conditions, low-carbon heating technologies must deliver reliable comfort at sub-zero outdoor temperatures while remaining financially viable in both investment and operation. Against this backdrop, international assessments and technology reviews consistently identify heat pumps – and, within this family, geothermal and shallow-geothermal (ground source) systems – as key options for the cost-effective decarbonization of buildings and district heating networks [1–4].

Global statistics on direct geothermal energy use confirm steady growth across residential, commercial, and industrial sectors, with heat pump applications accounting for an increasing share of installed capacity [4]. At the same time, the practical exploitation of shallow-geothermal resources is shaped by permitting regimes, hydrogeological conditions, and environmental safeguards (e.g., groundwater protection), which vary considerably between countries and regions [2]. Long-term scenarios project rapid expansion of electric heat pump capacity in line with Paris-compatible pathways, driven by technology learning, electrification of heat, and supporting policy frameworks [1,3]. However, in cold continental climates thermal loads are highly seasonal and strongly concentrated in winter, creating specific challenges for system sizing, operating strategies, and multi-year ground temperature management [5,6].

Heat pumps as a key technology in the energy transition.

Heat pumps (HPs) upgrade low-temperature energy from environmental sources (air, water, ground) into useful heat at higher temperature levels, using electricity as the driving input. Because they typically deliver seasonal performance factors above unity, they can outperform combustion-based boilers when supplied with low-carbon electricity. Recent surveys document substantial progress in compressors, heat exchangers, working fluids, and control algorithms for both domestic and industrial HPs, along with a strong, policy-driven increase in their deployment expected over the current decade [3,7–9].

For industrial processes and district energy systems, high-temperature heat pumps (HTHPs) now routinely reach sink temperatures on the order of 160 °C, allowing them to replace fossil-fuel boilers where electricity prices and carbon intensity are favorable [10]. The research literature also explores cascade and hybrid configurations to expand the operating envelope at low ambient temperatures. Studies of cascade systems quantify combined thermodynamic, exergoeconomic, and environmental trade-offs and demonstrate the effectiveness of multi-objective optimization approaches in HP design [11–15]. In parallel, finite-time and finite-size thermodynamics and ecological criteria have been applied to classical cycles (such as

Brayton) to incorporate realistic irreversibilities and provide guidance on parameter selection for heat pumps under practical constraints [16,17].

Beyond single-cycle arrangements, solar assisted compression heat pumps (SACHPs) and other hybrid systems increase the renewable share of delivered heat and stabilize performance in harsh climates. Recent reviews synthesize modeling approaches, configuration variants, and applications of SACHPs – including collector integration, refrigerant choice, and control strategies – and propose design routes tailored to climates with large temperature swings [14,18,19]. As these concepts move towards wider deployment, the ongoing transition to low-GWP refrigerants remains a critical cross-cutting issue. Experiments and numerical studies compare candidate working fluids and quantify their influence on COP, exergy efficiency, and environmental indicators, providing the evidence base for replacing high-GWP refrigerants [10,20,21]. At the same time, optimization studies investigate operating temperatures, intermediate pressures, and condenser/evaporator characteristics across residential, commercial, and industrial applications, seeking joint improvements in efficiency, cost, and environmental performance [3,9,12].

Development and application of ground source heat pumps (GSHPs).

Within the broader HP family, ground source heat pumps (GSHPs) exploit the relatively stable subsurface temperature to achieve high efficiencies in cold climates. Their technological development has been strongly supported by advances such as the thermal response test (TRT), which enables in-situ characterization of ground thermal properties and underpins the design of borehole heat exchangers (BHEs) [22,23]. Current GSHP solutions include closed-loop vertical and horizontal BHE fields, open-loop groundwater systems, and energy piles; many of these configurations can be combined with borehole thermal energy storage (BTES) to provide seasonal balancing [6,24,25]. Global utilization surveys and case studies document a wide application range – from single buildings to campus- or district-scale systems – and highlight the diversity of geological settings and regulatory environments that must be considered during project development [2,4,26].

Modeling tools have evolved from simple steady-state design methods to detailed transient models at both component and system level, capturing compressor cycling, ground loop dynamics, and control logic. Transient simulations of GSHPs under cycling operation clarify how part-load conditions influence seasonal performance and sizing [27]. Beyond conventional single-loop arrangements, recent work has examined shallow bore concepts, solar-coupled configurations, and other hybrids intended to reduce capital cost while preserving or improving efficiency [14,15,28–30]. Dedicated studies analyze low-GWP alternatives to legacy refrigerants in GSHP applications and quantify associated energy–exergy trade-offs [20], whereas broader domestic HP reviews summarize trends in component selection and techno-economic assessment relevant to GSHP deployment [9]. Overall, the literature confirms that GSHPs have particular advantages in cold continental climates, especially at sub-zero ambient temperatures where air-source HP performance degrades more rapidly [5,14,15,31].

Challenges in GSHP deployment.

Despite their favorable fundamentals, GSHP systems face several technical, economic, and regulatory obstacles. In cold continental regions such as Kazakhstan, one of the main technical issues is seasonal thermal imbalance: winter-dominated extraction from the ground can progressively cool the soil around BHEs, increasing compressor power demand, lowering COP, and, in extreme cases, causing local freezing that further reduces heat transfer. Mitigating these effects requires careful BHE field design (depth, spacing, arrangement) and, where appropriate, active balancing strategies such as solar recharging or seasonal storage, supported by TRT-based parameterization and dynamic simulation [5,13,23,25,32]. Geotechnical solutions such as energy piles enable simultaneous structural and thermal functions but call for analysis of thermo-mechanical interactions and long-term reliability [24]. Open-loop systems that tap shallow aquifers may be attractive where hydrogeological conditions are favorable, yet they are constrained by groundwater protection rules and licensing requirements [2,26].

From an economic perspective, the high upfront cost of drilling and BHE installation remains a major barrier compared with conventional boiler replacements, even when lifecycle analysis favors GSHPs. Consequently, many studies underline the importance of system-level optimization – including refrigerant selection, source and sink temperature levels, and heat exchanger sizing – to manage both capital and operating expenditures in realistic climatic and regulatory contexts [12,31,33]. Reviews of solar assisted GSHPs, hybrid storage schemes, and geocooling report strategies for mitigating thermal imbalance and reducing required BHE length, supported by monitoring data from residential systems and seasonal storage projects [18,19,25,34]. At the same time, the sector-wide shift to low-GWP refrigerants introduces new design constraints: although hydrocarbons and HFOs can substantially reduce direct climate impact, issues such as atmospheric degradation products (e.g., TFA formation) and safety classifications must be considered at an early stage in both engineering design and policy decisions [10,20,21].

Finite-time thermodynamics (FTT): foundations for cycle-reservoir optimization.

Modern thermodynamic optimization recognizes that real devices operate under finite-time and finite-size constraints, with non-negligible irreversibilities. Foundational work on entropy-generation minimization introduced tractable models that integrate heat transfer, fluid mechanics, and thermodynamics to optimize irreversible devices subject to resource and time limits [35–37]. Building on these ideas, subsequent research developed endoreversible and irreversible formulations and ecological criteria for power and refrigeration cycles (including Brayton-type systems), thereby linking traditional performance objectives to finite-rate heat transfer and finite heat-capacity couplings [16,17]. For heat pump cycles, finite-reservoir and variable-temperature-reservoir models show how source and sink temperatures, heat exchanger conductances, and capacity rates jointly influence COP, exergy efficiency, and required power input [38,39].

These principles can be naturally extended to GSHP systems, which may be idealized as a cycle coupled to multiple finite reservoirs through four heat exchangers:

the ground/BHE (heat source), the evaporator-side loop (cold loop), the condenser-side loop (hot loop), and the user side (heat sink). In this four-reservoir representation, the way in which limited heat exchanger resources (effectiveness and overall conductance) and heat capacity rates are distributed among interfaces directly controls entropy production and overall cycle performance. FTT offers a coherent framework to: (i) formulate cycle-reservoir optimization problems under realistic constraints; (ii) interpret trade-offs between temperature lift and COP; and (iii) derive allocation rules for heat exchanger resources tailored to continental climate loads [17,38,39]. In this sense, FTT provides the theoretical basis for the system-level optimization of GSHPs needed to address the technical challenges outlined above.

3E (energy-exergy-environmental) analysis for practical relevance.

While FTT structures the physics of irreversible optimization, practical GSHP design in real markets must also satisfy multi-criteria requirements consistent with decarbonization and affordability. The 3E framework – combining energy, exergy, and environmental analysis – links performance indicators (such as COP and exergy efficiency) with environmental metrics (such as refrigerant GWP and lifecycle emissions), allowing rigorous comparison of design alternatives. Studies of cascade heat pumps and district systems augmented by ground heat sources demonstrate that energy and exergy criteria correlate strongly with total cost rates and environmental indices, and highlight the need to jointly optimize operating temperatures, refrigerant combinations, and inter-stage conditions [12,33,40]. Comparative assessments for Russian cold-climate cities, for example, show that GSHPs can outperform air-source HPs both thermodynamically and economically under severe winter conditions, provided that systems are correctly sized and optimized [31]. For residential and mixed-use buildings, geocooling and solar assisted schemes further mitigate seasonal thermal imbalance and reduce capital intensity, improving the overall energy-exergy-economic-environmental profile in continental climates [5,18,19,34].

At the component level, the choice of low-GWP refrigerants has a decisive impact on both exergy efficiency and environmental performance; multi-objective analyses and substitution studies therefore provide concrete guidance for GSHP designers [10,20,21]. Shallow-bore and solar-coupled GSHP concepts show promising thermodynamic and economic outcomes in both laboratory experiments and field demonstrations [28–30,41]. Recent reviews of domestic heat pumps and cold-climate GSHPs synthesize key system-level levers – including control strategies, storage integration, and seasonal operating modes – that are essential for robust long-term performance and bankability in harsh climates [5,9]. Taken together, this body of work supports a unified design philosophy in which FTT-based cycle-reservoir optimization is combined with 3E-based evaluation of working fluids, temperature levels, and heat exchanger resources, forming the conceptual foundation for the present thesis.

Research gaps.

Although GSHPs and related optimization methods have been widely studied, several issues still restrict the transfer of existing results into robust design guidance, particularly for cold continental climates such as Kazakhstan.

First, finite-time thermodynamics is rarely applied to GSHPs in a fully system-level way. Most FTT-based heat pump studies consider idealized cycles or one-two

aggregated reservoirs and do not explicitly represent the four coupled heat exchangers (ground, evaporator, condenser, building/user side) [16,17,39,42]. Consequently, there is limited guidance on how thermal and geometric resources (heat exchanger effectiveness and capacity rates) should be allocated across all four interfaces when heat extraction from the ground or heat delivery to the load is prescribed.

Second, many GSHP and cascaded/solar assisted studies perform 3E (energy-exergy-environmental) analyses, but often with steady-state or case-specific models that do not embed finite-time irreversibilities into the core optimization [12,31,33,40]. This reduces their generality for large temperature lifts, long heating seasons, and winter-dominant loads and obscures clear relationships between cycle irreversibility, temperature lift, heat exchanger allocation, COP, and input power.

Third, long term ground thermal imbalance and multi-year ground temperature evolution are not treated in a unified way. Existing work on geocooling, borehole thermal energy storage, energy piles, and solar recharging usually analyzes configurations separately and rarely co-optimizes exchanger resources, operating temperatures, and possible storage/solar coupling within a single framework [5,24,25,30,34].

Fourth, the ongoing transition to low-GWP refrigerants is mostly assessed via separate COP or TEWI comparisons, without systematically coupling refrigerant choice to finite-time thermodynamics, heat exchanger allocation, and realistic operating constraints. This leaves designers without integrated tools that connect thermodynamic performance, environmental impact, and refrigerant selection for continental climates [3,10,20,21].

Finally, at the regional scale, despite Kazakhstan's high potential for GSHP deployment, there are still only a few validated system-level models and 3E assessments calibrated to local climatic and operating conditions. This weakens the evidence base for confident design recommendations and policy decisions.

The aim of this research is to develop theoretical and methodological framework for the thermodynamic optimization of ground source heat pump (GSHP) systems by integrating finite-time thermodynamics (FTT) models, 3E (energy, exergy, environmental) analysis, and experimental validation under continental climatic conditions.

Objectives of the research:

1. Formulate an FTT (finite-time thermodynamics) optimization framework for GSHPs with four heat exchangers and derive criteria for allocating thermal and geometric resources among them.
2. Set up and solve numerical optimization problems for imposed operating conditions (imposed ground heat extraction and imposed heat delivery), reflecting typical design and control constraints.
3. Carry out parametric studies of heat exchanger effectiveness, capacity rates, and irreversibility indicators in non-dimensional form to map performance trends and trade-offs.
4. Develop a 3E (energy, exergy, environmental) analysis framework and validate it using Almaty GSHP data.

5. Provide design and operational guidelines for GSHPs in continental climates, based on the combined FTT and 3E results.

Object of the research: ground source heat pump systems for heating applications in continental climatic conditions.

Subject of the research: thermodynamic optimization of GSHP performance, with emphasis on cycle irreversibility, allocation of heat exchanger resources, refrigerant selection, and efficiency-environmental trade-offs.

Research methods integrate finite-time thermodynamic modeling with energy-exergy analysis and environmental assessment to evaluate and optimize GSHP performance. The workflow combines numerical simulation, experimental testing, and benchmarking against measured data and published studies.

Scientific novelty of the research is as follows:

1. A unified finite-time thermodynamics (FTT) framework for GSHPs that treats system-level cycle-reservoir coupling across the four heat exchangers (ground, evaporator, condenser, and user side). This framework explicitly accounts for finite heat transfer rates and irreversibility, providing a consistent basis for analyzing both endoreversible and irreversible GSHP systems in continental climates.

2. New optimization criteria for operation under imposed conditions – specifically imposed heat extraction and heat production rates. The thesis formulates multi-variable optimization problems that directly reflect real design and operating constraints, enabling the determination of performance limits and trade-offs relevant for sizing, control, and seasonal load coverage.

3. Modeling of heat pump irreversibility to derive allocation rules for heat exchanger effectiveness and capacity rates. By embedding irreversibilities within the FTT framework, the work identifies how limited thermal and geometric resources should be distributed among the four heat exchangers to maximize COP or minimize input power under given operating conditions.

4. A comprehensive, validated 3E (energy-exergy-environmental) analysis of GSHP performance, supported by experimental operating data under continental climate conditions. The proposed 3E framework links thermodynamic indicators (COP, exergy efficiency) with environmental metrics (TEWI) and is calibrated and validated using measurements from a GSHP installation in Almaty, yielding climate-specific insight into performance and emissions.

5. Generalizable design rules for GSHP configuration in continental climates, covering heat exchanger resource allocation, refrigerant selection, and operating temperature ranges. These rules synthesize the FTT optimization and 3E results into practical guidance that can be transferred to other GSHP and related heat pump applications, supporting low-GWP refrigerant choices, robust borehole sizing, and operating strategies that balance efficiency, environmental impact, and cost.

Theoretical and practical significance of the research.

The theoretical significance of this research **stems from** the development and application of finite-time thermodynamic (FTT) methods to the optimization of ground source heat pump (GSHP) systems. By formulating models that explicitly account for irreversibilities, entropy production, and finite heat transfer rates, the study extends

classical thermodynamic optimization to practical energy systems. The proposed methodology introduces optimization criteria for imposed heat transfer rates that can be generalized to other heat pump cycles and energy conversion devices. In this way, the dissertation contributes to the advancement of thermodynamic theory by linking idealized models with real operating conditions. The results also have theoretical importance through the integration of FTT with 3E (energy, exergy, and environmental) analysis, providing a combined framework that evaluates heating systems using both efficiency-based and environmental performance indicators.

The practical significance of the research lies in the direct applicability of the developed models, methodologies, and guidelines to the design and optimization of GSHP systems in continental climates, such as those of Kazakhstan and other cold regions. The validated results provide engineers and designers with structured recommendations on allocating heat exchanger resources, selecting refrigerants, and choosing operating conditions. These findings can be used to increase efficiency, lower operating costs, and improve environmental performance of GSHP systems, supporting their deployment as sustainable alternatives to fossil-fuel heating.

Furthermore, the conclusions obtained in this work can support national and regional energy strategies by quantifying the potential contribution of GSHPs to carbon reduction and energy transition goals. The integration of theoretical optimization with experimental validation under local conditions ensures that the recommendations are not only academically rigorous but also directly applicable in practice, enabling policymakers, utility providers, and private companies to adopt GSHP technologies with greater confidence.

Scientific provisions submitted for defense:

1. A finite-time thermodynamic optimization methodology for GSHPs that treats system-level coupling across four heat exchange interfaces (ground, evaporator, condenser, user side).
2. Thermodynamic models of GSHP operation under imposed heat transfer conditions, including imposed ground heat extraction and imposed heat production rates.
3. Optimality criteria for allocating heat exchanger effectiveness and capacity rates in the presence of irreversibility.
4. A validated 3E (energy-exergy-environmental) framework for assessing thermal efficiency and environmental performance, based on experimental data from a GSHP installation in Almaty.

Reliability and validity of the scientific provisions, conclusions, and results of the thesis.

The reliability of this thesis is based on rigorous first-principles modelling and established thermodynamic doctrine. All GSHP models are derived from mass, energy, and exergy balance equations consistent with the first and second laws, while finite-time thermodynamics explicitly represents finite heat-transfer rates, irreversibilities, and entropy production. This provides internal consistency and theoretical rigor for the optimization criteria and allocation rules for heat exchanger effectiveness and capacity rates. Environmental quantification follows internationally recognized 3E practice,

including lifecycle climate metrics such as TEWI, which establish a clear link between thermodynamic performance and environmental impact.

Validity is demonstrated through several external checks. Model predictions are experimentally validated against measurements from a GSHP installation in Almaty (e.g., COP, ground temperature response) and show agreement with methodologies and trends reported in international GSHP and cascade HP studies. The results have undergone scholarly approbation via peer-reviewed publications and conference presentations [7,8,11,13–15,32]. Taken together, the combination of first-principles modelling, empirical validation under continental-climate operation, and consistency with the literature confirms the robustness of the scientific provisions and the practical applicability of the conclusions for GSHP design and optimization in continental climates.

Connection of the thesis with other research projects.

This thesis was carried out within the framework of the following scientific research projects:

1. AP26102323 “Optimization of efficiency and configuration of high-temperature heat pumps for integrating renewable energy sources and utilizing waste heat”, grant funding of the Committee of Science of the Ministry of Science and Higher Education of the Republic of Kazakhstan, 2025-2027.
2. AP14871988 “Development of a solar-thermal desalination plant based on a heat pump”, grant funding of the Committee of Science of the Ministry of Science and Higher Education of the Republic of Kazakhstan, 2022-2024.
3. AP08857319 “Study of heat transfer enhancement mechanisms of vertical type borehole heat exchanger to ensure high heat pump performance”, grant funding of the Committee of Science of the Ministry of Science and Higher Education of the Republic of Kazakhstan, 2020-2022.
4. APP-SSG-17/0280F “Cascade solar assisted heat pump for space heating and domestic hot water in continental climate regions”, supported by the Science Committee of the Ministry of Education and Science of the Republic of Kazakhstan and World Bank under the “Fostering Productive Innovation”, 2018-2020.
5. AP05132668 “Development of an auto-cascade solar heat pump for high-potential residential heating in continental climates”, grant funding of the Committee of Science of the Ministry of Science and Higher Education of the Republic of Kazakhstan, 2018-2020.

The results presented in this thesis were obtained in direct connection with these projects, and some of the methodologies and models developed were integrated into project reports and publications prepared within their scope. The thesis also benefited from international collaboration with research groups at the Université de Lorraine (France), within the framework of joint publications and academic mobility.

Publications.

The author has published 7 scientific papers on the topic of the dissertation, including **4 articles in international scientific journals indexed in Scopus and Web of Science:**

1. Yerdesh Ye., et al. Numerical simulation on solar collector and cascade heat pump combi water heating systems in Kazakhstan climates, Renewable Energy, Volume 145, 2020, pp. 1222-1234, https://doi.org/10.1016/j.renene.2019.06.102 (Q1, IF 8.001, Percentile 88, SJR 1.825) (**First author**).
2. Yerdesh Ye., et al. Experimental and theoretical investigations of a ground source heat pump system for water and space heating applications in Kazakhstan, MDPI Energies, Volume 15, №22, 2022, pp. 1-25, https://doi.org/10.3390/en15228336 (Q3, IF 3.2, Percentile 83, SJR 0.632) (**First author**).
3. Karlina Ye., Yerdesh Ye., et al. Numerical simulation study of thermal performance in hot water storage tanks with external and internal heat exchangers, MDPI Energies, Volume 17, №22, 2024, pp.1-18, https://doi.org/10.3390/en17225623 (Q3, IF 3.2, Percentile 85, SJR 0.713) (**Corresponding author**).
4. Baimbetov D., Yerdesh Ye., et al. Thermal analysis of a compression heat pump-assisted solar still for Caspian regions of Kazakhstan, Journal of Thermal Analysis and Calorimetry, Volume 149, №19, 2024, pp. 11269-11291, https://doi.org/10.1007/s10973-024-13446-4 (Q2, IF 3.1, Percentile 85, SJR 0.551) (**Co-author**).

2 publications in international conference proceedings indexed in Scopus:

5. Toleukhanov A., Belyayev Ye., Yerdesh Ye., et al. Simulation-based mathematical modeling of borehole heat exchanger thermal performance for ground source heat pumps, Journal of Mathematical Sciences, Conference Paper, Vol. 291, №2, 2025, pp. 323-335, https://doi.org/10.1007/s10958-025-07811-3 (Percentile 10, SJR 0.153)
6. Belyayev Ye., Toleukhanov A., Yerdesh Ye., et al. Energy and exergy performance study of ground source heat pump in continental climate conditions, AIP Conference Proceedings, Volume 3126, №1, 2024, pp. 1-8, https://doi.org/10.1063/5.0200363 (Percentile 10, SJR 0.153)

1 article in international scientific journal:

7. Yerdesh Ye., et al. Air-to-water cascade heat pump thermal performance modelling for continental climate regions, Entropie Thermodynamique, Volume 3, №1, 2022, pp. 1-16, https://doi.org/10.21494/ISTE.OP.2022.0836 (**First author**).

Personal contribution of the author.

The author defined the research objectives, conducted the literature review, and developed mathematical models of GSHP systems within a finite-time thermodynamics (FTT) framework. The author implemented the 3E (energy-exergy-environmental) methodology, performed numerical simulations and optimization, and analyzed results to derive new optimization criteria and design guidelines for heat exchanger allocation, refrigerant selection, and operating conditions.

The author also contributed to the experimental program: preparing the test stand, collecting thermal and electrical data, and validating the models under Kazakhstan's continental climate (Almaty installation). The dissertation's main text, analyses, and interpretation were written by the author; co-authors provided scientific supervision and methodological support. Results from joint works are co-owned by all contributors, and external materials are cited in the relevant sections.

Methodological framework of the research.

The methodological framework of this dissertation combines two complementary pillars: (i) finite-time thermodynamics (FTT) modeling and optimization of GSHP systems, and (ii) 3E (energy-exergy-environmental) analysis supported by experimental validation under continental climatic conditions.

(i) FTT modeling and optimization.

Classical thermodynamic analyses often rely on reversible or idealized cycles, which fail to capture the influence of real-world irreversibilities such as finite heat transfer rates, entropy production, and frictional losses. To address this gap, the dissertation develops fluidless FTT models of GSHP systems that explicitly incorporate cycle irreversibilities.

- *System representation:* The GSHP is modeled as a cycle interfacing with four thermal reservoirs (ground source, cold loop, hot loop, and user-side sink). Heat exchangers are represented by effectiveness-capacity rate relationships.
- *HP model variants.* Three formulations are analyzed:
  1) Reversible (endoreversible) model as a reference;
  2) Irreversible model with irreversibility ratio;
  3) Irreversible model with entropy production rate.
- *Imposed conditions:* Optimization is performed under two types of imposed constraints:
  1) Imposed heat extraction rate from the ground;
  2) Imposed heat production rate to the user.
- *Non-dimensionalization:* All governing equations are reformulated in terms of dimensionless parameters to generalize the results and reduce dependency on specific cases.
- *Optimization problems:* Objective functions include minimization of compressor power consumption and/or maximization of COP, subject to thermodynamic and design constraints. Optimization problems are solved numerically.

– *Parametric analysis:* Systematic variation of parameters is performed to quantify their influence on optimal performance. The results identify critical parameters and establish general optimization rules.

(ii) 3E analysis and experimental validation.

The dissertation applies 3E analysis to GSHP system, which includes energy, exergy, and environmental performance indicators.

– *Energy and exergy models:* First- and second-law balances are used to calculate heating capacity, COP, and exergy efficiency.
– *Environmental assessment:* Total equivalent warming impact (TEWI) is calculated, considering both direct refrigerant leakage and indirect emissions from electricity consumption.
– *Validation:* Experimental data from a GSHP installation in Almaty, Kazakhstan are used to calibrate and validate the models.
– *Scenario analysis:* The validated model is applied to explore different refrigerants, source/sink temperatures, and heating loads.

Thesis structure and scope.

The thesis consists of an introduction, two chapters, a conclusion, a list of references. The work is 81 pages long and contains 29 figures and 6 tables.

Main content of the thesis.

The introduction presents the relevance of the research, formulates the aim and objectives, emphasizes the scientific novelty, and highlights the theoretical and practical significance of the results. It also notes the approbation of the main findings at international conferences and their publication in peer-reviewed journals, and outlines the structure and contents of the thesis.

The main part comprises two chapters and ten sections.

Chapter 1 develops a finite-time thermodynamics (FTT) framework for optimizing ground source heat pump (GSHP) systems. It reviews GSHPs and FTT methods, formulates mathematical models of endoreversible and irreversible heat pump cycles, and considers two imposed operating cases. The results yield new relationships for optimal allocation of heat exchanger effectiveness and capacity rates, and clarify how cycle irreversibility and temperature lift affect performance, providing a theoretical basis for GSHP design rules.

Chapter 2 presents a 3E (energy-exergy-environmental) analysis of GSHPs, validated using experimental data from a pilot installation in Almaty, Kazakhstan. It describes the experimental setup, develops and validates conventional GSHP models against measured data, and analyzes performance under different operating conditions, including refrigerant selection, exergy efficiency, and TEWI. The findings demonstrate the practical applicability of the methodology for GSHP design in continental climates.

The conclusion synthesizes the principal results, formulates scientific and practical outcomes, and offers recommendations for the design and operation of GSHP systems. The thesis also includes a list of references.

1 FINITE-TIME THERMODYNAMIC (FTT) OPTIMIZATION OF GROUND SOURCE HEAT PUMP (GSHP) SYSTEMS

Ground source heat pump (GSHP) systems are widely recognized for their high efficiency and potential to reduce greenhouse gas emissions in residential and industrial heating applications. Nevertheless, their actual performance in practice is constrained by a variety of irreversibilities, including finite heat transfer rates, entropy generation, and limitations of the heat exchanger configuration. Classical thermodynamic approaches, based on the Carnot cycle or steady-state exergy analysis, provide idealized upper bounds for performance but do not capture the realistic penalties introduced by these irreversibilities. For this reason, a more refined theoretical framework is required to evaluate GSHPs under conditions that reflect real-world operating constraints.

Finite-time thermodynamics (FTT) has emerged as a powerful tool for bridging this gap between theory and practice. Unlike classical thermodynamics, which assumes reversible processes, FTT explicitly accounts for finite temperature differences, finite heat exchanger surface areas, and dissipation effects [36,37]. By formulating optimization problems that incorporate these constraints, FTT enables the derivation of realistic performance bounds and optimal allocation strategies for thermal resources. The relevance of FTT has been demonstrated in a wide range of energy conversion systems, from heat engines to refrigeration and heat pump cycles, but its application to GSHPs remains limited.

GSHP systems present a particularly interesting case for FTT analysis. Their cycle interacts simultaneously with multiple thermal reservoirs – ground source, evaporator, condenser, and user-side heat sink. The allocation of thermal and geometric resources among these exchangers has a direct impact on the overall coefficient of performance (COP) and compressor power consumption. Moreover, the asymmetry of source and sink conditions in continental climates, where soil temperatures are low and heat demand is high, accentuates the influence of irreversibility on system efficiency. A finite-time optimization framework is therefore well suited to identify design and operational strategies that minimize power input while ensuring reliable heat delivery.

The present chapter develops such a framework, starting with a review of the theoretical background and prior work on finite-time thermodynamics. Section 1.1 provides a structured literature review, beginning with the classical foundations of FTT, followed by its application to refrigeration and heat pump cycles, and concluding with the few existing studies relevant to GSHPs. The gaps identified in this review serve as motivation for the GSHP description in Section 1.2 and the development of the mathematical model and optimization methodology in Section 1.3. A schematic of the GSHP cycle with its four thermal reservoirs is shown in Figure 1, providing a visual context for the analyses that follow.

1.1 Literature review on FTT and GSHP optimization

Classical foundations of finite-time thermodynamics (FTT).

The classical bounds of thermodynamics, particularly those established by Carnot, have long been recognized as unattainable in practice. The Carnot efficiency (or coefficient of performance, COP, for reversed cycles) presupposes reversible processes and infinite thermal reservoirs, which necessarily imply infinitesimally slow cycles and vanishing power output. Such assumptions render the classical bounds of limited practical value for engineering systems that must deliver finite power or cooling/heating rates. The inadequacy of these reversible bounds motivated the development of finite-time thermodynamics (FTT), which explicitly considers finite heat-transfer rates, finite cycle times, heat leaks, and dissipative effects such as fluid friction [43,44].

The first systematic formulations appeared in the 1950s, when Novikov and Chambadal independently derived the efficiency of power plants under finite-rate heat transfer [43,44]. Two decades later, Curzon and Ahlborn extended this reasoning to derive the now-famous Curzon-Ahlborn efficiency [45]:

$$\eta_{CA} = 1 - \sqrt{\frac{T_c}{T_h}},$$

which represents the efficiency of an endoreversible Carnot engine operating at maximum power between hot and cold reservoirs at temperatures T_h and T_c. This result has become a cornerstone of FTT and has been generalized to numerous configurations and objective functions.

A simple example illustrates the gap between idealized Carnot bounds and finite-time optima. For an engine operating between 600 K and 300 K, the reversible Carnot efficiency is $\eta_{rev} = 50\%$, while the Curzon-Ahlborn efficiency for the same reservoirs is only $\eta_{CA} = 1 - \sqrt{300/600} \approx 29.3\%$ [45]. This substantial reduction, consistent with measured performance of real plants, underlines the necessity of FTT methods when realistic power densities are considered.

Subsequent developments broadened the scope beyond maximum power to alternative optimization criteria. Ecological optimization, introduced by Angulo-Brown, balances power output against entropy generation to yield more environmentally meaningful operating points [16]. Similarly, entropy generation minimization (EGM), proposed by Bejan, frames the problem as minimizing irreversibility for a given thermal duty, leading to practical design insights for heat exchangers and thermal cycles [46].

FTT has also incorporated multi-objective trade-offs, such as maximizing COP while constraining heating/cooling load, or minimizing work input for an imposed thermal duty [47,48]. Many studies demonstrate that finite heat exchanger surface area allocation and finite capacity-rate reservoirs critically influence optima. For instance, Sarkar et al. [49] showed that optimum allocation can reduce the total conductance

requirement by 20-30% compared with equal partitioning, thereby improving compactness and cost-effectiveness. Such quantitative results confirm that FTT-based designs approach achievable real-world efficiencies rather than unattainable theoretical maxima.

Despite its progress, classical FTT models typically employ simplified working-fluid assumptions ("fluidless" cycles) and Newtonian heat-transfer laws, limiting their direct applicability to complex, real-world devices. Nonetheless, they provide the theoretical foundation for extending finite-time principles to refrigeration, heat pumps, and eventually ground source heat pump systems.

FTT in refrigeration and heat pumps systems.

The application of FTT to refrigerators and heat pumps (HPs) extends the classical framework to reversed cycles, where the performance is measured by the coefficient of performance (COP) and the delivered cooling or heating load. The challenge arises because, unlike engines, refrigerators and HPs exhibit fundamentally different trade-offs: while COP diverges near reversible operation, it collapses at high loads, making optimization more subtle [47,48].

Quantitative findings reinforce the theoretical arguments. Sahin & Kodal [47] showed that the optimal thermoeconomic COP of an endoreversible refrigerator peaks at ~4.0 when operating between 270 K and 300 K with finite conductance, compared with a Carnot COP of 9.0 under the same conditions. Salah El-Din [48] demonstrated that incorporating variable-temperature reservoirs typically reduces the optimal COP by 15-25% relative to constant-reservoir assumptions.

Further developments integrated ecological and exergy-based criteria. Chen and Wu [50] analyzed exergy-based ecological optimization of irreversible Carnot HPs, balancing heating load against entropy generation. Bi et al. [51] found that for an endoreversible air-source HP, the ecological optimum corresponded to a COP of ~3.5 at a heating load density of 2.8 kW m^{-2}, whereas the maximum COP (>6) was achievable only at impractically low loads. Qin et al. [38] extended these approaches to a four-reservoir absorption HP, reporting optimum COP values of 1.4-1.8 depending on irreversibility distribution, consistent with experimental absorption system performance.

More recently, Ye and Holubec [39] proposed low-dissipation models for heat pumps, bridging the gap between low-dissipation and endoreversible regimes. They analytically proved that the maximum COP at imposed heating load is constrained to 50-70% of the Carnot COP, depending on asymmetry of dissipation. This result formalizes the gap between idealized and realistic operation.

Across these studies, the COP-load trade-off emerges as a defining feature: real HPs cannot simultaneously deliver high COP and large heating output, and optimal operation lies in compromise regions determined by irreversibility allocation. Heat exchanger distribution is another key lever. Sarkar et al. [49] showed that optimal area ratios between condenser and evaporator can reduce total conductance requirements by 20-30%, compared with uniform allocation strategies.

Generalized FTT formulations have also introduced performance maps in COP–load space with loop-shaped characteristics, unifying thermoelectric, Brayton, Rankine, and absorption cycles under common dissipation structures [52]. Objective

functions have expanded to include ecological COP (ECOP), exergy-based criteria, and thermoeconomic profit-rate functions [50,53]. Multi-objective optimization techniques – especially evolutionary algorithms – have been applied to balance COP, exergetic efficiency, and ecological goals. For example, Ahmadi et al. [54] optimized a Brayton HP using NSGA-II and reported Pareto-optimal COPs of 2.0-2.4, exergetic efficiencies of 35-42%, and ecological COP peaking at ~1.7.

Taken together, these numerical ranges emphasize that FTT shifts the focus from unattainable maxima (e.g., Carnot COP > 8) to realistic compromises (COP ~2-4) achievable with constrained resources. Collectively, these works establish FTT as a unified framework for analyzing HPs under realistic constraints, offering reusable principles: imposed-load formulations, optimal heat exchanger (HX) allocation, irreversibility trade-offs, and generalized objective criteria. These principles naturally extend to ground source heat pump (GSHP) systems, where both the cycle and its reservoirs (ground and building) impose finite-time and finite-size limitations.

Applications to GSHPs.

Ground source heat pumps (GSHPs) couple vapor-compression cycles to the earth through buried ground heat exchangers (GHEs), which act as finite-capacitance thermal reservoirs. Unlike the idealized infinite thermostats of classical models, the ground exhibits finite thermal conductance, time-varying temperature, and seasonal imbalance. These characteristics make GSHPs a natural candidate for FTT analysis, even though the literature has only partly integrated FTT principles.

Adebayo and Mwesigye [5] provide a comprehensive review of GSHPs in cold climates, highlighting challenges such as seasonal imbalance, long-term ground cooling, and high drilling costs. They emphasize the need for advanced models that capture transient ground behavior, hybridization (e.g., solar-assisted GSHPs), and thermal storage integration. Olympios and Markides [9] similarly review domestic HPs, noting that while GSHPs achieve high seasonal COP (SCOP), optimization often neglects finite HX surfaces and irreversibility trade-offs.

Some works have explicitly applied FTT reasoning. Arz, Feidt, and Costea [42,55] studied the influence of boundary conditions on GSHP optimization, showing that optimal HX allocation depends strongly on the imposed condition (soil temperature, heat flux, or COP). They reported that for an imposed heating load of 10 kW, minimum compressor work occurred when ~55-60% of the total HX area was assigned to the ground side – significantly different from the classical 50/50 equipartition rule. Feidt and Costea [55] developed a new FTT-based optimization approach explicitly coupling cycle performance to finite-capacitance reservoirs. They found that for a Carnot-like GSHP, the COP at minimum energy expense could be up to 15% lower than the reversible COP, but still superior to equal-area allocations. Rachedi et al. [56] analyzed a transcritical CO_2-based endoreversible cycle driven by a geothermal source at 90 °C, reporting optimum COPs of 3.0-3.5 and showing that finite reservoir conductance can yield performance above Curzon-Ahlborn predictions.

At the borefield scale, hybrid semi-analytical models (e.g., thermal response test, line-source methods) provide reduced-order representations of transient ground heat transfer, enabling integration with cycle-level FTT models [5]. Such models reveal how

borehole number, spacing, and length interact with imposed seasonal loads, echoing FTT principles of finite reservoir capacity.

The GSHP literature also contains abundant 4E (energy-exergy-economic-environmental) analyses, many of which implicitly align with FTT levers. For instance, minimizing compressor work for imposed heating load parallels minimizing energy expense at imposed Q_h in FTT formulations. Exergoeconomic studies show that COP-optimal operation rarely coincides with cost-optimal operation, reinforcing the need for multi-objective formulations [5,9]. From broader techno-economic reviews, Olympios & Markides [9] showed that seasonal performance factors (SPFs) of GSHPs in domestic heating typically range 3.0-4.5, while Adebayo and Mwesigye [5] reported that in cold-climate applications, SPFs decline to 2.5-3.2 due to seasonal imbalance and ground cooling. They also highlighted that hybrid GSHP–solar storage systems can improve SPF by 20-25% while reducing borehole length requirements by ~30%.

These numerical findings confirm that finite-resource constraints (soil conductance, HX area, seasonal drift) systematically limit GSHP COP to about 3-4, aligning with both FTT predictions and field data. Overall, while GSHP studies frequently employ thermoeconomic or dynamic borefield models, a general FTT framework that integrates cycle irreversibility, finite HX surfaces, and seasonal ground behavior has not yet been established.

Research gaps.

Despite the richness of both FTT and GSHP literatures, a clear research gap remains at their intersection. No general FTT-based GSHP framework currently exists that simultaneously accounts for:

- cycle-reservoir coupling with finite thermal capacitance and time-varying ground temperature,
- finite heat exchanger (HX) surfaces for both ground and internal exchangers, with optimal allocation under imposed loads,
- the presence of multiple thermal reservoirs (ground, building, evaporator, condenser), effectively forming a four-reservoir problem,

Addressing this gap is timely. GSHP deployment is expanding rapidly in Europe, Asia, and North America [5,9], where the technology is increasingly positioned as a cornerstone of building-sector decarbonization. Yet current optimization approaches remain fragmented: cycle-level FTT studies neglect reservoir dynamics, while borefield models rarely incorporate finite-time principles.

This thesis seeks to bridge that divide by developing a finite-time thermodynamic framework for GSHP systems with four thermal reservoirs. The proposed approach embeds cycle-reservoir coupling, finite HX surfaces, and imposed-load formulations within a unified optimization methodology. Specifically, it investigates an optimized four-heat-exchanger (4-HX) configuration that allows rational allocation of thermal and geometric resources.

The optimization problem is constrained by key thermodynamic and design parameters, including the heat extraction rate from the ground ($\dot{Q}_g$), the heat delivery

rate to the user ($\dot{Q}_p$). In this study, either $\dot{Q}_g$ or $\dot{Q}_p$ is imposed, and the optimization seeks to minimize power consumption or, equivalently, maximize COP.

This work builds earlier contributions [42,55] and provides, for the first time, a comprehensive FTT-based framework for the thermodynamic optimization of GSHPs under imposed heat extraction and delivery profiles. The following sections describe the GSHP system (Section 1.2) and present the mathematical modeling and optimization methodology (Section 1.3), which together form the foundation of the thesis.

1.2 Description of the GSHP system

The ground source heat pump (GSHP) system, schematically illustrated in Figure 1, operates as a closed-loop vapor compression cycle coupled with two secondary fluid circuits. Thermal interaction with the ground is established through a ground heat exchanger (GHE), most commonly configured as vertical or horizontal U-tubes. The GHE extracts low-grade thermal energy from the surrounding soil, where the temperature remains relatively stable at T_s, and delivers it to the cycle as the primary heat source for subsequent upgrading.

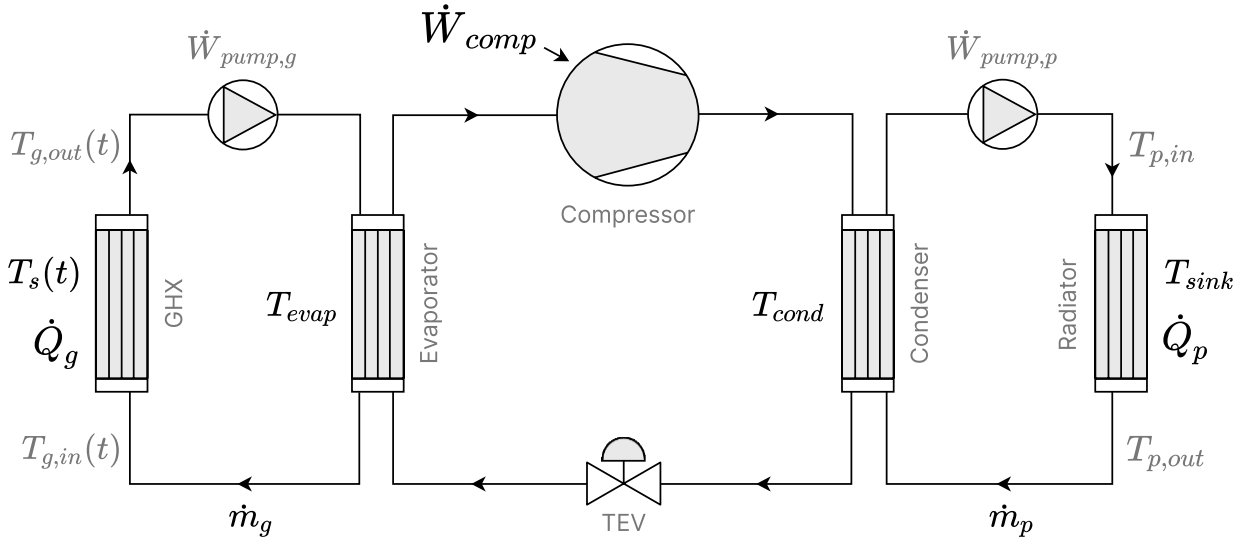

Figure 1 – Schematic diagram of the GSHP

In the cold loop, an antifreeze solution (typically ethylene or propylene glycol) circulates through the GHE, absorbing heat from the ground and transferring it to the evaporator of the vapor compression cycle. Within the evaporator, the refrigerant absorbs this energy and undergoes phase change from liquid to vapor. The vapor is then compressed, resulting in a substantial increase in pressure and temperature. The high-enthalpy refrigerant subsequently flows into the condenser, where it releases heat to the hot loop, most often water-based, which supplies thermal energy to the user-side system (e.g., radiators, fan coils, underfloor heating) at the prescribed sink temperature

T_{sink}. After condensation, the refrigerant passes through a thermal expansion valve (TEV), which reduces its pressure and temperature before re-entering the evaporator, thereby completing the cycle.

Both the cold and hot loops operate as closed circuits, with circulating pumps maintaining the prescribed flow rates of the secondary heat transfer fluids. In these auxiliary loops, thermal exchange occurs without phase change, relying solely on sensible heat transfer.

In this chapter of the thesis, the analysis explicitly considers the four heat exchangers integrated within these coupled loops: ground, evaporator, condenser, and radiator. Their finite effectiveness (ε_i) and heat capacity rates (c_i) govern the thermal coupling between the reservoirs and thus the overall efficiency of the GSHP cycle. The thermodynamic optimization framework developed here addresses this resource allocation problem: how to distribute limited exchanger conductance and capacity between components in order to minimize compressor power consumption ($\dot{W}$) or maximize the coefficient of performance (COP), under imposed operating conditions defined either by the ground-side heat extraction rate or the user-side heat production rate. This formulation directly links physical design parameters with performance metrics, enabling a systematic study of optimal GSHP operation under finite-time thermodynamic constraints.

1.3 FTT model and optimization problem formulation

The mathematical model is developed from fundamental thermodynamic balances, with the governing equations derived in analytical form and independent of specific thermophysical properties of working fluids. This establishes a fluidless framework, in which performance is determined by heat exchanger effectiveness and capacity rates rather than refrigerant details. The GSHP configuration consists of a cold loop and a hot loop (Figure 1), both treated as adiabatic subsystems, i.e., without thermal losses to the surroundings.

On the cold side (ground loop), the energy balance is expressed in terms of the heat transfer rate $\dot{Q}$:

$$\dot{Q}_g = \dot{Q}_{evap},$$

where subscripts g and $evap$ correspond to the ground and evaporator heat exchangers, respectively. The heat transfer rates can be expressed in terms of heat exchanger effectiveness and heat capacity rate as follows [37,42]:

$$\dot{Q}_g = \varepsilon_g \dot{c}_g \left(T_s - T_{g,in}\right) = \dot{c}_g \left(T_{g,out} - T_{g,in}\right),$$

$$\dot{Q}_{evap} = \varepsilon_{evap} \dot{c}_g \left(T_{g,out} - T_{evap}\right)$$

where:

- ε is the effectiveness of the heat exchanger,
- $\dot{c} = \dot{m}c_p$ is the heat capacity rate of the loop,
- T_s, $T_{g,in}$, and $T_{g,out}$ are the temperature of the heat source (ground), inlet, and outlet of the ground heat exchanger, respectively.

The evaporator temperature in the HP cycle can be derived from the heat extraction rate $\dot{Q}_g$:

$$T_{evap} = T_s - \alpha'_g \dot{Q}_g, \tag{1}$$

where $\alpha'_g = \frac{1}{\dot{c}_g}\left(\frac{1}{\varepsilon_g} + \frac{1}{\varepsilon_{evap}} - 1\right)$.

On the hot side (heat delivery loop), the corresponding energy balance can be expressed as:

$$\dot{Q}_p = \dot{Q}_{cond},$$

where the subscripts p and $cond$ refer respectively to the heat production (radiator) and condenser heat exchangers. In this equation, the heat transfer rates are given by [37,42]:

$$\dot{Q}_p = \varepsilon_p \dot{c}_p\left(T_{p,in} - T_{sink}\right) = \dot{c}_p\left(T_{p,in} - T_{p,out}\right),$$

$$\dot{Q}_{cond} = \varepsilon_{cond} \dot{c}_p\left(T_{cond} - T_{p,out}\right),$$

where T_{sink}, $T_{p,in}$, and $T_{p,out}$ denote respectively the temperatures of the heat sink (consumer comfort setpoint), and the inlet and outlet of the radiator. The condenser temperature can be determined as:

$$T_{cond} = T_{sink} + \alpha'_p \dot{Q}_p, \tag{2}$$

where $\alpha'_p = \frac{1}{\dot{c}_p}\left(\frac{1}{\varepsilon_p} + \frac{1}{\varepsilon_{cond}} - 1\right)$.

The governing energy and entropy balance relations for the cycle are:

$$\dot{Q}_p = \dot{Q}_g + \dot{W}, \tag{3}$$

$$\frac{\dot{Q}_p}{T_{cond}} = \frac{\dot{Q}_g}{T_{evap}}, \tag{4a}$$

$$\frac{\dot{Q}_p}{T_{cond}} = I\frac{\dot{Q}_g}{T_{evap}}, \qquad I \geq 1, \tag{4b}$$

$$\frac{\dot{Q}_p}{T_{cond}} = \frac{\dot{Q}_g}{T_{evap}} + \dot{S}, \quad \dot{S} \geq 0\,, \tag{4c}$$

where $\dot{W}$ is the power consumption of the GSHP, I is the irreversibility ratio, and $\dot{S}$ is the entropy production rate.

Equation (4a) represents the reversible (endoreversible) case, while Equations (4b) and (4c) incorporate the effects of irreversibility through the irreversibility ratio (I) and the entropy production rate ($\dot{S}$), respectively.

Two operating scenarios are examined: one with an imposed heat extraction rate (Subsection 1.3.1) and another with an imposed heat production rate (Subsection 1.3.2). For both cases, the models are evaluated under the two irreversibility formulations, allowing a direct comparison of their influence on the predicted thermodynamic performance of the system.

1.3.1 Case A: model under imposed ground heat extraction

In this scenario, the analysis considers the case where the heat extraction rate from the ground side is externally imposed, i.e.,

$$\dot{Q}_g = \dot{Q}_{g0}.$$

Three model formulations are examined to evaluate how different representations of irreversibility influence the resulting cycle performance.

a) Reversible (endoreversible) model.

This formulation represents the baseline case in which heat exchanger allocations (ε_i) and capacity rates (c_i) are evaluated without accounting for additional irreversibilities. The resulting expressions serve as a reference for comparison with the irreversible models, where performance degradation due to finite entropy production or irreversibility ratio (I) is explicitly included.

For the reversible cycle, substituting $\dot{Q}_g = \dot{Q}_{g0}$ into the governing relations (Eqs. (1) and (3)) yields the following expressions for the evaporator temperature and energy balance:

$$T_{evap} = T_s - \alpha'_g \dot{Q}_{g0},$$

$$\dot{Q}_p = \dot{Q}_{g0} + \dot{W}.$$

By combining the energy balance Eq. (3) with the reversible entropy balance Eq. (4a), we obtain:

$$\frac{T_{evap}}{\dot{Q}_{g0}} = \frac{T_{cond}}{\dot{Q}_p},$$

substituting the expressions for the evaporator and condenser temperatures from Eqs. (1) and (2), this relation can be further rewritten as:

$$\frac{T_s}{\dot{Q}_{g0}} - \alpha'_g = \frac{T_{sink}}{\dot{Q}_p} + \alpha'_p,$$

$$\frac{T_s}{\dot{Q}_{g0}} - \frac{T_{sink}}{\dot{Q}_{g0} + \dot{W}} = \alpha',$$

where $\alpha' = \alpha'_g + \alpha'_p$. By rearranging the preceding relation, the expression for the compressor power consumption in the reversible case can be written as:

$$\dot{W} = \dot{Q}_{g0}\left[\frac{T_{sink}}{T_s - \alpha'\dot{Q}_{g0}} - 1\right]. \quad (5)$$

b) Irreversible model based on the irreversibility ratio.

In the case of the irreversible model formulated using the irreversibility ratio I, the imposed condition $\dot{Q}_g = \dot{Q}_{g0}$ is substituted into Eqs. (1) and (2) to determine the evaporator and condenser temperatures. By then combining these relations with the energy balance Eq. (3) and the entropy balance for the irreversible case Eq. (4b), we obtain:

$$\frac{T_{evap}}{\dot{Q}_{g0}} = I\frac{T_{cond}}{\dot{Q}_p},$$

$$\frac{T_s}{\dot{Q}_{g0}} - \alpha'_g = I\frac{T_{sink}}{\dot{Q}_p} + I\alpha'_{p,}$$

$$\frac{T_s}{\dot{Q}_{g0}} - \frac{I \cdot T_{sink}}{\dot{Q}_{g0} + \dot{W}} = \alpha'_I,$$

where $\alpha'_{\mathrm{I}} = \alpha'_g + I\alpha'_p$.

The corresponding expression for the compressor power consumption is then obtained as:

$$\dot{W} = \dot{Q}_{g0}\left[\frac{I \cdot T_{sink}}{T_s - \alpha'_I\dot{Q}_{g0}} - 1\right]. \quad (6)$$

c) Irreversible model based on the entropy production rate.

For the formulation based on the entropy production rate $\dot{S}$, the imposed condition $\dot{Q}_g = \dot{Q}_{g0}$ is applied. Substituting into Eqs. (1), (2), and (3), together with the entropy balance for this case Eq. (4c), yields:

$$\frac{\dot{Q}_{g0} + \dot{W}}{T_{sink} + \alpha'_p(\dot{Q}_{g0} + \dot{W})} = \frac{\dot{Q}_{g0}}{T_s - \alpha'_g \dot{Q}_{g0}} + \dot{S}.$$

This leads to the following expression of the power consumption:

$$\dot{W} = \frac{[\dot{Q}_{g0} + \dot{S}(T_s - \alpha'_g \dot{Q}_{g0})](T_{sink} - \alpha'_p \dot{Q}_{g0}) - \dot{Q}_{g0}(T_s - \alpha'_g \dot{Q}_{g0})}{T_s - \alpha'_g \dot{Q}_{g0} - \alpha'_p[\dot{Q}_{g0} + \dot{S}(T_s - \alpha'_g \dot{Q}_{g0})]}.$$

By algebraic rearrangement, this expression can be written in the more compact form:

$$\dot{W} = \dot{Q}_{g0}\left[\frac{\alpha'_{s,g} T_{sink}}{\alpha'_{s,p} T_s - \alpha'_s \dot{Q}_{g0}} - 1\right] + \frac{\dot{S} T_s T_{sink}}{\alpha'_{s,p} T_s - \alpha'_s \dot{Q}_{g0}}, \tag{7}$$

where:

$$\alpha'_s = \alpha'_g + \alpha'_p - \dot{S}\alpha'_g \alpha'_p,$$

$$\alpha'_{s,g} = 1 - \dot{S}\alpha'_g,$$

$$\alpha'_{s,p} = 1 - \dot{S}\alpha'_p.$$

For the purposes of optimization and parametric sensitivity analysis, it is convenient to introduce the following non-dimensional variables, defined under the condition $\sum \dot{c}_i = \dot{c}_t$:

$$w = \frac{\dot{W}}{\dot{c}_t T_{sink}}, \; q_{g0} = \frac{\dot{Q}_{g0}}{\dot{c}_t T_{sink}}, \; \tau = \frac{T_s}{T_{sink}}, \quad c_i = \frac{\dot{c}_i}{\dot{c}_t}, \qquad s = \frac{\dot{S}}{\dot{c}_t}.$$

These normalized quantities enable the reformulation of Eqs. (5)-(7) in dimensionless form, thereby facilitating a direct comparison of reversible and irreversible models as well as a more systematic exploration of the optimization problem.

From Eq. (3), the coefficient of performance (COP) is:

$$COP = \frac{q_{g0}}{w} + 1.$$

For the reversible case, the dimensionless form of the power consumption (Eq. (5)) and the corresponding expression for COP are given by:

$$w = q_{g0}\left[\frac{1}{\tau-\alpha q_{g0}} - 1\right], \tag{8a}$$

$$COP = \frac{1}{\alpha q_{g0}+1-\tau}, \tag{8b}$$

where $\alpha = \alpha_g + \alpha_p$, such that:

$$\alpha_g = \frac{1}{c_g}\left(\frac{1}{\varepsilon_g} + \frac{1}{\varepsilon_{evap}} - 1\right),$$

$$\alpha_p = \frac{1}{c_g}\left(\frac{1}{\varepsilon_p} + \frac{1}{\varepsilon_{cond}} - 1\right).$$

For the irreversible model based on the irreversibility ratio, the dimensionless form of Eq. (6) and the COP expression are:

$$w = q_{g0}\left[\frac{I}{\tau-\alpha_I q_{g0}} - 1\right], \tag{9a}$$

$$COP = \frac{I}{\alpha_I q_{g0}+I-\tau}, \tag{9b}$$

where $\alpha_I = \alpha_g + I\alpha_p$.

For the irreversible model based on the entropy production rate, the dimensionless form of Eq. (7) and the COP are:

$$w = q_{g0}\left[\frac{\alpha_{s,g}}{\alpha_{s,p}\tau-\alpha_s q_{g0}} - 1\right] + \frac{s\tau}{\alpha_{s,p}\tau-\alpha_s q_{g0}}, \tag{10a}$$

$$COP = \frac{\alpha_{s,g}+\frac{s\tau}{q_{g0}}}{\alpha_s q_{g0}+\alpha_{s,g}-\alpha_{s,p}\tau+\frac{s\tau}{q_{g0}}}, \tag{10b}$$

where

$$\alpha_s = \alpha_g + \alpha_p - s\alpha_g\alpha_p,$$

$$\alpha_{s,g} = 1 - s\alpha_g,$$

$$\alpha_{s,g} = 1 - s\alpha_g.$$

1.3.2 Case B: model under imposed heat delivery to load

In this case, the GSHP is analysed under the condition that the heat production rate on the load side is externally specified and fixed at a prescribed value:

$$\dot{Q}_p = \dot{Q}_{p0}.$$

Under this condition, Eqs. (1) and (3) yield the following relations:

$$T_{cond} = T_{sink} + \alpha'_p \dot{Q}_{p0},$$

$$\dot{Q}_{p0} = \dot{Q}_g + \dot{W}.$$

By combining the energy balance Eq. (3) with the entropy balance formulations Eqs. (4a), (4b), and (4c), the compressor power consumption $\dot{W}$ for the case of imposed heat production rate can be derived in three forms, corresponding to the reversible, irreversibility ratio, and entropy production rate models, respectively:

$$\dot{W} = \dot{Q}_{p0}\left[1 - \frac{T_s}{\alpha' \dot{Q}_{p0} + T_{sink}}\right], \tag{11}$$

where $\alpha' = \alpha'_g + \alpha'_p$.

$$\dot{W} = \dot{Q}_{p0}\left[1 - \frac{T_s}{\alpha'_I \dot{Q}_{p0} + I T_{sink}}\right], \tag{12}$$

where $\alpha'_I = \alpha'_g + I\alpha'_p$.

$$\dot{W} = \dot{Q}_{p0}\left[1 - \frac{\alpha'_{s,p} T_s}{\alpha'_s \dot{Q}_{p0} + \alpha'_{s,g} T_{sink}}\right] + \frac{\dot{S} T_s T_{sink}}{\alpha'_s \dot{Q}_{p0} + \alpha'_{s,g} T_{sink}}, \tag{13}$$

where

$$\alpha'_s = \alpha'_g + \alpha'_p - \dot{S}\alpha'_g \alpha'_p,$$

$$\alpha'_{s,g} = 1 - \dot{S}\alpha'_g,$$

$$\alpha'_{s,p} = 1 - \dot{S}\alpha'_p.$$

From the energy balance in Eq. (3), the coefficient of performance (COP) of the GSHP with imposed heat production rate is defined as

$$COP = \frac{q_{p0}}{w}.$$

Furthermore, the expressions for compressor power consumption given in Eqs. (11), (12), and (13) can be cast into non-dimensional form as follows.

For the reversible model:

$$w = q_{p0}\left[1 - \frac{\tau}{\alpha q_{p0} + 1}\right], \tag{14a}$$

$$COP = \frac{\alpha q_{p0}+1}{\alpha q_{p0}+1-\tau}, \tag{14b}$$

where $\alpha = \alpha_g + \alpha_p$.

For the model with irreversibility ratio:

$$w = q_{p0}\left[1 - \frac{\tau}{\alpha_I q_{p0}+I}\right], \tag{15a}$$

$$COP = \frac{\alpha_I q_{p0}+I}{\alpha_I q_{p0}+I-\tau}, \tag{15b}$$

where $\alpha_I = \alpha_g + I\alpha_p$.

For the model with entropy production rate:

$$w = q_0\left[1 - \frac{\alpha_{s,p}\tau}{\alpha_s q_{p0}+\alpha_{s,g}}\right] + \frac{s\tau}{\alpha_s q_{p0}+\alpha_{s,g}}, \tag{16a}$$

$$COP = \frac{\alpha_s q_{p0}+\alpha_{s,g}}{\alpha_s q_{p0}+\alpha_{s,g}-\alpha_{s,p}\tau+\frac{s\tau}{q_{p0}}}, \tag{16b}$$

where

$$\alpha_s = \alpha_g + \alpha_p - s\alpha_g\alpha_p,$$

$$\alpha_{s,g} = 1 - s\alpha_g,$$

$$\alpha_{s,p} = 1 - s\alpha_p.$$

These non-dimensional expressions offer a common framework for comparing the three modeling approaches and assessing how the imposed heat delivery q_{p0}, temperature ratio τ, and irreversibility parameters (I, s)affect the required compressor power and the resulting COP of the GSHP.

1.3.3 Objective functions, constraints, and solution method

The optimization framework is established using the objective functions derived in Eqs. (8)-(10) for the case of imposed heat extraction rate (q_{g0}), and Eqs. (14)-(16) for the case of imposed heat production rate q_{p0}.

The objectives are twofold:

1. Minimization of power consumption of the GSHP cycle, corresponding to Eqs. (8a), (9a), (10a), (14a), (15a), and (16a).
2. Maximization of the coefficient of performance (COP), corresponding to Eqs. (8b), (9b), (10b), (14b), (15b), and (16b).

Both objectives are evaluated subject to the following system of constraints:

$$\varepsilon_g + \varepsilon_{evap} + \varepsilon_p + \varepsilon_{cond} = \varepsilon_t, \tag{17a}$$

$$c_g + c_p = c_t, \tag{17b}$$

$$0 < \varepsilon_i < 1, \text{ and } 0 < c_i < 1, \tag{18}$$

where, $\varepsilon_i,\ c_i$ are the optimization variables, $\varepsilon_t,\ c_t$ are the constraint parameters, q_{g0} (or q_{p0},) τ, I (and s) are the optimization parameters. The constraint $0 < \varepsilon_i < 1$ represents a technical limitation, where the effectiveness of the heat exchangers varies between 0 and 1.

By analyzing objective functions together with the constraint system (Eqs. (17-18)), it can be shown that the allocation of optimal values for exchanger effectiveness ε_i and capacity rates c_i is governed by the following relationships:

$$\begin{gathered}\varepsilon_g^* = \varepsilon_{evap}^*, \qquad \varepsilon_p^* = \varepsilon_{cond}^*, \text{ and} \\ \varepsilon_g^* + \varepsilon_p^* = \varepsilon_{evap}^* + \varepsilon_{cond}^* = \frac{\varepsilon_t}{2},\end{gathered} \tag{19a}$$

$$c_g^* + c_p^* = c_t. \tag{19b}$$

Furthermore, in the case of the reversible models (Eqs. (8, 14)), the optimal allocation reduces to a uniform distribution across all exchangers, given by:

$$\varepsilon_g^* = \varepsilon_p^* = \varepsilon_{evap}^* = \varepsilon_{cond}^* = \frac{\varepsilon_t}{4}, \tag{20a}$$

$$c_g^* = c_p^* = \tfrac{c_t}{2}. \tag{20b}$$

The objective functions for minimizing power consumption (Eqs. (8a), (9a), (10a), (14a), (15a), and (16a)) are strictly concave within the domain $0 < \varepsilon_i < 1{,}0 < c_i < 1$, and thus admit a unique interior minimizer when subject to linear equality constraints. Similarly, the COP-maximizing functions (Eqs. (8b), (9b), (10b), (14b), (15b), and (16b)) are strictly convex over the same domain, ensuring a unique interior maximizer.

The optimization problems formulated above are solved numerically using a custom Python implementation combined with the SLSQP (Sequential Least Squares Programming) algorithm available in the SciPy library[57]. To reduce computational effort and improve convergence robustness, each parametric optimization run is initialized using the solution from the preceding step with slightly perturbed parameter values, thereby providing a warm start that accelerates convergence while maintaining numerical stability.

1.3.4 Parameter ranges for parametric study

In the following section, the influence of parameter variation on the optimal solutions and objective values (i.e., minimum power consumption and/or maximum COP) is examined. For this purpose, the parameter ranges are defined as follows:

- *Total effectiveness and capacity rate:*
  The parameters ε_t, c_t are taken as $\varepsilon_t \geq 1$ and $c_t \geq 0.1$, respectively, as there is no practical justification for considering values outside these ranges.
- *Temperature ratio:*
  The parameter $\tau = T_s/T_{sink}$ is considered within the range $0.8 \leq \tau < 1$. This reflects typical GSHP operating conditions, where the ground (soil) temperature T_s typically lies within 273-293 K, and the heat sink temperature T_{sink} ranges from 298-323 K.
- *Imposed heat extraction rate:*
  The parameter q_{g0} is estimated to lie within the range $0 < q_{g0} < 10^{-2}$, based on its definition:

$$q_{g0} = \frac{\dot{Q}_{g0}}{\dot{c}_t T_{sink}} = \frac{\dot{c}_g (T_{g,out} - T_{g,in})}{\dot{c}_t T_{sink}} = c_g \frac{\Delta T_g}{T_{sink}}.$$

  For GSHP systems, the capacity rate c_g satisfies $0 < c_g < c_t \sim 1$, while the ground temperature difference is typically within $0\ K < \Delta T_g < 20\ K$.
- *Irreversibility ratio:*
  The parameter I is taken within the range $1 \leq I \leq 1.5$, which corresponds to realistic heat pump systems with moderate thermodynamic losses. Higher values are excluded as they represent unrealistic or inefficient operating conditions.
- *Entropy production rate:*
  To enable comparison between the two irreversibility formulations, the non-dimensional entropy production parameter s is expressed as a function of parameters I, q_{g0} (or q_{p0}), t_s, ε_t, c_t. These formulations, corresponding to the

imposed heat extraction and production cases, are derived from Equations. (4b) and (4c), under the assumptions $c_g^* \approx \frac{c_t}{2}$ and $\varepsilon_g^* = \varepsilon_{evap}^* \approx \frac{\varepsilon_t}{4}$, leading to the expressions presented in Eqs. (21a) and (21b), respectively:

$$s = \frac{\dot{S}}{\dot{c}_t} = \frac{(I-1)\dot{Q}_g}{\dot{c}_t T_{evap}} = \frac{(I-1)q_{g0}T_{sink}}{T_{evap}} \approx \frac{(I-1)q_{g0}}{\tau - \frac{2q_{g0}}{c_t}\left(\frac{8}{\varepsilon_t}-1\right)}, \tag{21a}$$

$$s = \frac{\dot{S}}{\dot{c}_t} = \frac{(I-1)\dot{Q}_p}{\dot{c}_t I \cdot T_{cond}} = \frac{(I-1)q_{p0}T_{sink}}{I \cdot T_{cond}} \approx \frac{(I-1)q_{p0}}{I + \frac{2Iq_{p0}}{c_t}\left(\frac{8}{\varepsilon_t}-1\right)}. \tag{21b}$$

1.4 Results and discussion

Numerical solutions were obtained by applying the defined objective functions to optimize the GSHP performance with respect to the allocation of heat exchanger effectiveness and heat capacity rates. In addition, a parametric analysis was carried out to examine how the optimal solutions and system performance metrics evolve under varying operating conditions.

Figure 2 illustrates the variation in power consumption (w) as a function of heat exchanger effectivenesses (ε_g, ε_p), highlighting its minimum for three cases: reversible, irreversible based on the irreversibility ratio (I), and irreversible based on the entropy production rate (s). To ensure that both approaches describe the same irreversibility, the entropy production rate (s) is expressed using Eq. (21a) as a function of the parameters $I, q_0, \tau, \varepsilon_t, c_t$.

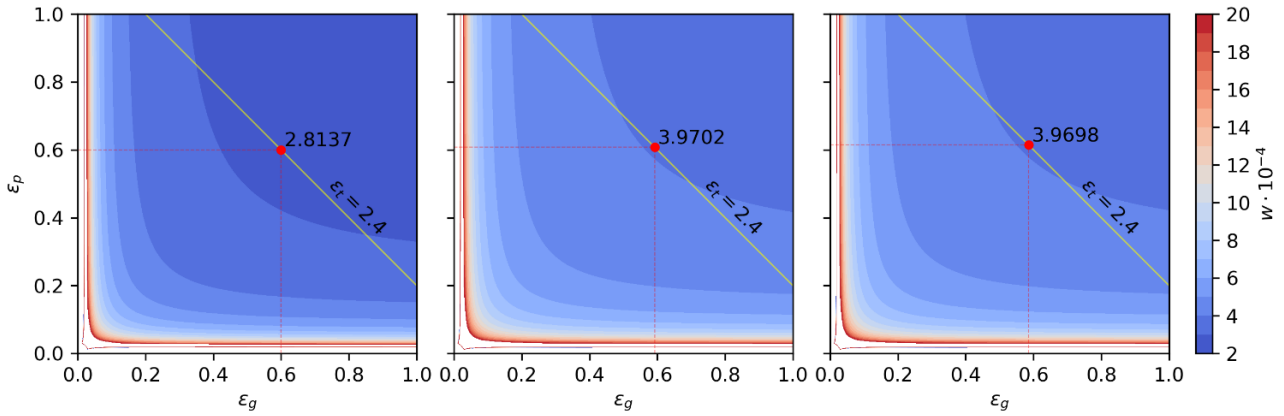

Figure 2 – Power consumption (w) as a function of ε_g and ε_p, for fixed parameters $q_{g0} = 2 \cdot 10^{-3}$, $\tau = 0.9$, $I = 1.05$, $\varepsilon_t = 2.4$, $c_g = c_p = 0.4$:
a) reversible model; b) irreversible model based on the irreversibility ratio I;
c) irreversible model based on the entropy production rate s.
The minimum (red dot) is determined with respect to the constraint (yellow line).

Figure 2 is presented solely in terms of ε_g and ε_p, as the optimal solutions are interconnected through Eq. (19a). It clearly demonstrates that higher heat exchanger effectiveness leads to lower power consumption by the heat pump compressor, while irreversibility increases the required power. The value of w increases significantly in regions where ε_g, ε_p values approach zero. A similar dependence is observed for the case of power consumption as a function of c_g and c_p (see Figure 3). Regions corresponding to $w > 2 \cdot 10^{-3}$ are omitted from the figure, since they lack practical significance (for instance, at $q_{g0} = 2 \cdot 10^{-3}$, this condition corresponds to $COP \leq 2$).

Figure 3 shows the variation in power consumption (w) as a function of heat capacity rates (c_g, c_p), highlighting its minimum for three cases: reversible, irreversible based on the irreversibility ratio (I), and irreversible based on the entropy production rate (s).

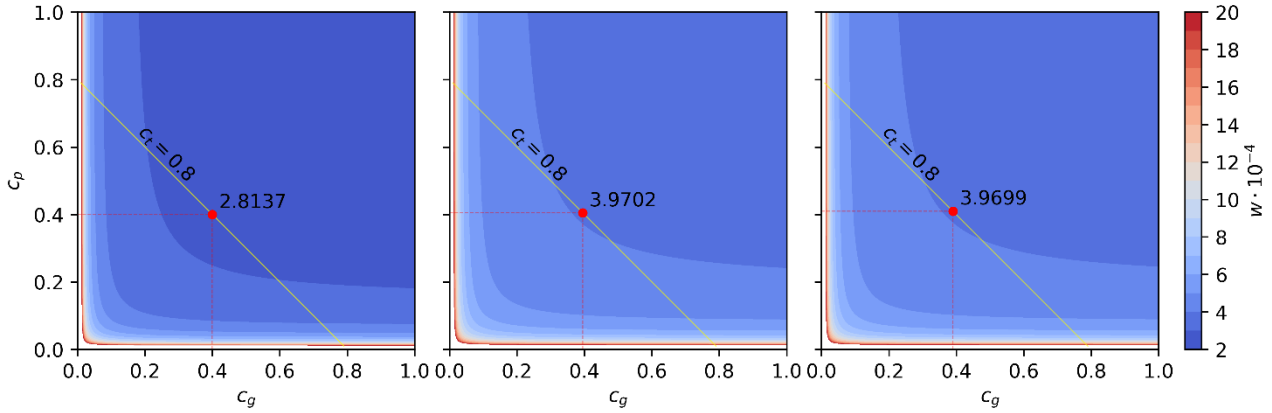

Figure 3 – Power consumption (w) as a function of c_g and c_p, for fixed parameters $q_{g0} = 2 \cdot 10^{-3}$, $\tau = 0.9$, $I = 1.05$, $c_t = 0.8$, $\varepsilon_g = \varepsilon_{evap} = \varepsilon_p = \varepsilon_{cond} = 0.4$:
a) reversible model; b) irreversible model based on the irreversibility ratio I;
c) irreversible model based on the entropy production rate s.
The minimum (red dot) is determined with respect to the constraint (yellow line).

For the reversible case, Figures 2 and 3 correspond Eqs. (20a) and (20b). When irreversibilities within the heat pump cycle are taken into account, the optimal value of ε_p (ε_{cond}) becomes slightly greater than that of ε_g (ε_{evap}). Likewise, the optimal value of c_p is slightly greater than that of c_g. This behaviour is demonstrated on Figure 4, which shows the optimal values and solutions for different level of cycle irreversibility.

In Figure 4a, the values for maximum coefficient of performance $\max(COP)$ and minimum power consumption $\min(w)$ are illustrated along the coordinate axis for various irreversibility conditions. It can be seen from the figure that as irreversibility ratio I increases, the upper limit of $\max(COP)$ decreases. A small increase from $I = 1$ to $I = 1.1$ causes a 39% drop in $\max(COP)$. As I increases to 1.3, the total reduction exceeds 62%, indicating a strong sensitivity of system performance to irreversibility. At the same time, $\min(w)$ increases significantly (by 81%) at $I = 1.1$, and reaching over 3.4 times the reversible value at $I = 1.3$. For each incremental increase of I, the power requirement rises substantially: 81% from $I = 1.0$ to $I = 1.1$, then by 45% and

31% for $I = 1.2$ and $I = 1.3$. These results underline the severe efficiency penalty imposed by system irreversibility. The system exhibits high initial sensitivity to irreversibility, with diminishing marginal effects as I increases.

According to the mathematical formulation of the optimization problem, the solution that yields the minimum w also corresponds to the solution that yields the maximum COP. Therefore, the results presented in the remainder of the section will be discussed in terms of min(w) only.

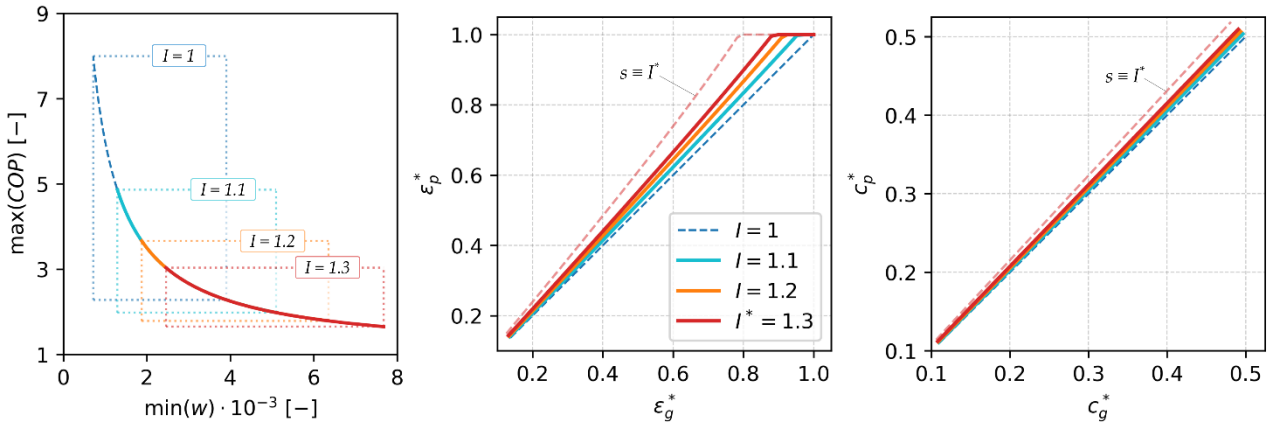

Figure 4 – Optimal values and solutions under various irreversibility conditions: a) optimal values and b) ε_i^* with $c_t = 0.8$ and $\varepsilon_t \in (0, 4)$;
c) c_i^* with $\varepsilon_t = 3.2$ and $c_t \in (0, 1)$;
For fixed parameters $q_{g0} = 5 \cdot 10^{-3}$, $\tau = 0.9$, with reversible case (dashed blue line). Entropy production rate s is estimated by Eq. (21a), corresponding to $I = 1.3$ (dashed red line)

Figure 4b and 4c show the variation of optimal solutions (heat exchanger effectiveness ε^* and capacity rate c^*) in both source (subscript g) and sink (subscript p) loops. As mentioned above, the results substantiate the equalities $\varepsilon_p^* = \varepsilon_g^*$ and $c_p^* = c_g^*$ as indicated in Eqs. (20a-20b) for the optimal heat exchanger effectiveness and optimal heat capacity rates in the reversible case (see dashed blue lines). Under irreversible conditions ($I > 1$), this symmetry is broken. As a consequence of irreversibility, the results observe that $\varepsilon_p^* > \varepsilon_g^*$ (and thus $\varepsilon_{cond}^* > \varepsilon_{evap}^*$) and $c_p^* > c_g^*$. This results from the greater demand for thermal performance on the delivery side (condenser/radiator) to compensate for irreversibility in the compression process. Furthermore, Figure 4b shows abrupt changes in the optimal solutions ε_p^* (heat exchanger effectiveness in the heat delivery loop) due to the technical constraint $\varepsilon_i^* < 1$, with the solutions asymptotically approaching 1.

It can also be observed that, despite achieving identical optimal values of COP and w under the two approaches to accounting for irreversibility (Figure 4a), the corresponding optimal solutions differ between the two approaches (Figures 4b-4c).

Building on this, the analysis proceeds to examine the influence of optimization and constraint parameters on minimum power consumption, as well as on the optimal heat exchanger effectiveness, optimal heat capacity rate, and their sensitivity to these parameters (Figures 5-9). Note that in these figures, the optimal effectiveness of the radiator and the optimal heat capacity rate of the heat delivery (hot) loop are presented, while the other optimal solutions can be determined using Eqs. (19a-19b).

Figure 5 presents the impact of the effectiveness parameter ε_t on the optimal value, the corresponding solutions, and their sensitivity to this parameter. Although both approaches to accounting for cycle irreversibility result in the same minimum power consumption, the optimal solutions for heat exchanger effectiveness and optimal heat capacity rates differ from one another and from the reversible case.

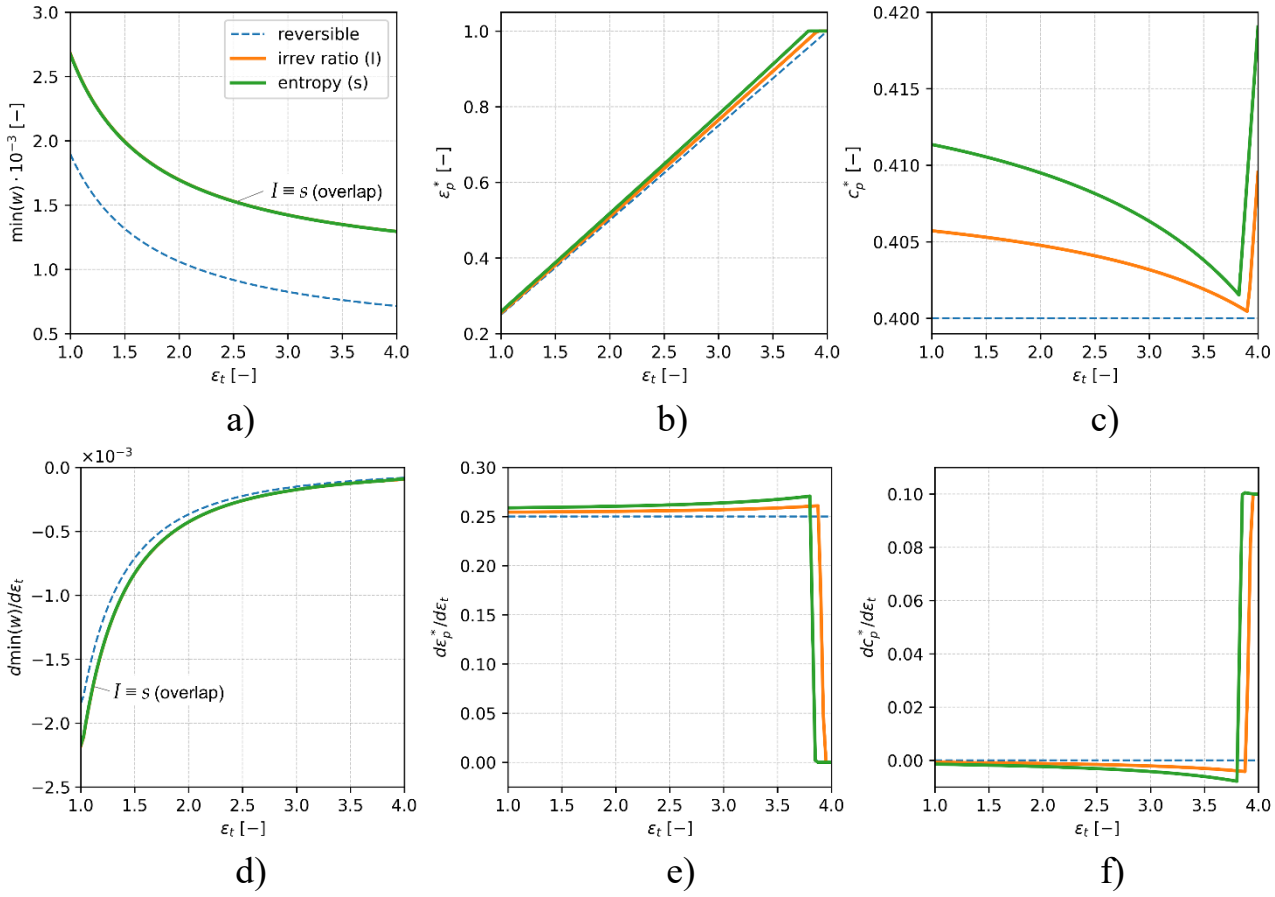

Figure 5 – Influence of parameter ε_t on optimal value of power consumption, for fixed parameters $q_{g0} = 5 \cdot 10^{-3}$, $\tau = 0.9$, $I = 1.1$, and $c_t = 0.8$:
a) minimum power consumption min(w); b) optimal HX effectiveness ε_i^*;
c) optimal heat capacity rate c_i^*, and d), e), f) sensitivity to parameter ε_t, respectively.

In Figure 5a, it can be observed that increasing heat exchanger effectiveness (ε_t) reduces the minimum power required to extract the imposed heat (q_{g0}) from the ground across all cases. However, the magnitude and rate of reduction differ significantly. Under the reversible model, power demand decreases rapidly with increasing ε_t, reaching the lowest values overall. In contrast, both irreversible models show higher

baseline power demands and slower rates of decrease, reflecting the persistent penalty of irreversibility. In all cases, the sensitivity of $\min(\mathrm{w})$ to changes in total effectiveness is similar in trend, as their monotonous increase drops down significantly for high values of ε_t. Specifically, the sensitivity drops from around $-2 \cdot 10^{-3}$ to $-1 \cdot 10^{-4}$, indicating that the marginal benefit of increasing total effectiveness becomes less pronounced at higher values (Figure 5d). For example, increasing ε_t from 3.0 to 3.5 reduces the $\min(\mathrm{w})$ by 7.7% and 5.2% in the reversible and irreversible case, respectively.

Figure 5b shows that optimal heat exchanger effectiveness ε_p^* increases almost linearly (and exactly linearly in the reversible case) with the parameter ε_t, reaching the technical limit $\varepsilon_p^* = 1$. This sensitivity is clearly illustrated in Figure 5e.

Reaching this technical limit also influences the optimal heat capacity rate c_p^*, as depicted in Figures 5c-5f. In the reversible case, the sensitivity of c_p^* is zero (Figure 5f). However, in irreversible cases, the sensitivities remain slightly negative and close to zero until the technical limitation ($\varepsilon_p^* < 1$) is reached. Beyond this point, the ε_t parameter's impact becomes positive for c_p^*.

Figure 6 demonstrates the impact of the heat capacity rate parameter c_t on the optimal value and solutions. As the total capacity rate c_t increases, the minimum required power $\min(\mathrm{w})$ decreases substantially across all cases (Figure 6a). In the reversible case, $\min(\mathrm{w})$ drops sharply – by 63% as c_t increases from 0.1 to 0.3. In the irreversible model, the same increase in c_t reduces $\min(\mathrm{w})$ by about 56%, though the absolute power requirement remains higher (more than 50%) overall. The largest absolute gains are observed in the low-capacity regime (i.e., $c_t < 0.4$), where the sensitivity of $\min(\mathrm{w})$ to c_t is highest (on the order of 10^{-2}) and decreases rapidly (until on the order of 10^{-4}) as the parameter increases further. For example, increasing c_t from 0.4 to 0.8 reduces the $\min(\mathrm{w})$ by 27.5% and 20% in the reversible and irreversible case, respectively. These trends indicate that increasing the system's total heat capacity rate is an effective strategy to reduce power consumption, particularly in the low-capacity range. However, the marginal benefit diminishes at higher c_t.

As illustrated in Figure 6b, the optimal heat exchanger effectiveness ε_p^* remains constant across all c_t values, except in the entropy-based irreversibility model, where a slight increase is observed. In this case, ε_p^* shows a positive sensitivity to c_t on the order of 10^{-3}, particularly for $c_t < 0.4$. This behavior is due to the explicit dependence of entropy production rate s on c_t (see Eq. (21a)). Additionally, Figure 6c shows that c_p^* increases linearly with c_t across all models, indicating that the sink-side capacity scales proportionally with the total available capacity.

Figure 7 compares the two parameters, s and I, which quantify irreversibility, illustrating their effects on optimal values and solutions. Using Eq. (21a) to determine parameter s yields essentially the same minimum power consumption $\min(\mathrm{w})$ as parameter I (Figure 7a). The results confirm that increasing irreversibility leads to a substantial rise in the $\min(w)$. As I increases from 1.0 to 1.2, the $\min(w)$ increases by a factor of 2.5; at $I = 1.4$, it rises 4 times compared to the reversible case. This dramatic

growth highlights the strong thermodynamic penalty associated with irreversibility. The sensitivity of min (w) to I remains approximately constant, around $6 \cdot 10^{-3}$.

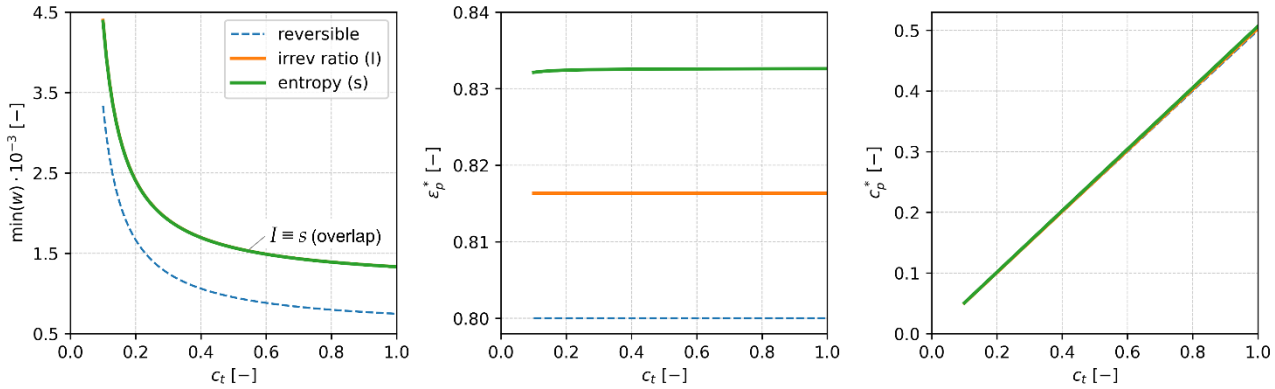

a) b) c)

Figure 6 – Influence of parameter c_t on optimal value of power consumption, for fixed parameters $q_{g0} = 5 \cdot 10^{-3}$, $\tau = 0.9$, $I = 1.1$, and $\varepsilon_t = 3.2$:
a) minimum power consumption min(w); b) optimal HX effectiveness ε_i^*;
c) optimal heat capacity rate c_i^*.

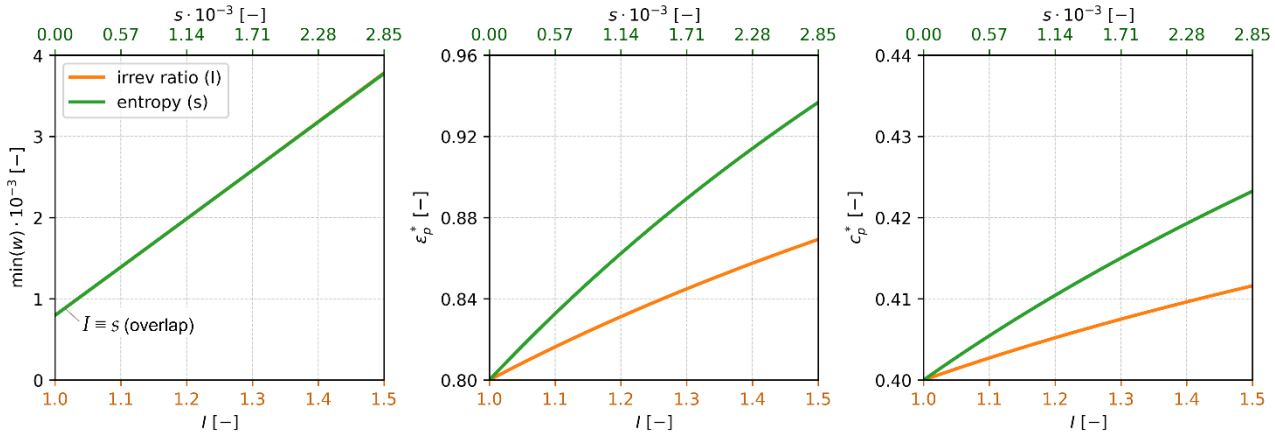

a) b) c)

Figure 7 – Influence of parameters I and s on optimal value of power consumption, for fixed parameters $q_{g0} = 5 \cdot 10^{-3}$, $\tau = 0.9$, $c_t = 0.8$, and $\varepsilon_t = 3.2$:
a) minimum power consumption min(w); b) optimal HX effectiveness ε_i^*;
c) optimal heat capacity rate c_i^*.

Moreover, as highlighted in earlier analyses, these parameters (s and I) distinctly influence the optimal solutions. As irreversibility increases, the optimal heat exchanger effectiveness ε_p^* and capacity rate ratio c_p^* both increase. A notable observation from Figures 7b and 7c is that the entropy production rate s has a stronger influence on the optimal design parameters than the irreversibility ratio I. As irreversibility increases, the heat delivery loop must compensate through greater thermal performance. This is

reflected in the steeper rise of both ε_p^* and c_p^*, indicating the need for more effective and higher-capacity heat exchangers on the sink-side of the GSHP system.

The difference in optimal solutions arises from the way irreversibility is incorporated into the objective function. The I-based approach treats irreversibility as a simple multiplicative penalty on work input, leading to a more uniform influence across the system. In contrast, the entropy-based formulation explicitly includes s in the objective, making it more sensitive to local irreversibilities – particularly those in the heat exchangers. As a result, even small improvements in heat exchanger performance yield greater reductions in the objective function, driving the optimization toward higher values of ε_p^* and c_p^* compared to the I-based model.

Figures 8 and 9 depict the influence of the imposed heat extraction rate (q_{g0}) and temperature (τ) parameters on the minimum power consumption min(w). Figure 7a illustrates that increasing the heat extraction from the ground (q_{g0}) necessitates a higher min(w), with irreversibility further amplifying this requirement. For example, at $q_{g0} = 4 \cdot 10^{-3}$ and $8 \cdot 10^{-3}$, introducing irreversibility with $I = 1.1$ increases the required min (w) by approximately 78% and 65%, respectively. However, variations in the parameter q_{g0} do not affect the optimal solutions (see Figures 8b and 8c).

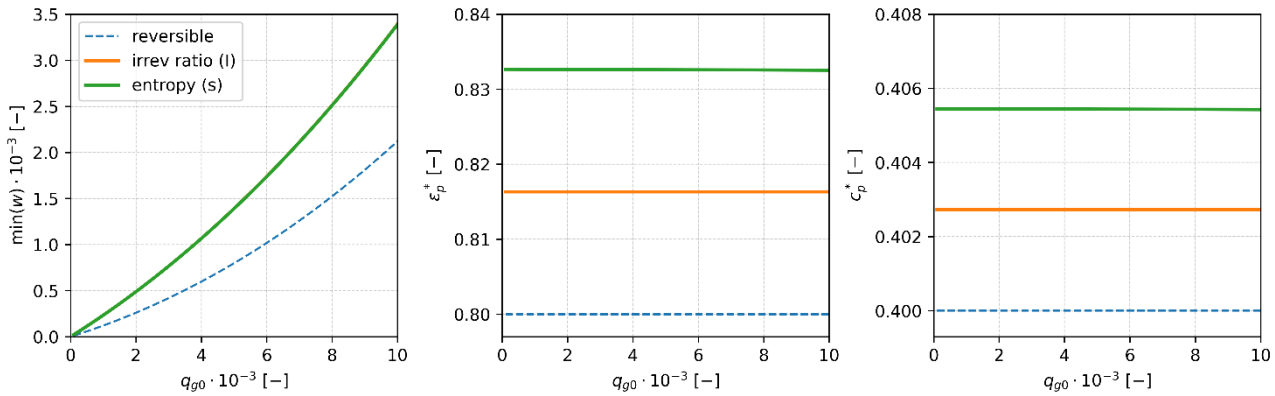

Figure 8 – Influence of parameter q_{g0} on optimal value of power consumption, for fixed parameters $\tau = 0.9$, $I = 1.1$, $c_t = 0.8$, and $\varepsilon_t = 3.2$:
a) minimum power consumption min(w); b) optimal HX effectiveness ε_i^*;
c) optimal heat capacity rate c_i^*.

Figure 9 demonstrates that an increase in the temperature parameter τ reduces the minimum required power consumption. This reduction occurs because a higher τ narrows the temperature difference between the heat source (T_s) and the heat sink (T_{sink}), thus decreasing the compressor work. The irreversible model predicts consistently higher min (w) values than the reversible case, though both exhibit a similar downward trend. For example, increasing τ from 0.8 to 0.9 results in a 38% decrease in min (w) for the irreversible model, and nearly 49% decrease for the reversible case. The sensitivity to changes in τ is negative and relatively small (on the

order of 10^{-3}). Nevertheless, the optimal solutions ε_p^* and c_p^* remain unaffected by variations in τ (see Figures 9b and 9c).

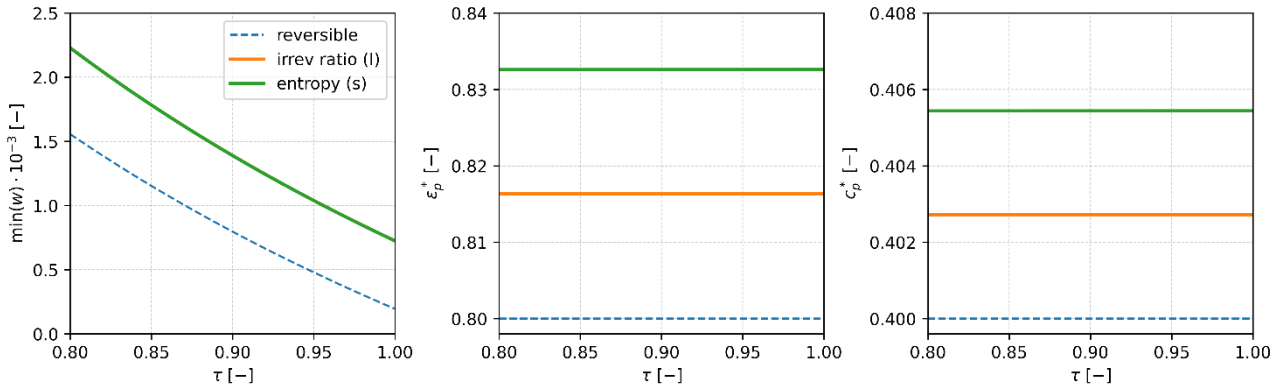

a) b) c)

Figure 9 – Influence of parameter τ on optimal value of power consumption, for fixed parameters $q_{g0} = 5 \cdot 10^{-3}$, $I = 1.1$, $c_t = 0.8$, and $\varepsilon_t = 3.2$:
a) minimum power consumption min(w); b) optimal HX effectiveness ε_i^*;
c) optimal heat capacity rate c_i^*.

The parametric analysis under an imposed heat extraction rate scenario demonstrates that key parameters – heat exchanger effectiveness, heat capacity rate, heat extraction rate, and temperature – significantly influence both the minimum power consumption and the corresponding optimal solutions. Increased heat exchanger effectiveness and heat capacity rate both reduce the minimum required power; the former causes the optimal effectiveness to approach its technical limit, while the latter drives a linear increase in the optimal heat capacity rate. A higher imposed heat extraction rate increases the minimum power requirement without affecting the optimal solution values, and an increase in the temperature parameter reduces the required power but also leaves the optimal solutions unchanged. Additionally, elevated cycle irreversibility consistently increases compressor power demand and shifts the optimal solutions toward higher values in the heat delivery loop.

To extend the analysis, optimization was conducted using the objective functions defined in Eqs. (14)-(16) under the condition of an imposed heat production rate. This scenario enables the evaluation of system behavior when heat output is fixed – a relevant case for many practical applications. A subsequent parametric analysis revealed that the influence of key system parameters on both the minimum power consumption and the corresponding optimal solutions remains consistent with the trends observed in the heat extraction scenario.

Figure 10 illustrates the optimal values and solutions under varying irreversibility conditions for an imposed heat production rate. In Figure 10a, the maximum COP ($\max(COP)$) and corresponding minimum power consumption ($\min(w)$) are presented across different levels of irreversibility. As expected, increasing irreversibility leads to a reduction in the upper bound of the $\max(COP)$. As I increases from 1.0 to 1.3, the $\max(COP)$ drops substantially – from 7.43 in the

reversible case to 3.02 at $I = 1.3$, corresponding to a 59% reduction. The initial sensitivity is pronounced: even a modest rise from $I = 1.0$ to 1.1 causes a 36% drop in performance. Results confirm that $\max(COP)$ becomes progressively less responsive to further increases in irreversibility. Concurrently, the $\min(w)$ rises significantly. At $I = 1.1$, the required $\min(w)$ increases by 54% compared to the reversible case. As I reaches 1.3, the power requirement more than doubles (+137%). However, the rate of increase in power input diminishes with increasing I.

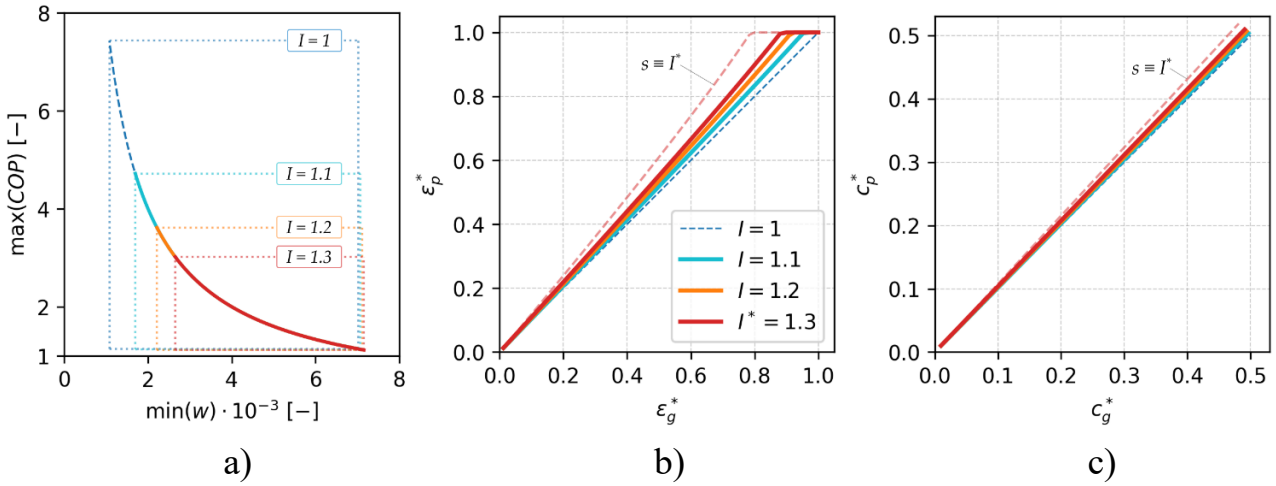

Figure 10 – Optimal values and solutions under various irreversibility conditions:
a) optimal values and b) ε_i^* with $c_t = 0.8$ and $\varepsilon_t \in (0, 4)$;
c) c_i^* with $\varepsilon_t = 3.2$ and $c_t \in (0, 1)$;
For fixed parameters $q_{p0} = 8 \cdot 10^{-3}$, $\tau = 0.9$, with reversible case (dashed blue line). Entropy production rate s is estimated by Eq. (21b), corresponding to $I = 1.3$ (dashed red line)

As previously noted, the results in Figures 10b-10c closely resemble those in Figures 4b-4c and confirm the equalities $\varepsilon_p^* = \varepsilon_g^*$ and $c_p^* = c_g^*$ in the reversible case, consistent with Eqs. (20a)-(20b). Under irreversible conditions, however, a clear trend emerges: the optimal heat exchanger effectiveness and heat capacity rate in the heat delivery loop are consistently higher than those in the heat extraction loop. The upward divergence in these parameters with increasing I confirms the need to allocate more thermal resources (e.g., larger or more effective heat exchangers, stronger circulation) on the delivery side of the GSHP as system irreversibility increases.

The analysis demonstrates that increasing thermodynamic irreversibility has a profound impact on GSHP system performance. Optimal system configuration also shifts under irreversible conditions: the sink-side heat exchanger requires higher effectiveness and capacity rate than the source side, indicating an asymmetric design priority. These findings underscore the critical importance of minimizing irreversibility and strategically allocating thermal resources to maintain high efficiency in practical GSHP applications.

1.5 Chapter summary

This chapter has developed a finite-time thermodynamic optimization framework for ground source heat pump (GSHP) systems operating under imposed heat extraction and heat delivery rates. The results demonstrate that increasing system irreversibility, quantified by either the irreversibility ratio or the entropy production rate, can reduce the maximum coefficient of performance (COP) by up to 62% and increase compressor power consumption by more than 3.4 times compared to reversible conditions. Performance is particularly sensitive to the delivery-side heat exchanger: increasing the total capacity rate c_t from 0.4 to 0.8 reduces power demand by up to 27.5%, while raising the total heat exchanger effectiveness ε_t from 3.0 to 3.5 yields an additional 5–7.7% reduction. A higher source temperature (i.e., increasing the temperature ratio from 0.8 to 0.9) decreases power consumption by 38-49%, depending on the irreversibility level. Taken together, these results highlight the central role of irreversibility control and targeted enhancement of delivery-side components in achieving high GSHP efficiency.

The optimization results reveal that under reversible conditions, exchanger effectiveness and capacity rates are symmetrically distributed between the source and sink sides. When irreversibilities are introduced, this symmetry is lost: the delivery (sink) side systematically requires higher exchanger effectiveness and capacity allocation than the source side. This asymmetric allocation highlights the need to prioritize sink-side enhancements (condenser, radiator) in practical GSHP design.

Parametric studies confirm that increasing the total heat exchanger effectiveness ε_t and capacity rate c_t reduces compressor power demand, with the largest benefits obtained in low-capacity and mid-effectiveness ranges. Similarly, raising the ground source temperature or narrowing the source-sink temperature gap substantially reduces required compressor work. On the other hand, increasing the imposed extraction or production rate proportionally raises power demand, although the optimal allocation of exchanger parameters remains unaffected.

Comparison of the two irreversibility treatments shows that, although both yield the same minimum power consumption and maximum COP, they predict different optimal allocations of exchanger effectiveness and capacity rates. The entropy-based formulation proves more sensitive to local exchanger performance, which explains the stronger prioritization of sink-side allocation. This indicates that the choice of irreversibility model can influence detailed design recommendations even when global performance indicators coincide.

Overall, the chapter demonstrates that minimizing irreversibility and redistributing exchanger resources toward the delivery side are key to high-efficiency GSHP operation. The proposed framework provides general rules for heat exchanger allocation and a theoretical basis that can be used in future work to treat imposed power or COP constraints and to couple thermodynamic optimization with thermoeconomic and environmental objectives under more realistic, time-varying operating conditions.

2 3E (ENERGY-EXERGY-ENVIRONMENTAL) MODELING AND EXPERIMENTAL VALIDATION OF GROUND SOURCE HEAT PUMP (GSHP) SYSTEM

Having formulated the finite-time thermodynamic (FTT) optimization framework, the thesis next turns to a broader performance assessment of GSHP systems that simultaneously accounts for energy efficiency, exergy usage, and environmental impact. Chapter 2 is devoted to building an integrated 3E (energy-exergy-environmental) model that connects the theoretical optimization results with practical operating conditions. Using this model, the thermodynamic predictions are confronted with experimental data from a GSHP pilot installation in Almaty, Kazakhstan, and are applied to select appropriate refrigerants, operating regimes, and heat exchanger configurations for continental climates.

In this way, the 3E analysis does more than evaluate technical performance: it also characterizes the sustainability and ecological footprint of the system. By combining these perspectives, Chapter 2 closes the gap between abstract design rules and real-world implementation, showing how optimized GSHP configurations can be both highly efficient and environmentally acceptable for large-scale deployment.

2.1 Literature review on 3E modeling and analysis of GSHP systems

Heat pumps and GSHPs in continental climates.

Recent reviews show that long heating seasons and large temperature lifts make conventional boiler based heating highly energy- and carbon-intensive in continental regions, whereas the stable subsurface temperatures used by GSHPs allow higher seasonal performance when systems are properly designed and controlled [5,9]]. Comparative 3E/4E studies of air source and ground source heat pumps confirm that GSHPs can deliver greater primary energy savings and lower emissions, although their competitiveness remains sensitive to drilling costs and local ground properties [31]. These findings position GSHPs as a key decarbonization option for continental climates, while highlighting the need for climate-specific design and robust ground characterisation.

GSHP performance has been widely investigated using energy and exergy analyses. Early work on ground-coupled and horizontal systems showed that heat-exchanger configuration and ground coupling strongly affect COP and exergy efficiency [58,59], and later studies extended these methods to vertical-bore and district-heating applications with realistic operating profiles and exergoeconomic metrics [33,60]. Other contributions stress the influence of working fluid and system integration: studies of BZT refrigerants and low-GWP R410A substitutes demonstrate that refrigerant choice can substantially modify energetic and exergetic performance [20,61], while monitored building-scale systems reveal that borehole layout, ground boundary conditions, and medium-deep thermal storage shape seasonal behaviour [34,62,63]. Geothermal systems coupled with storage and advanced building-side technologies – such as fresh-air pre-conditioning and thermally activated structures –

further underline the decisive role of interactions between the heat pump, ground loop and building envelope[64–66].

Within this broader literature, several studies focus on continental and Central Asian conditions. Using engineering-based geothermal classifications [67], thermal response tests have been employed to characterise borehole performance and to obtain local ground conductivity and thermal resistance data for Kazakhstan [22,68]. Numerical analyses of solar assisted cascade heat pump systems for domestic hot water have been conducted for Kazakhstan's continental climates, indicating the potential of hybrid configurations [14]. More recently, combined experimental and theoretical investigations of a GSHP installation in the Almaty region have reported COP and exergy performance under real weather conditions, providing one of the first integrated GSHP case studies for Kazakhstan [13]. In parallel, field evidence from green buildings in cold northern China shows systematic discrepancies between design expectations and actual GSHP operation, underscoring the need for methodologies that explicitly couple cycle-level thermodynamics with ground-side design and building operation strategies [69].

3E frameworks for heat pumps and GSHPs.

3E (energy-exergy-environmental) and 4E (adding economic or exergoeconomic dimensions) frameworks have become standard tools for evaluating heat pump systems beyond simple COP-based metrics. Recent reviews of GSHPs in cold climates and of domestic heat pump integration emphasise that meaningful assessment must consider energetic efficiency, exergy quality, environmental impact and economic feasibility in a unified way [3,5,9]. A representative example is the 4E comparison of air source and ground source heat pumps for the ten coldest Russian cities, which shows that GSHPs can outperform ASHPs in primary energy use, exergy efficiency, life-cycle emissions and operating cost, while their advantage remains sensitive to drilling expenses and local boundary conditions [31]. Similar multi-criteria perspectives are evident in geothermal and hybrid systems: a full 4E evaluation of a flash-binary geothermal CCHP cycle illustrates how configuration choices influence energy utilisation, exergy destruction, exergoeconomic costs and exergoenvironmental penalties [70], while exergetic and thermo-ecological assessments of heat pumps driven by renewable electricity underline the importance of electricity mix and exergy-based environmental indicators for defining "sustainable" operation [71]. At the building and district scale, exergoeconomic analyses of geothermal-assisted district heating and GSHPs with thermal storage confirm the usefulness of combined exergy-cost metrics for identifying economically meaningful efficiency improvements [33,72].

Within this context, a substantial methodological literature couples 3E/4E frameworks with optimisation for refrigeration and heat-pump-type cycles. For CO_2/NH_3 cascade systems, 3E analyses and multi-objective optimisation have been applied to balance energy efficiency, exergy destruction and environmental impact under varying operating conditions and intercooler configurations [12,73]. For vapour compression systems, thermo-economic optimisation across different refrigerant combinations shows how working fluid selection interacts with component design to determine both first- and second-law performance and life-cycle cost [40]. Thermoeconomic design studies of heat pump systems, explicitly accounting for

compressor and condenser inventory costs, demonstrate that optimum design points may differ markedly from those indicated by purely energetic criteria [74]. Beyond stand-alone heat pumps, techno-economic assessments of micro-CHP systems based on geothermal and solar energy, solar district heating with seasonal thermal storage, and flexible geothermal cogeneration extend these multi-criteria methods to more complex integrated energy systems [75–77]. Overall, these contributions show that 3E/4E frameworks, especially when combined with multi-objective optimisation, are effective for exposing trade-offs between efficiency, cost and environmental performance in thermally driven systems.

Theoretical work on performance limits and ecological optimisation complements these applied 3E/4E studies. Reviews of GSHP development and modeling in cold regions point to a persistent gap between component-level or idealised analyses and system-level, experimentally supported 3E assessments that are tailored to local ground and climate conditions [5]. Reviews of domestic heat pump design and integration similarly call for more studies that combine rigorous thermodynamic treatment with realistic operating regimes and explicit cost and environmental metrics [9]. These gaps motivate the present work, which adopts a 3E framework for GSHP systems and aims to link cycle thermodynamics, ground-side coupling and environmental performance within a unified, system-level description suited to continental climates.

Experimental validation and dynamic modeling of GSHP systems.

Many studies have therefore focused on detailed monitoring and energy-exergy analysis of operating systems. Ground-coupled and vertical-bore GSHPs for space heating and domestic hot water have been characterised under realistic loads, with COP and exergy efficiency evaluated over representative operating profiles [58,60]. At the building scale, geocooling with borehole heat exchangers, groundwater-source heat pumps with fresh-air pre-conditioning, and heat-recovery GSHPs coupled to thermally activated building structures (TABS) all show that building-side integration and control exert a decisive influence on seasonal performance [34,64,66]. For alternative working fluids and layouts, experimental characterisation of CO_2 water-to-water heat pumps with integrated storage provides useful benchmarks for transcritical operation under variable loads [41].

On the ground side, extensive work has addressed the characterisation and modeling of borehole and shallow ground heat exchangers. Thermal response tests and monitored operation have been used to derive effective ground thermal properties and to compare different BHE designs and installation configurations [22,68,78], while prediction equations for modular ground heat exchangers have been proposed to support preliminary design and capacity estimation [79]. Three-dimensional and transient models refine this picture further: novel shallow-bore concepts with and without phase-change material have been analysed and experimentally validated [28,80]; atmosphere-soil interactions have been incorporated into slinky-type horizontal GHE models [81]; and the effects of surface boundary conditions, layered geology and groundwater flow have been quantified for horizontal systems [62]. Medium-deep borehole thermal energy storage schemes, relevant for large-scale GSHP applications, have also been examined, demonstrating how storage design governs

long-term temperature evolution and recoverable heat [63]. At the system level, hardware-in-the-loop experiments on GSHPs with thermal storage combined with exergetic and exergoeconomic analysis, as well as numerical optimisation of geothermal heating systems with storage for office buildings in cold regions, illustrate how dynamic models can inform design and operation under realistic load patterns [65,72].

Dynamic, system-level modeling of GSHPs under variable and cycling conditions has likewise received considerable attention. A transient geothermal heat pump model that explicitly resolves on-off cycling and short-term dynamics has been formulated and experimentally validated, showing that simplified steady-state approaches can misrepresent seasonal performance and part-load behaviour [27,82]. Comparative analyses of design versus actual operation in green buildings reveal systematic performance gaps: GSHP systems in cold northern China often operate below their design COP because of control strategies, load profiles and ground-side constraints [69]. In the Central Asian context, numerical simulations of solar collector plus cascade heat pump combi systems have been performed for Kazakhstan's continental climates [14,15], while combined experimental campaigns and thermodynamic modeling of a GSHP installation in the Almaty region provide one of the few integrated datasets linking measured performance and model predictions for Kazakhstan [13]. Collectively, these studies underline the importance of validated transient models and detailed ground-side characterisation for predicting GSHP behaviour under realistic operating conditions.

Environmental performance and refrigerant selection for HP and GSHP systems.

Environmental assessments and refrigerant-selection studies extend conventional heat pump analysis by explicitly linking cycle design to greenhouse-gas emissions and broader sustainability criteria. Recent reviews of GSHPs and domestic heat pumps emphasise that, in addition to COP and exergy efficiency, robust evaluation must account for both direct refrigerant leakage and indirect emissions from electricity consumption, especially in cold climates with carbon-intensive grids [5,9]. In the vapour-compression literature, thermo-economic and multi-criteria analyses show that the choice and combination of refrigerants can substantially modify first- and second-law performance as well as life-cycle costs, so that the optimal design point often shifts relative to that suggested by purely energetic criteria [40]. Thermo-ecological evaluations further underline that the environmental "quality" of heat pump operation depends not only on device efficiency, but also on the carbon intensity of the driving energy and on exergy-based ecological indicators [71].

For GSHP and related water-to-water systems, numerous studies have examined alternative working fluids and their environmental implications. Early work on BZT-type fluids assessed energetic and exergetic performance in geothermal heat pumps, showing that unconventional working fluids can offer favourable thermodynamic characteristics but must be evaluated against safety and environmental constraints [61]. Subsequent analyses of low-GWP substitutes for R410A in GSHPs found that several candidates can maintain or enhance COP and exergy efficiency while reducing direct climate impact, underscoring the need to integrate refrigerant choice into GSHP design

[20]. Experimental drop-in studies on water-to-water heat pumps have evaluated hydrofluoroolefin and blend alternatives to R134a, indicating that fluids such as R1234yf, R1234ze(E), R450A and R513A can deliver substantially lower GWP with acceptable performance penalties or, in some cases, efficiency gains [3,83,84]. Complementary investigations of transcritical CO_2 water-to-water heat pumps with integrated storage demonstrate that CO_2 can combine competitive performance with negligible direct GWP, provided that system design is adapted to its specific thermodynamic behaviour [41].

Synthesis of literature and research gaps.

The reviewed literature establishes GSHPs as a promising low-carbon alternative to conventional boilers in cold and continental climates, provided that drilling costs, ground properties and building integration are carefully addressed. A substantial body of work has analysed GSHPs and related heat pump systems using energy, exergy and environmental indicators, and 3E/4E frameworks have proven effective in revealing trade-offs between efficiency, cost and emissions. Detailed borehole characterisation, transient ground models and hardware-in-the-loop experiments have improved understanding of subsurface coupling, while environmental and refrigerant-selection studies have clarified how low-GWP fluids and electricity mix shape overall climate impact.

At the same time, several gaps remain for GSHP applications in continental climates such as Kazakhstan's. First, most 3E/4E studies concern air source heat pumps, generic water-to-water systems or deep geothermal plants and do not combine system-level 3E analysis with experimentally validated GSHP operation under local ground and climate conditions. Second, the majority of GSHP assessments still rely on steady-state or component-level models, without explicitly linking energy and exergy indicators to the allocation of heat exchanger resources and irreversibilities derived from finite-time thermodynamics. Third, while low-GWP refrigerants and environmental metrics such as TEWI have been extensively investigated for conventional heat pumps, comparatively few studies evaluate alternative working fluids for GSHPs within a unified 3E framework that includes real borehole configurations and measured ground response. Finally, in the Central Asian context there is still a scarcity of long-term, experimentally anchored GSHP case studies that can serve as benchmarks for design and policy.

These gaps motivate the present chapter, which develops and validates a 3E (energy-exergy-environmental) framework for a GSHP installation in the Almaty region. By combining detailed experimental data with thermodynamic modeling and TEWI-based environmental assessment, the chapter seeks to provide climate-specific performance benchmarks and design guidance for GSHPs in continental regions, while complementing the finite-time optimisation results of Chapter 1.

To this end, the study uses measurements from a representative GSHP installation operating under Almaty's continental climate and subjects them to a detailed 3E analysis. The next section describes the configuration and operating conditions of this system, which form the physical basis for the subsequent thermodynamic modeling, performance evaluation, and comparison of alternative refrigerants and operating regimes within the unified 3E framework.

2.2 Experimental GSHP setup

The experimental ground source heat pump (GSHP) installation is located in Almaty and is schematically presented in Figure 11. The system is based on two vertical U-tube borehole heat exchangers (BHEs), one with a single U-pipe and one with a double U-pipe, each drilled to a depth of 50 m. These BHEs are used to extract low-grade thermal energy from the ground and supply it to a water-to-water heat pump with a nominal heating capacity of 5 kW. The heat pump is integrated with the borehole field to provide domestic hot water and space heating, and is coupled to a 300 L hot water storage tank that serves as a thermal buffer.

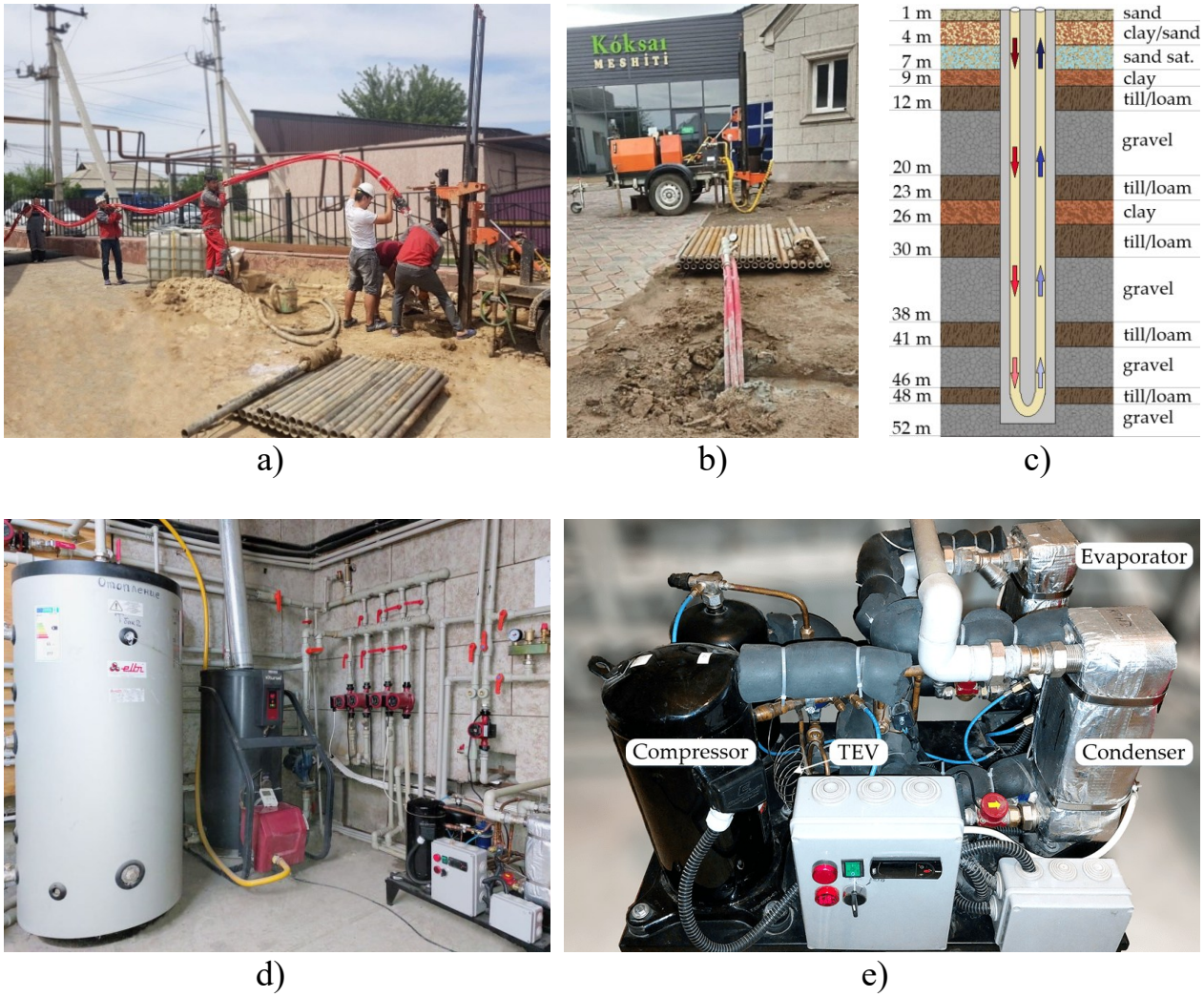

a) b) c)

d) e)

Figure 11 – Photographs of the experimental GSHP installation at the Koksai Mosque site in the Almaty region, Kazakhstan: a) drilling and installation of the BHE; b) completed and backfilled BHE; c) geological cross-section of the ground; d) heat distribution unit; e) water-to-water heat pump module.

For the installation of the BHEs, two wells of 50 m depth were drilled. High-density polyethylene (HDPE) pipes with an outer diameter of 32 mm are used as the U-shaped ground heat exchangers. After lowering the U-tubes into the boreholes, the annular space is backfilled with a grout mixture composed of approximately 70%

water, 24% cement and 6% bentonite, ensuring good thermal contact between the pipe and the surrounding soil. Once the ground heat exchangers (GHEs) are installed, the hydraulic circuit is pressurized and purged to remove air pockets and to check for leaks. A thermal response test (TRT) is then performed to identify the effective thermal conductivity of the ground and the thermal resistance of the BHEs, which are subsequently used in the model calibration. Comprehensive TRT results and interpretation are presented in Ref. [22].

The water-to-water heat pump can operate in both heating and cooling modes through a four-way reversing valve, although in this work only the heating mode is analyzed. Figure 12 shows the hydraulic and refrigerant circuits of the system, which consists of three main loops: the GHE loop, the refrigerant loop of the heat pump, and the hot-water storage loop. The GHE circuit includes the vertical U-tube BHE, a circulation pump, an expansion tank and the evaporator of the heat pump. The refrigerant loop comprises the compressor, condenser, expansion device and evaporator; additional accessories such as a filter-drier, liquid receiver and sight glass are installed in the liquid line to ensure stable operation. The hot-water storage loop contains the condenser, a circulation pump, the 300 L storage tank and an expansion tank. Temperatures and pressures at key points of the refrigerant circuit are monitored using thermocouples and pressure gauges (see Figure 12), providing the experimental data used for performance evaluation and subsequent 3E analysis.

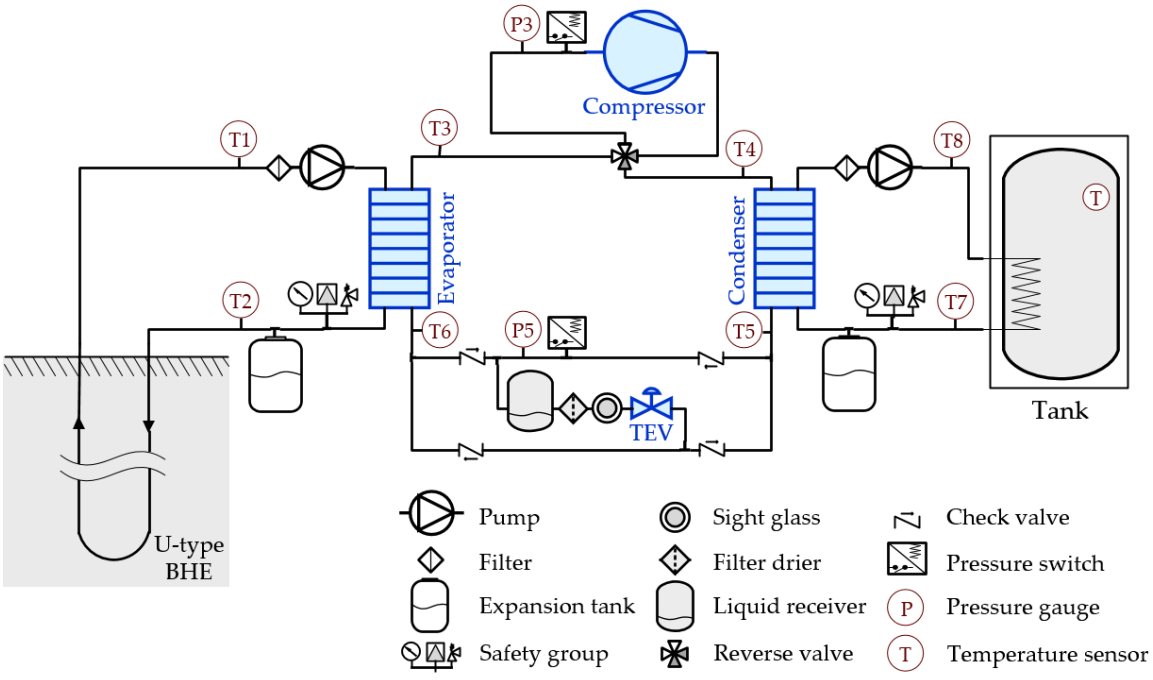

Figure 12 – Schematic of the experimental setup

Tables 1-3 summarize the main technical characteristics of the water-to-water heat pump and its auxiliary equipment, including the compressor, heat exchangers, and expanntion device. They specify the nominal capacities, design operating conditions, and key geometric parameters used in the performance evaluation and model calibration.

Table 1 – Compressor characteristics provided by the manufacturer [13]

Parameter	Unit	Compressor
Model	-	Copeland ZR28K3E-PFJ
Displacement @ 50 Hz	m³/h	6.83
Max. Internal Free Volume	L	2.90
Dimensions (L × W × H)	mm	246 × 246 × 377
Oil type	-	POE RL32-3MAF
Oil quantity	L	1.12
Heating capacity *	kW	4.83
Input power *	kW	1.38
COP *	-	2.57
Mass flow rate *	g/s	24.7

* Parameter obtained at T_{evap} = 0 °C and T_{cond} = 50 °C, T_{SH} = 10 °C, T_{SC} = 5 °C.

Table 2 – Expansion device specifications provided by the manufacturer [13]

Parameter	Unit	TEV
Model	-	Danfoss T2–4
Maximum evaporating temperature	°C	15
Minimum evaporating temperature	°C	−45
Max. working pressure	kPa	3400
Pressure drop *	kPa	1024
Nominal capacity *	kW	6.4
Min. capacity *	kW	1.6

* Parameters obtained at T_{evap} = 0 °C and T_{cond}= 50 °C, T_{SH} = 10 °C, T_{SC} = 5 °C.

Table 3 – Heat exchanger specifications provided by the manufacturer [13]

Parameter	Unit	Evaporator		Condenser	
Model	-	B3-027-20-H		B3-027-30-H	
Heat transfer area	m²	0.468		0.728	
Dimensions (L × W × H)	mm	111 × 54 × 311		111 × 81 × 311	
Weight	kg	3.8		5.1	
Material	-	AISI 316L		AISI 316L	
Flow arrangement	-	Counterflow		Counterflow	
Fluid side	-	R134a	Water	R134a	Water
Number of plates	-	10	9	15	14
Heat transfer coefficient *	W/(m²·K)	2177.1	5224.0	1347.1	7778.2
Total pressure drop *	kPa	10.47	1.89	0.21	2.35

* Parameters obtained at T_{evap} = 0 °C and T_{cond}= 50 °C, T_{SH} = 10 °C, T_{SC} = 5 °C.

Together, the layout in Figures 11-12 and the specifications in Tables 1-3 fully define the experimental GSHP installation used in this study. The configuration of the borehole field, heat pump, and hydraulic loops provides a realistic representation of a small-scale system operating under continental climatic conditions. On this basis, the next section develops a mathematical model and 3E analysis framework.

2.3 Energy, exergy, and environment (3E) modeling and analysis

In this section, the performance of the experimental GSHP system is evaluated within a 3E framework that combines energy, exergy, and environmental indicators. The energy analysis quantifies conventional performance metrics such as heating capacity and COP; the exergy analysis assesses the quality and irreversibility of the energy conversion processes; and the environmental assessment links these results to equivalent greenhouse gas emissions. To enable this evaluation, a thermodynamic GSHP model is formulated and applied to compute the 3E performance across a range of operating conditions and refrigerant options.

2.3.1 Thermodynamic model description of the GSHP system

Building on the experimental installation described in Section 2.2, this subsection formulates a thermodynamic model of the GSHP based on the first and second laws of thermodynamics. The vapor-compression cycle of the water-to-water heat pump is represented on a pressure-enthalpy (p-h) diagram in Figure 13.

The heat transfer fluid (HTF) leaving the borehole heat exchanger (BHE) enters the evaporator at state 1, where it releases heat to the refrigerant. In both the BHE and the evaporator, the HTF undergoes single-phase convective heat transfer. On the condenser side, the HTF is heated from state 7 to state 8 and then transfers heat to the water in the thermal storage tank; here again, the HTF heat exchange in the condenser and tank is modeled as single-phase forced convection.

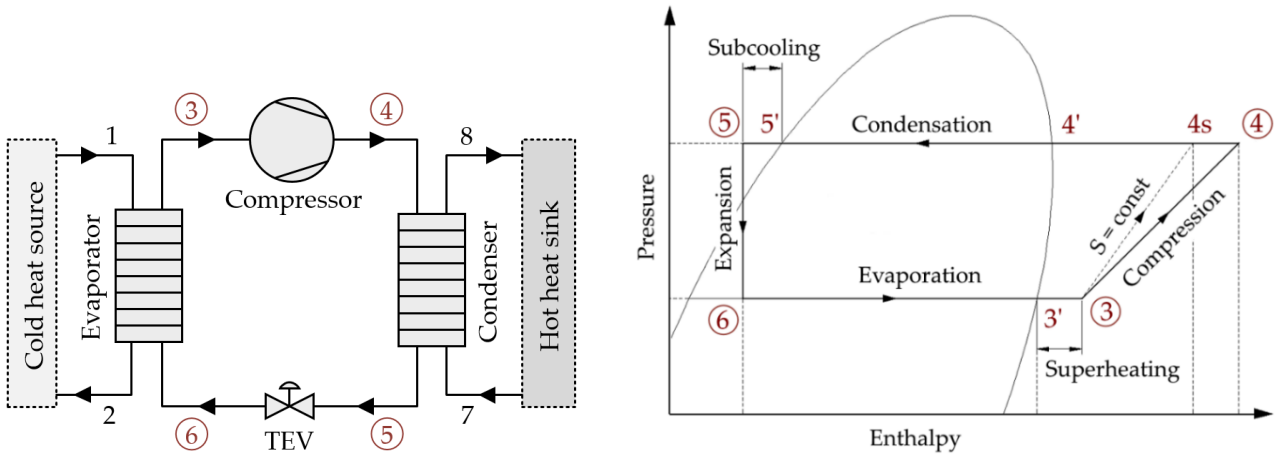

Figure 13 – Schematic representation of the thermodynamic model: a) Water-to-water heat pump; b) Pressure-enthalpy diagram.

In the refrigerant loop, states 3–4–5–6–3 describe the main processes of the vapor-compression cycle: compression (3–4), condensation (4–5), expansion (5–6), and evaporation (6–3). The segments 5′–5 and 3′–3 correspond to subcooling in the condenser and superheating in the evaporator, respectively, while 3–4s denotes the ideal isentropic compression process used as a reference for compressor efficiency

[13,14,36,37]; the actual compression path is given by 3–4. The points 3′, 4′ and 5′ represent saturation states on the p-h diagram. This state-point description provides the basis for writing the energy and exergy balance equations of the GSHP components in the subsequent analysis.

The following subsections introduce the governing equations used to evaluate the energy and exergy performance of the GSHP system, its main components, and the overall vapor-compression cycle, as well as the indicators employed to quantify its environmental impact. The formulations are based on standard simplifying assumptions: the compression process is treated as (quasi-)isentropic, evaporation and condensation are assumed to occur at constant pressure, and the expansion process is modeled as isenthalpic [11,13,18,19,29]. On this basis, energy and exergy balances are written in accordance with the first and second laws of thermodynamics [36,37], yielding expressions for capacities, COP, exergy efficiencies, and irreversibilities. These thermodynamic results are then coupled with environmental performance indicators, such as total equivalent warming impact (TEWI), providing a consistent 3E framework.

2.3.2 Energy performance analysis

1) Evaporator

In the GSHP system, the ground acts as the primary heat source and delivers energy to the heat pump through the borehole heat exchangers (BHEs). The temperature of the heat transfer fluid (HTF) at state 1, T_1, is taken to be equal to the ground source temperature, T_{source}. The approach temperature difference in the evaporator, T_{EAP}, and the refrigerant superheating, T_{SH}, are specified from experimental measurements. Under these conditions, the refrigerant temperature at the compressor suction, T_3, is given by Eq. (22) [11,13,37]:

$$T_3 = T_1 - T_{EAP} = T_{source} - T_{EAP} = T_{evap} + T_{SH} \tag{22}$$

The outlet temperature of the HTF from the evaporator, corresponding to state 2, is then evaluated using Eq. (23) [18]:

$$T_2 = T_1 - \frac{\dot{Q}_{evap}}{c_{p,1}\dot{m}_{pump-1}}. \tag{23}$$

The amount of heat received by the evaporator from the low-potential ground heat source and transferred to the refrigeration circuit, $\dot{Q}_{evap}$, is:

$$\dot{Q}_{evap} = \dot{m}_{ref}(h_3 - h_6). \tag{24}$$

2) Compressor

For the compressor, the refrigerant enthalpy at the outlet (state 4) is obtained from the usual definition of isentropic efficiency. Given the inlet state and the

corresponding ideal isentropic outlet state, the actual outlet enthalpy can be expressed as follows:

$$h_4 = h_3 + \frac{h_{4s} - h_3}{\eta_{isen}}. \tag{25}$$

The isentropic efficiency of the compressor is then evaluated using Eq. (26) [85]:

$$\eta_{isen} = \frac{T_{evap} + 273.15}{T_{cond} + 273.15} + 0.0025 \cdot T_{evap}\,, \tag{26}$$

On this basis, the compressor power and the corresponding electrical energy consumption are calculated as:

$$\dot{W}_{comp} = \dot{m}_{ref}(h_4 - h_3), \tag{27}$$

$$\dot{W}_{elec,comp} = \frac{\dot{W}_{comp}}{\eta'_{comp}}, \tag{28}$$

$$\eta'_{comp} = \frac{\eta_{comp}}{\eta_{isen}}. \tag{29}$$

Here, η'_{comp} represents the combined mechanical, transmission, and electric motor efficiency of the drive system [13,36,37], and η_{comp} denotes the ratio of ideal isentropic work to the actual electrical input. In this study, η_{comp} (in %) is taken as a function of the evaporating and condensing temperatures, T_{evap} and T_{cond}, according to the manufacturer's performance map for the Copeland ZR28K3E-PFJ compressor, which is approximated by the correlation in Eq. (30):

$$\begin{aligned}\eta_{comp} = c_1 T_{evap} + c_2 T_{cond} + c_3 T_{evap}^2 + c_4 T_{evap} T_{cond} + c_5 T_{cond}^2 + \\ + c_6 T_{evap}^3 + c_7 T_{evap}^2 T_{cond} + c_8 T_{evap} T_{cond}^2 + c_9 T_{cond}^3 + c_{10},\end{aligned} \tag{30}$$

with the regression coefficients $c_1 = -2.4341$, $c_2 = 1.367$, $c_3 = -0.062$, $c_4 = 0.103$, $c_5 = -0.0173$, $c_6 = -3.88\cdot10^{-5}$, $c_7 = 7.89\cdot10^{-4}$, $c_8 = -7.51\cdot10^{-4}$, $c_9 = 1.85\cdot10^{-6}$, $c_{10} = 33.6476$.

3) Condenser

On the sink side, the GSHP rejects heat to the water in the storage tank, which acts as the heat sink. The HTF temperature at state 7, T_7, is taken equal to the storage (heat sink) temperature, T_{sink}. The condenser approach temperature, T_{CAP}, and the refrigerant subcooling, T_{SC}, are obtained from experimental data. Under these

conditions, the refrigerant outlet temperature from the condenser is calculated using Eq. (31) [11,13,37]:

$$T_5 = T_7 + T_{CAP} = T_{sink} + T_{CAP} = T_{cond} - T_{SC} \tag{31}$$

The corresponding outlet temperature of the HTF at state 8 is then evaluated as:

$$T_8 = T_7 + \frac{\dot{Q}_{cond}}{c_{p,7}\dot{m}_{pump-2}}. \tag{32}$$

The amount of useful heat from the condenser, $\dot{Q}_{cond}$, is determined by:

$$\dot{Q}_{cond} = \dot{m}_{ref}(h_4 - h_5). \tag{33}$$

This condenser heat rate represents the main useful output of the GSHP in heating mode and is later used to determine the overall energy performance indicators, such as the heating COP.

4) Expansion device

The throttling process in the expansion device (valve) is modeled as isenthalpic. Accordingly, the refrigerant enthalpy at the outlet of the valve is taken equal to its enthalpy at the inlet, i.e., $h_6 = h_5$.

5) System-level performance parameters

The refrigerant mass flow rate is determined from the useful heat released in the condenser, using the enthalpy difference between the condenser inlet and outlet, as expressed:

$$\dot{m}_{ref} = \frac{\dot{Q}_{cond}}{h_4 - h_5}. \tag{34}$$

The total electrical power demand of the GSHP installation is obtained by summing the power consumption of the compressor and that of the two circulation pumps in the ground and load loops:

$$\dot{W}_{elec-total} = \dot{W}_{elec,comp} + \dot{W}_{elec,pump-1} + \dot{W}_{elec,pump-2}. \tag{35}$$

The volumetric refrigerating capacity at the evaporator outlet is then calculated as:

$$VRC = \rho_3(h_3 - h_6). \tag{36}$$

Finally, the energy performance of the system is characterized by two COP definitions. The first is the cycle COP of the vapor-compression heat pump, COP_{cycle},

associated with the 3–4–5–6 processes on the p-h diagram. The second is the overall COP of the GSHP system, COP_{system}, which relates the useful heat delivered at the condenser to the total electrical input of the compressor and pumps [5,9,18,37]:

$$COP_{cycle} = \frac{\dot{Q}_{cond}}{\dot{W}_{elec,comp}}, \tag{37}$$

$$COP_{system} = \frac{\dot{Q}_{cond}}{\dot{W}_{elec-total}}. \tag{38}$$

These system-level indicators are later used to compare different operating conditions and refrigerant options within the 3E framework.

2.3.3 Exergy performance analysis

1) Exergy destruction

Exergy analysis evaluates the maximum useful work that can be obtained from a system as it comes into equilibrium with a specified environment (the so-called "dead state") [11,13,18]. It is widely employed for the thermodynamic assessment and optimization of thermal systems, including GSHPs, because it identifies where and to what extent irreversibilities occur and thus which components are most inefficient [13,36,37].

For the vapor-compression heat pump, the exergy destruction in each component is obtained from the steady-state exergy rate balance, which can be written in the general form of Eq. (39):

$$\dot{E}^{dest} = \sum \dot{E}^{in} - \sum \dot{E}^{out} - \dot{W} + \dot{E}_Q. \tag{39}$$

In this expression, the first and second terms on the right-hand side represent the flow exergy at the inlet and outlet of a given component, the third term accounts for the mechanical or electrical work interaction, and the fourth term corresponds to exergy transfer associated with heat exchange between the component and its surroundings.

The specific flow exergy at a given state, as well as the corresponding exergy rate, are calculated from the local enthalpy and entropy relative to the dead state:

$$e_i = (h_i - h_0) - T_0(s_i - s_0), \tag{40}$$

$$\dot{E}_i = \dot{m}_i e_i = \dot{m}_i[(h_i - h_0) - T_0(s_i - s_0)]. \tag{41}$$

Using these definitions, the exergy destruction in each element of the heat pump cycle is given by Eqs. (42)-(45) for the evaporator, compressor, condenser and expansion valve, respectively [13]:

$$\dot{E}_{evap}^{dest} = \left(\dot{E}_1 + \dot{E}_6\right) - \left(\dot{E}_2 + \dot{E}_3\right), \tag{42}$$

$$\dot{E}_{comp}^{dest} = \dot{E}_3 + \dot{W}_{elec,comp} - \dot{E}_4, \tag{43}$$

$$\dot{E}_{cond}^{dest} = \left(\dot{E}_4 + \dot{E}_7\right) - \left(\dot{E}_5 + \dot{E}_8\right), \tag{44}$$

$$\dot{E}_{TEV}^{dest} = \dot{E}_5 - \dot{E}_6. \tag{45}$$

The total exergy destruction of the cycle is then determined as the sum of the (jth) component contributions:

$$\dot{E}_{\text{cycle}}^{\text{dest}} = \sum \dot{E}_j^{\text{dest}} = \dot{E}_{\text{comp}}^{\text{dest}} + \dot{E}_{\text{cond}}^{\text{dest}} + \dot{E}_{\text{TEV}}^{\text{dest}} + \dot{E}_{\text{evap}}^{\text{dest}}. \tag{46}$$

To evaluate the relative importance of each element, the share of exergy destruction in (jth) component RE_j^{dest} is expressed as a fraction of the total cycle exergy destruction, as given by Eq. (47):

$$RE_j^{dest} = \frac{\dot{E}_j^{dest}}{\dot{E}_{cycle}^{dest}}. \tag{47}$$

2) Exergy efficiency

Both the evaporator and condenser are brazed plate heat exchangers operating in counter-flow configuration (see Table 3). Their exergy efficiencies are defined as the ratio between the exergy gained by the working fluid and the exergy supplied or removed, and are evaluated by Eqs. (48) and (49), respectively [11,13]:

$$\eta_{evap}^{ex} = \frac{\dot{E}_1 - \dot{E}_2}{\dot{E}_3 - \dot{E}_6}. \tag{48}$$

$$\eta_{cond}^{ex} = \frac{\dot{E}_8 - \dot{E}_7}{\dot{E}_4 - \dot{E}_5}. \tag{49}$$

The vapor-compression process in the compressor is modeled as adiabatic. Under this assumption, the compressor exergy efficiency is obtained from the ratio of useful exergy increase of the refrigerant to the exergy associated with the mechanical/electrical work input:

$$\eta_{comp}^{ex} = \frac{\dot{E}_4 - \dot{E}_3}{\dot{W}_{elec,comp}}. \tag{50}$$

The throttling process in the expansion device is considered isenthalpic. Its exergy efficiency is therefore expressed as the ratio of the exergy rate at the outlet to that at the inlet of the valve, as given in Eq. (51) [86]:

$$\eta_{TEV}^{ex} = \frac{\dot{E}_6}{\dot{E}_5}. \tag{51}$$

At the system level, exergy efficiencies are defined both for the vapor-compression cycle alone and for the entire GSHP system, including the auxiliary components. These are calculated by Eqs. (52) and (54):

$$\eta_{cycle}^{ex} = \frac{\dot{E}_8 - \dot{E}_7}{\dot{W}_{elec,comp}}, \tag{52}$$

$$\eta_{system}^{ex} = \frac{\dot{E}_8 - \dot{E}_7}{\dot{W}_{elec-total}}. \tag{53}$$

Finally, the second-law (or rational) efficiency of the cycle is introduced by comparing the actual cycle COP to that of an ideal reverse Carnot cycle operating between the same source and sink temperatures [36,37]. This second-law efficiency is given by Eq. (54):

$$\eta_{2nd} = \frac{COP_{cycle}}{COP_{carnot}}. \tag{54}$$

where the COP of the reverse Carnot cycle, COP_{carnot}, is expressed in terms of the source and sink temperatures as follows:

$$COP_{carnot} = \frac{T_{sink}}{T_{sink} - T_{source}} = \frac{T_7}{T_7 - T_1}. \tag{55}$$

2.3.4 Environmental impact analysis

The environmental performance of the GSHP is assessed in terms of its total equivalent warming impact (TEWI), which accounts for both direct and indirect greenhouse gas emissions over the system lifetime. Direct emissions arise from refrigerant leakage and end-of-life losses, while indirect emissions are associated with the electricity consumed by the heat pump and auxiliary equipment. Following [13,18,87], TEWI is evaluated as:

$$TEWI = \underbrace{GWP \cdot m \cdot \left(\frac{L}{100} \cdot n + \left(1 - \frac{\alpha}{100}\right)\right)}_{direct} + \underbrace{E \cdot \beta \cdot n,}_{indirect} \quad (56)$$

where GWP is the global warming potential of the refrigerant (in CO_2 eq.), m is the charge of the refrigerant (in kg), L is the annual leakage rate (in %/year), n is the operating lifetime of the system (in years); α is the recovery/recycling factor (in %). The term E Denotes the annual electric energy consumption (in kWh/year), β is the indirect emission factor (in kg/kWh).

This formulation links the choice of refrigerant, system tightness, and energy efficiency to climate-relevant emissions, enabling a consistent comparison of different GSHP configurations within the 3E framework.

2.4 Results and discussion

This section reports the main findings of the study, combining experimental observations with the 3E (energy-exergy-environmental) assessment of the GSHP. First, the measured data from the Almaty installation are used to validate the thermodynamic model of the heat pump and its components. Then, the energy and exergy performance of the system is analyzed for different operating conditions and for a set of low-GWP refrigerants proposed as alternatives to R134a. Finally, the total equivalent warming impact (TEWI) of each refrigerant option is evaluated, allowing a joint comparison of technical efficiency and climate impact within a unified framework.

2.4.1 Experimental results

Measurements were performed using the instrumentation layout shown in Figure 12. Temperature and pressure sensors were installed at the main state points of the GSHP cycle, while flow meters were placed in the hydraulic loops between the BHE and the evaporator and between the condenser and the hot water storage tank. The resulting time series for the water heating experiments are summarized in Figures 14-18.

Figures 14 and 15 illustrate representative measurement data for the heat transfer fluid (HTF) and the refrigerant R134a at the nodal points indicated in Figure 12. Figure 14 shows the evolution of water temperature in the storage tank during a typical two-hour heating test. After an initial start-up period of approximately 10 minutes, during which the vapor compression cycle reaches steady operation, the HTF temperatures fall within the ranges $T_1 = 15.2$–12.4°C, $T_2 = 10$–8.5°C, $T_7 = 37$–50.6°C, and $T_8 = 43.2$–56.2°C, while the water in the tank is heated from 33°C to 47°C. Figure 15 reports the corresponding refrigerant temperatures: for R134a, the nodal temperatures vary in the ranges $T_3 = 13.6$–10.6°C, $T_4 = 57$–88°C, $T_5 = 42.5$–55.2°C, and $T_6 = 5.2$–4.3°C [13].

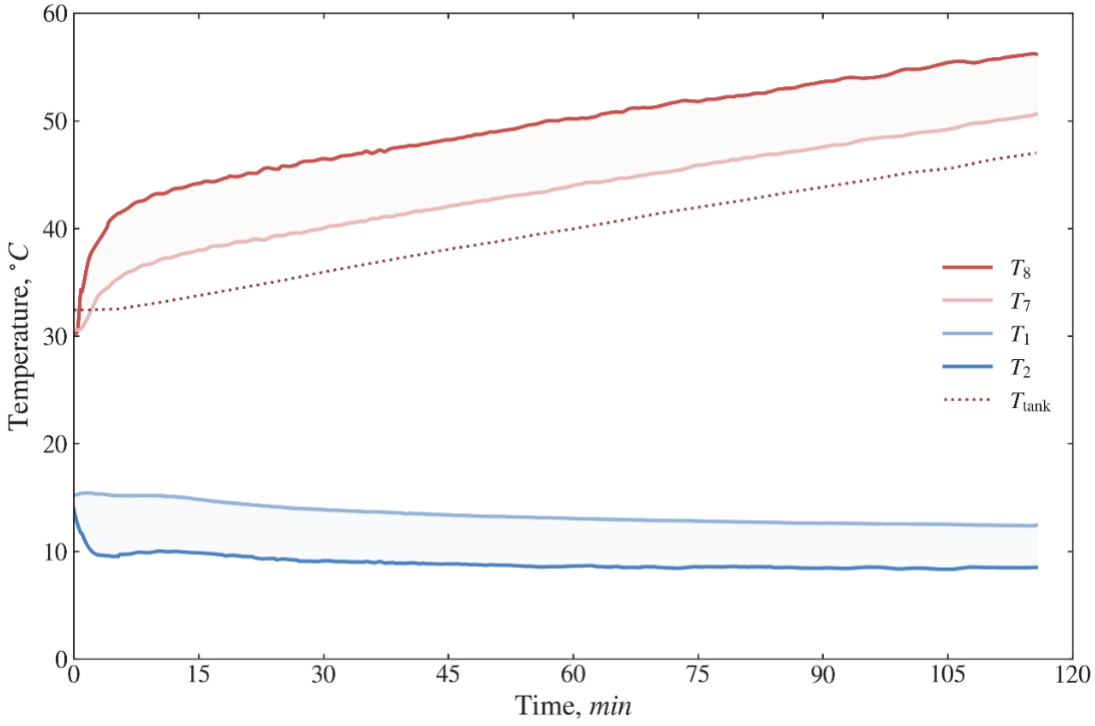

Figure 14 – Measured heat transfer fluid temperatures as a function of time

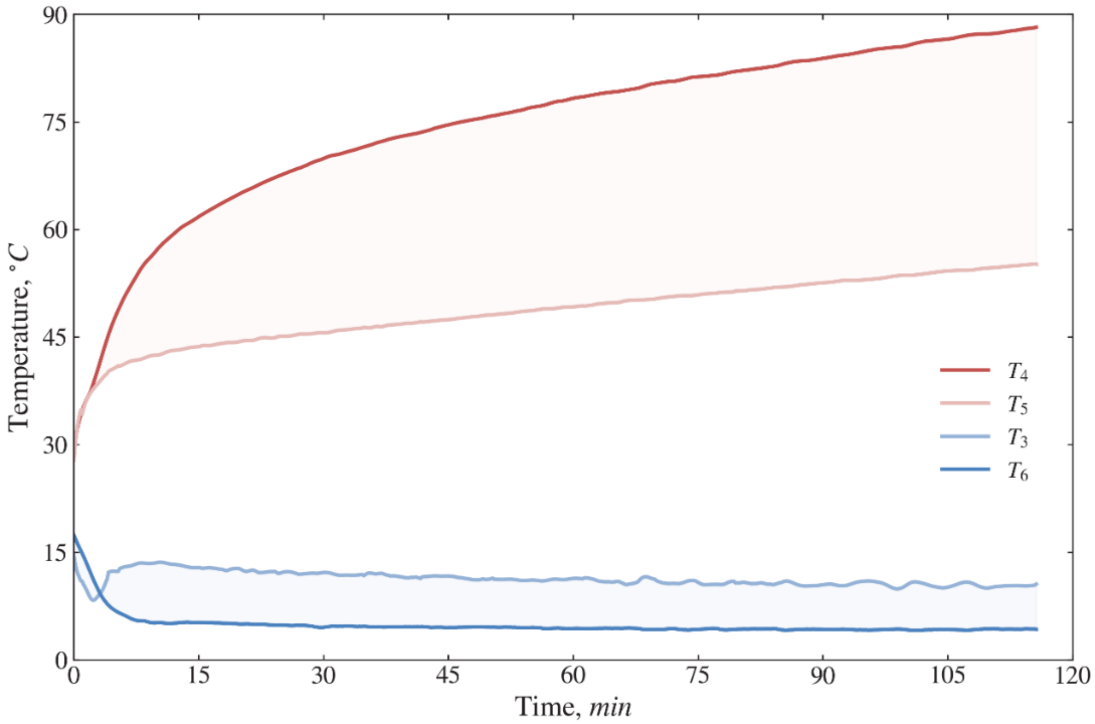

Figure 15 – Measured R134a refrigerant temperatures as a function of time

To characterize GSHP operation in accordance with the schematic in Figure 12 and the thermodynamic model given by Eqs. (22)-(56), the HTF temperature at state 1, T_1, is taken as the source temperature T_{source}, while the HTF temperature at state 7, T_7, is taken as the sink temperature T_{sink}. In this work, all measurements and subsequent

calculations are carried out for T_{sink} values in the range of 40-50 °C, representative of domestic hot water and low-temperature space heating applications.

The results of several experimental runs, showing the variation of T_{source} and the compressor electrical power $\dot{W}_{elec,comp}$, are presented in Figures 16 and 17, respectively. As shown in Figure 16, the source temperature varies within a relatively narrow range, from 12.45 °C to 13.83 °C. The local subsurface at the test site consists mainly of gravel and till/loam [22,32], and for this ground structure the operation of the installed GSHP yields a regression relationship between the relevant temperatures, which is later used for model validation (see Table 4) [11,13]. An analogous correlation for the measured compressor electricity consumption $\dot{W}_{elec,comp}$is presented in Figure 17, where values fall in the range 1.33-1.61 kW.

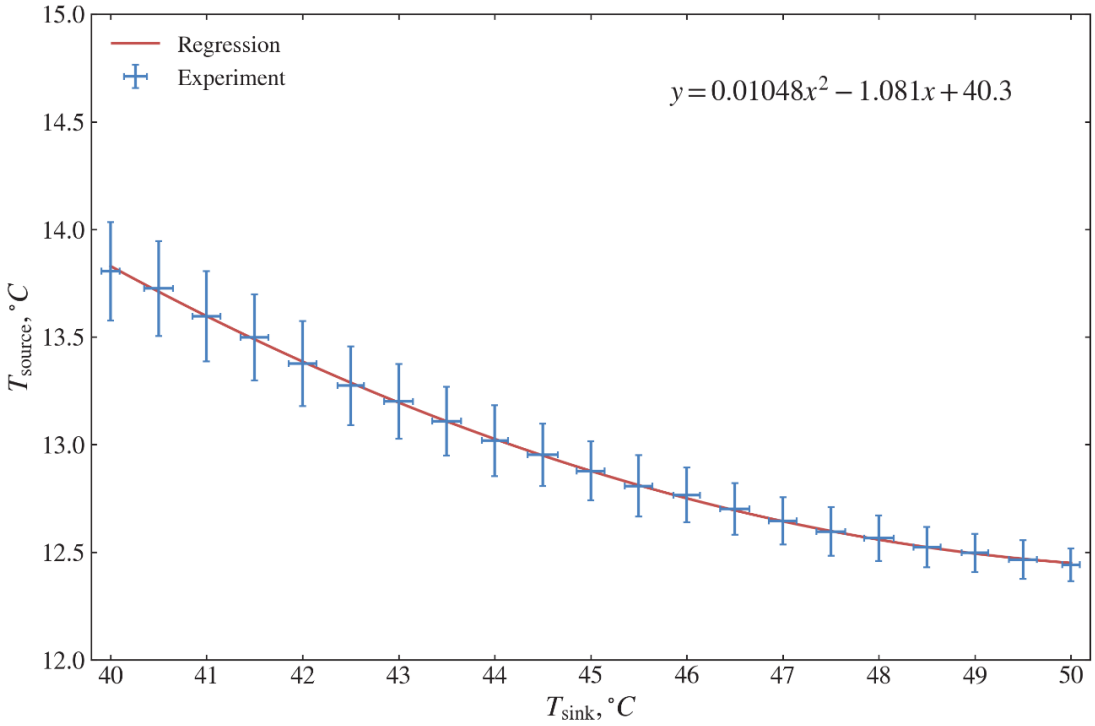

Figure 16 – Heat source temperature as a function of heat sink temperature

Furthermore, to compare the measured and calculated results, the following parameters such as superheating T_{SH}, sub-cooling T_{SC}, evaporator approach temperature T_{EAP}, and condenser approach temperature T_{CAP} are used and encountered in Equations (22) and (31) [11,13,15]. These quantities are directly related to the operating behavior of the vapor compression cycle, including the refrigerant charge in the system and the setting of the thermostatic expansion valve. Figure 18 presents the values of T_{SH}, T_{SC}, T_{EAP}, and T_{CAP} obtained from the temperature measurements and subsequent calculations.

For each of these parameters, linear regression relationships are identified. The observed ranges are $T_{SH} = 11.2–11.7°C$, $T_{SC} = 1.6–2.3°C$, $T_{EAP} = 1.8–2.1°C$, and $T_{CAP} = 4.7–5.6°C$. These values and their regressions are subsequently used for model validation (see Table 4).

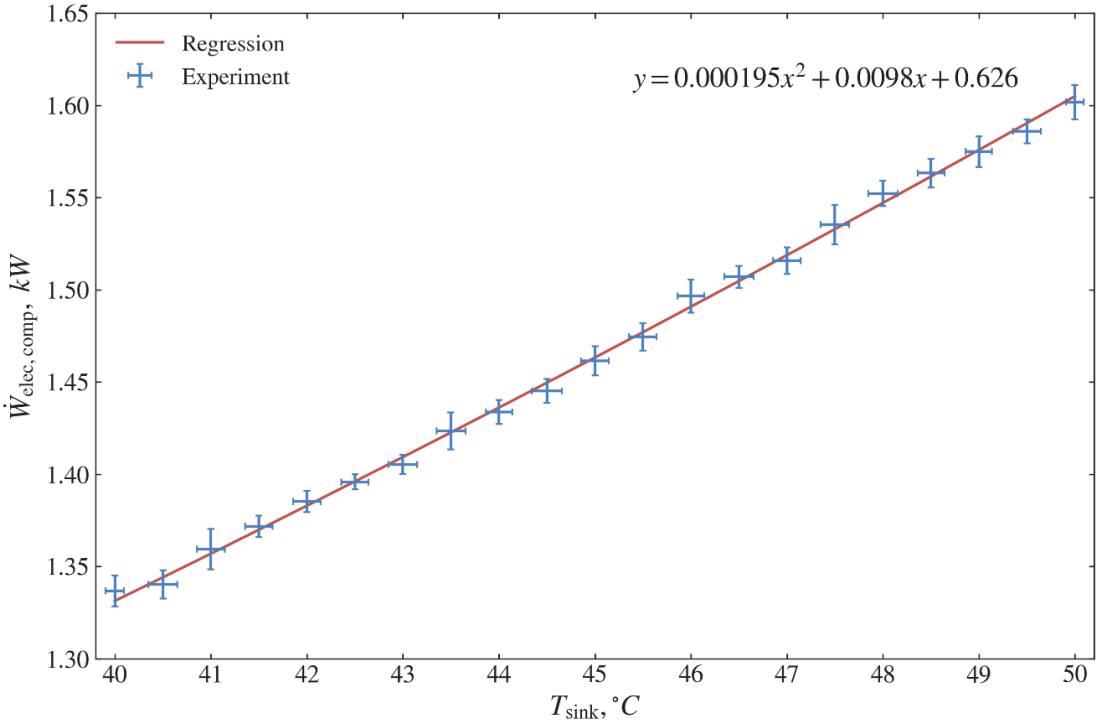

Figure 17 – Measured compressor electrical power as a function of heat sink temperature

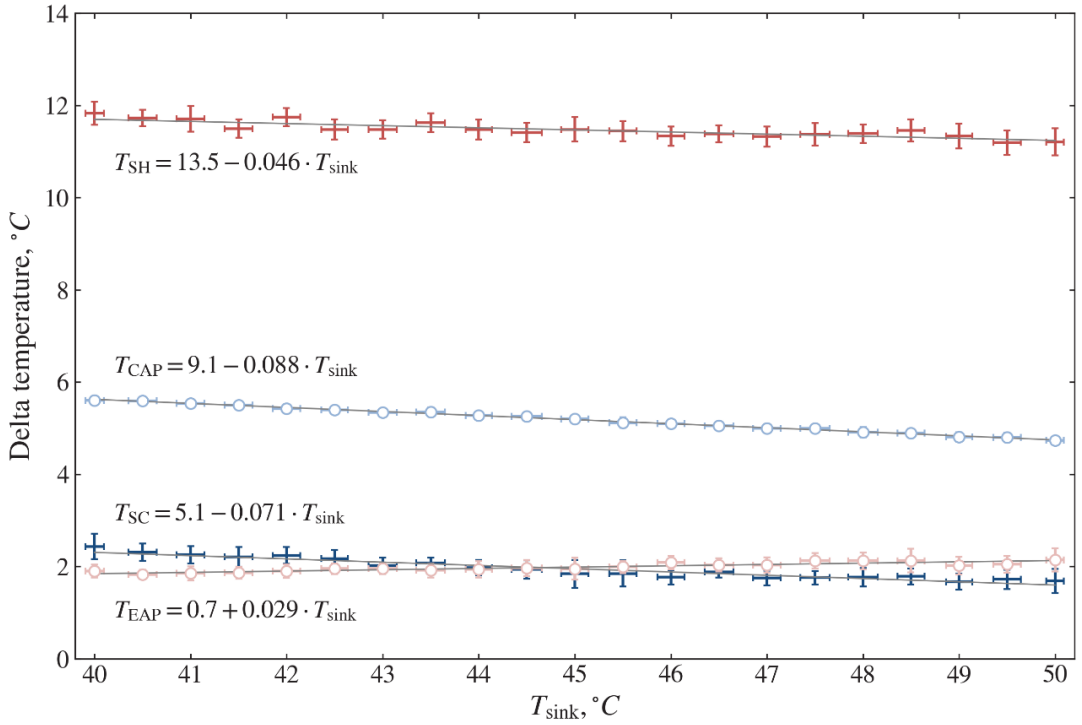

Figure 18 – Superheating, subcooling, and evaporator/condenser approach temperature differences vs. heat sink temperature, estimated from measured data

Table 4 – Operating conditions adopted in the thermodynamic model [13]

Parameter	Designation	Unit	Value *
Heat sink temperature	T_{sink}	°C	40–50 {50}
Heat source temperature	T_{source}	°C	$T_{\text{source}} = 0.01048 \times T_{\text{sink}}^2 - 1.081 \times T_{\text{sink}} + 40.3$ {13}
Compressor electricity consumption	$\dot{W}_{\text{elec,comp}}$	kW	$\dot{W}_{\text{elec,comp}} = 0.000195 \times T_{\text{sink}}^2 + 0.0098 \times T_{\text{sink}} + 0.626$
Compressor efficiency	η_{comp}	%	Equation (30)
Superheating temperature	T_{SH}	°C	$T_{\text{SH}} = 13.5 - 0.046 \times T_{\text{sink}}$ {8}
Sub-cooling temperature	T_{SC}	°C	$T_{\text{SC}} = 5.1 - 0.071 \times T_{\text{sink}}$ {2}
Evaporator approach temperature	T_{EAP}	°C	$T_{\text{EAP}} = 0.7 + 0.029 \times T_{\text{sink}}$ {2}
Condenser approach temperature	T_{CAP}	°C	$T_{\text{CAP}} = 9.1 - 0.088 \times T_{\text{sink}}$ {2}
Dead state temperature	T_0	°C	20
Dead state pressure	P_0	kPa	101.325
Pumps volume flow rate	$\dot{V}_{\text{pump}-1}$	m^3/h	0.595
	$\dot{V}_{\text{pump}-2}$		0.543
Pumps power consumption	$\dot{W}_{\text{elec,pump}-1}$	W	60
	$\dot{W}_{\text{elec,pump}-2}$		40

* The values in brackets { } are used for the calculations in Subsection 2.4.3.

2.4.2 Thermodynamic model validation

This subsection compares the experimental measurements with the predictions of the thermodynamic model for key performance indicators, including refrigerant and HTF temperatures in the cycle, heat fluxes in the evaporator and condenser, and the COP of both the heat pump cycle and the overall GSHP system. For the calculations based on Eqs. (22)-(38), the operating conditions summarized in Table 4 are used as input. The resulting model outputs are then confronted with the experimental data to assess the accuracy of the proposed formulation and to validate its use for subsequent 3E analysis.

Figure 19 presents the variation of selected nodal temperatures as a function of the sink temperature T_{sink}. The experimental and calculated refrigerant temperatures at the compressor suction (T_3) and at the condenser outlet (T_5) show very good agreement. At the evaporator inlet (T_6), the temperature difference between the model and the measurements lies in the range 3.16-4.01 °C, with an average deviation of 3.66 °C. For the compressor discharge temperature (T_4), the discrepancy ranges from 0.06 to 6.12 °C. The larger spread at this point is mainly attributed to the fact that the thermodynamic model does not explicitly account for the additional irreversibilities associated with the four-way reversing valve [11,13].

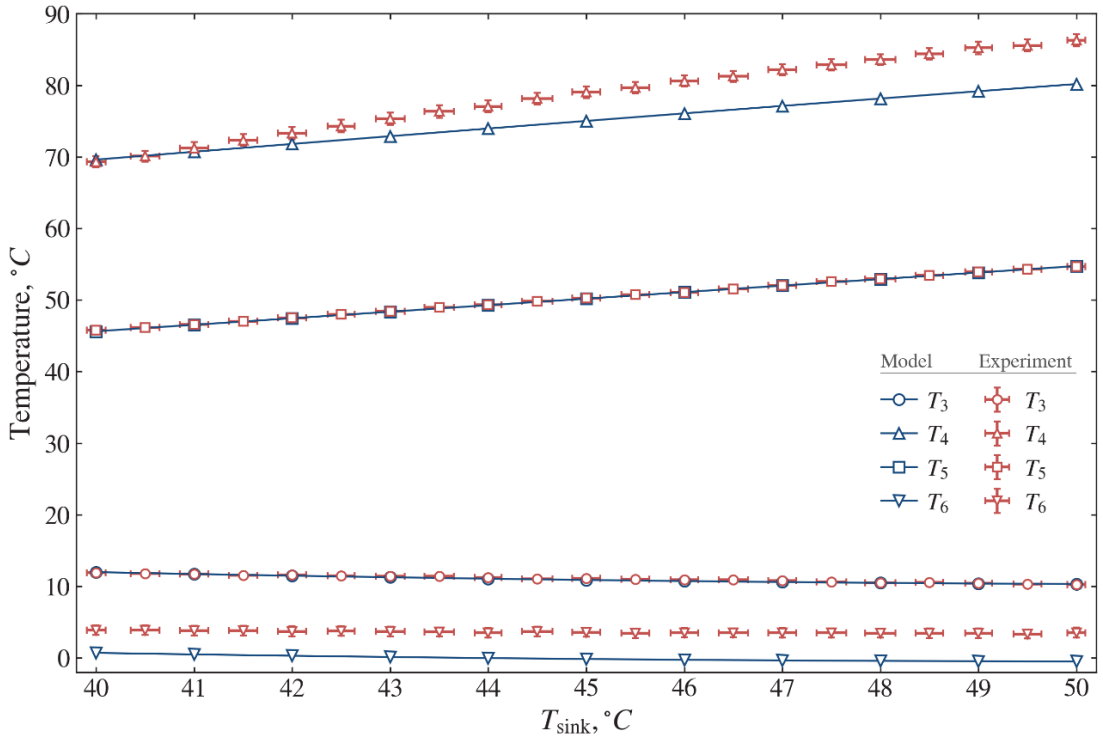

Figure 19 – Comparison of measured and predicted nodal temperatures as a function of heat sink temperature

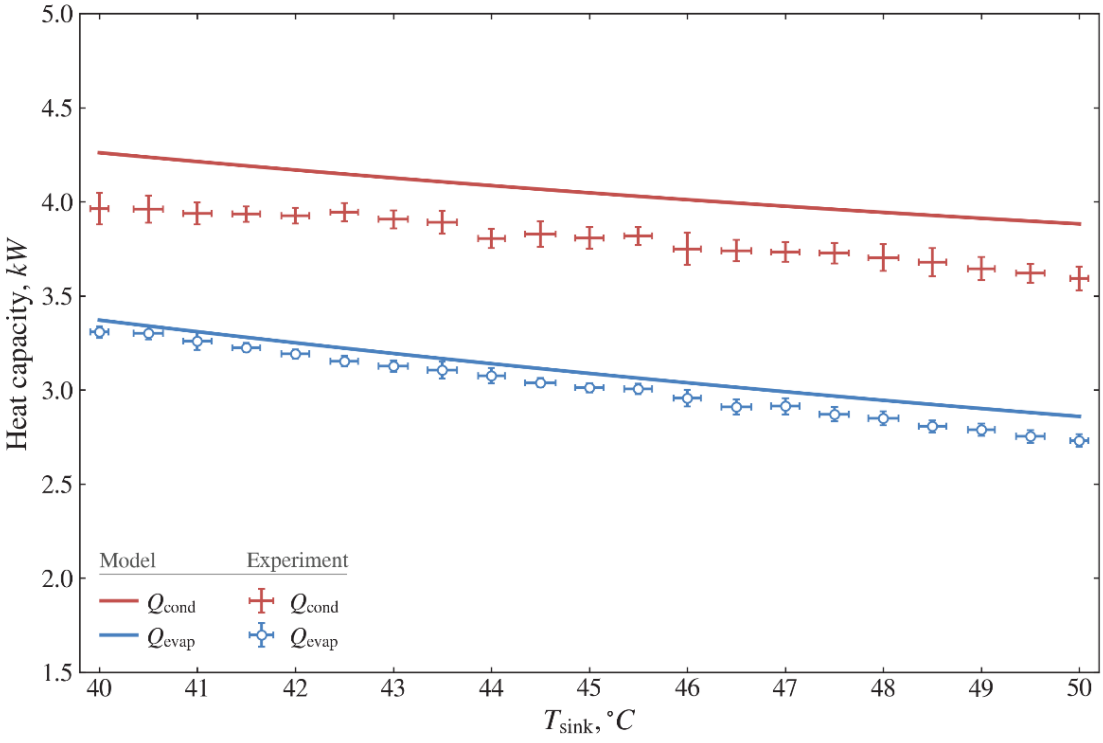

Figure 20 – Comparison of measured and predicted condenser and evaporator heat capacities as a function of heat sink temperature

Figure 20 compares the predicted and measured heat transfer rates in the evaporator and condenser. The useful heat delivered by the condenser, $\dot{Q}_{\text{cond}}$, is measured in the range 3.59-3.96 kW, whereas the simulated values fall between 3.88 and 4.26 kW. The average systematic deviation is 6.2%, corresponding to about 251 W. This bias largely reflects the neglect of pressure drops and external heat losses in the present model. For the evaporator, the measured heat input $\dot{Q}_{\text{evap}}$varies from 2.73 to 3.31 kW, while the calculated values are in the range 2.86-3.37 kW, with an average deviation of 2.6% (about 79.6 W) [11,13].

Figure 21 compares the predicted and measured COP values of both the vapor compression cycle and the overall GSHP system as functions of the heat sink temperature. The experimental cycle COP, COP_{cycle}, lies in the range 2.24-2.97, whereas the corresponding theoretical values obtained from Eq. (37) fall between 2.42 and 3.20, with an average deviation of about 6.2%. For the system COP, COP_{system}, the measured values range from 2.11 to 2.76, while the values calculated using Eq. (38) vary from 2.28 to 2.98. The minimum, maximum, and mean discrepancies between measured and predicted system COP are 4.9%, 7.5%, and 6.2%, respectively [11,13].

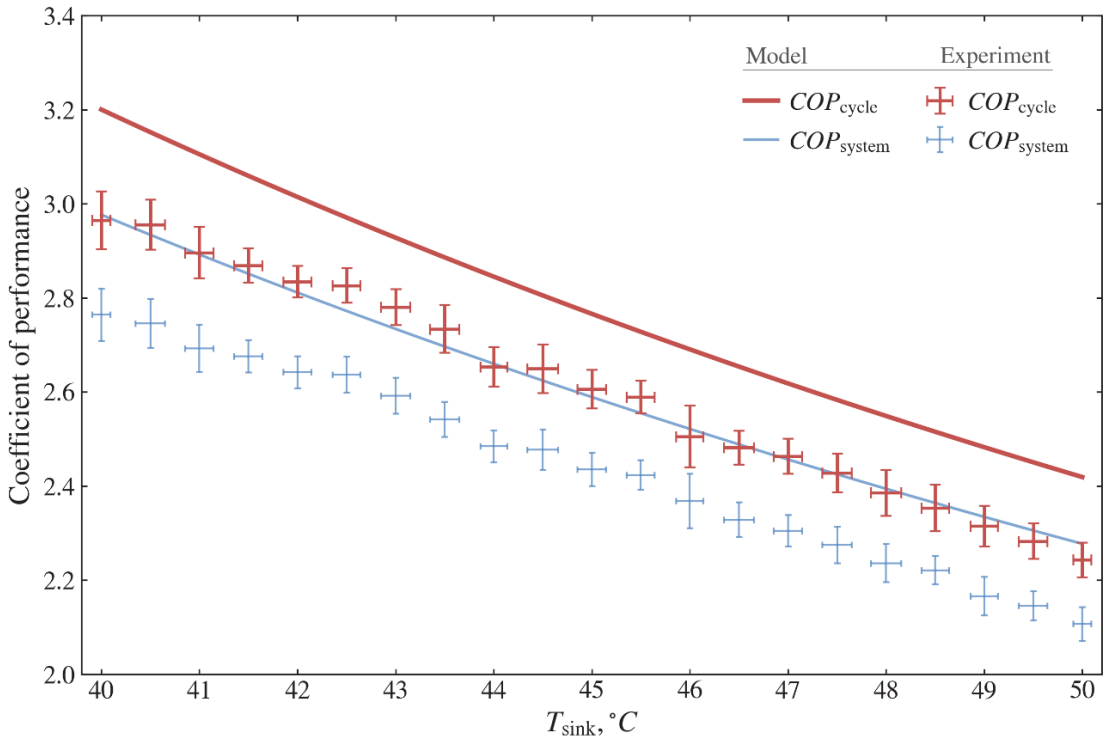

Figure 21 – Comparison of measured and predicted cycle and system COPs as a function of heat sink temperature

These levels of agreement indicate that the developed thermodynamic model is sufficiently accurate to represent the GSHP performance and can be reliably used for subsequent 3E analysis and refrigerant comparisons.

2.4.3 Thermodynamic and environmental performance evaluation

On the basis of the validated thermodynamic model, the GSHP performance is simulated for several low-GWP refrigerants proposed as alternatives to R134a. The selection criteria for these working fluids include commercial availability, similar thermodynamic and transport properties to R134a, low global warming potential, and non- or mildly flammable characteristics compatible with current safety standards. For each candidate, the model is used to predict energy and exergy performance indicators together with the associated environmental impact. Table 5 summarizes the main thermophysical properties of the selected refrigerants.

Table 5 – Thermophysical properties of the selected refrigerants

Property	Unit	R134a	R152a	R450A	R513A	R1234yf	R1234ze(E)
GWP for 100 years	CO_2 eq.	1430	124	547	573	4	7
Molar mass	g/mol	102.03	66.05	108.6	108.4	114.0	114.0
Normal boiling point	°C	−26.1	−24.7	−23.1	−29.2	−29.4	−19.0
Critical pressure	MPa	4.06	4.50	4.01	3.77	3.38	3.64
Critical temperature	°C	101.1	113.15	75.1	96.5	94.7	109.4
UFL	vol. %	-	16.9	-	-	12.3	11.3
LFL	vol. %	-	3.9	-	-	6.2	5.7
Auto-ignition temperature	°C	-	455	-	-	405	368

The thermodynamic analysis is carried out using the model defined by Eqs. (22)-(56) and the operating conditions listed in Table 4. In these simulations, instead of prescribing the electrical power input, the useful heating capacity is fixed at $\dot{Q}_{\text{cond}} = 5$ kW.

Figure 22 illustrates the relationship between the required refrigerant mass flow rate $\dot{m}_{\text{ref}}$ and the specific latent heat of vaporization of the candidate refrigerants. The highest value of latent heat corresponds to R152a and leads to the lowest $\dot{m}_{\text{ref}}$, whereas R1234yf exhibits the lowest latent heat and therefore requires the largest $\dot{m}_{\text{ref}}$. As seen in Figure 22, the refrigerant mass flow rate decreases as the specific latent heat of vaporization increases, reflecting the inverse proportionality between $\dot{m}_{\text{ref}}$ and the enthalpy change at evaporation for a fixed heating capacity.

Figure 23 compares the required refrigerant mass flow rate and volumetric refrigerating capacity (VRC) at a fixed heating capacity for R134a and the selected low-GWP alternatives. For the same condenser heat output, a lower mass flow rate $\dot{m}_{\text{ref}}$ combined with a higher VRC implies a smaller required compressor displacement. In this regard, R152a appears as the most favorable option: the required mass flow rate is about 17.5 g/s, with a VRC of 1949 kJ/m³.

For R450A and R1234ze(E), the required mass flow rates (31.4 g/s and 32.0 g/s, respectively) are similar to that of R134a, but both exhibit lower VRC values, implying a larger compressor volume for the same heating capacity. By contrast, R513A and R1234yf yield VRC values closer to that of R134a but only at the expense of higher mass flow rates.

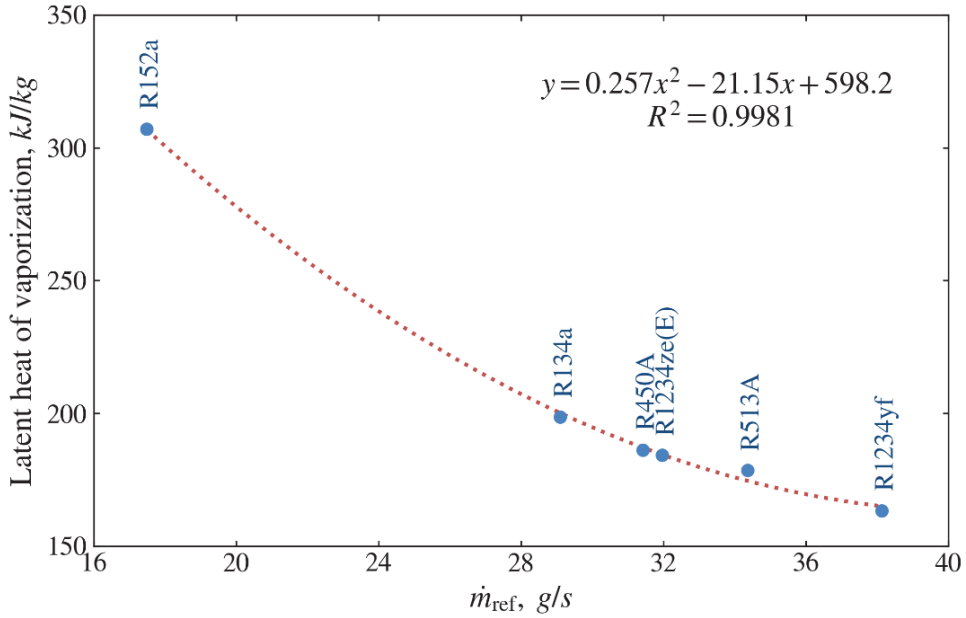

Figure 22 – Required refrigerant mass flow rate for a fixed heating capacity vs. refrigerant latent heat of vaporization

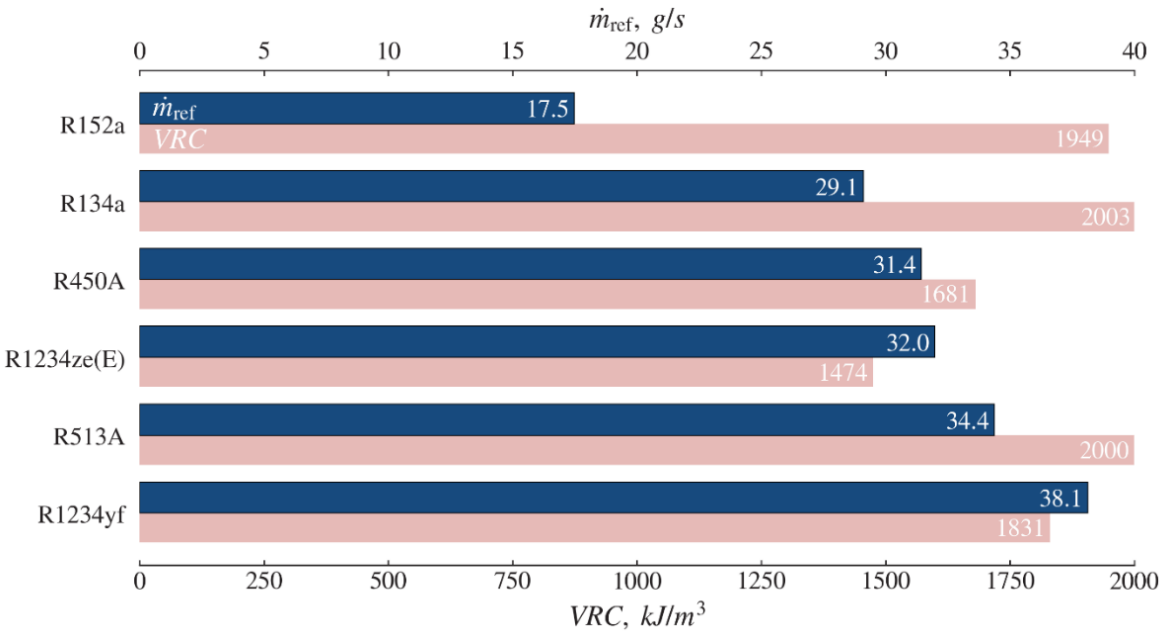

Figure 23 – Required refrigerant mass flow rate and volumetric refrigerating capacity for a fixed heating capacity for different refrigerants

Figures 24 and 25 compare, respectively, the absolute and relative exergy destructions of the main components and of the overall cycle for the different refrigerants. Among the candidates, the lowest total system exergy destruction, $\dot{E}^{dest}_{system}$, is obtained for R152a (965 W), whereas the highest value, 1119 W, is found for R1234yf. At the component level, the compressor consistently exhibits the largest exergy destruction, followed in order by the expansion valve, evaporator, and condenser.

As shown in Figure 25, the expansion valve plays a notable role in the increase of system exergy destruction for the alternative refrigerants. The relative exergy destruction of the expansion device, RE_{TEV}^{dest}, rises from about 16% to 23%, while the shares associated with the other components change only slightly (by about 1-3%). With reference to Table 4, since both the source temperature T_{source} and the HTF flow rate $\dot{V}_{pump\text{-}1}$ are fixed at the evaporator, the exergy destruction $\dot{E}_{evap}^{dest}$ is similar for all refrigerants. By contrast, although T_{sink} and $\dot{V}_{pump\text{-}2}$ are kept constant at the condenser, the condenser exergy destruction $\dot{E}_{cond}^{dest}$ varies because the discharge temperature T_4 depends on the specific thermodynamic properties of each refrigerant.

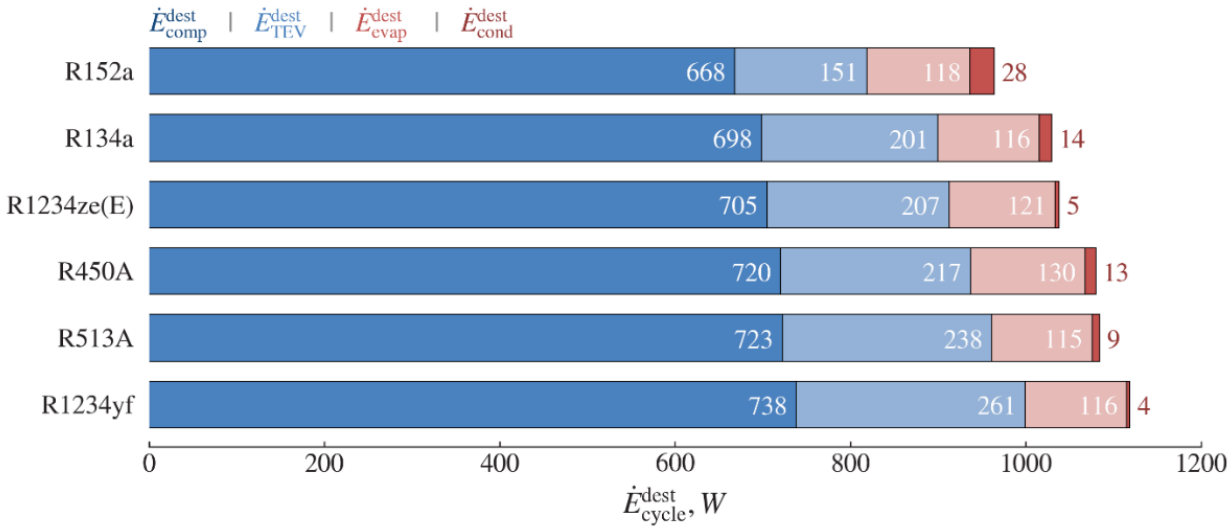

Figure 24 – Exergy destruction in individual components and in the overall cycle for different refrigerants

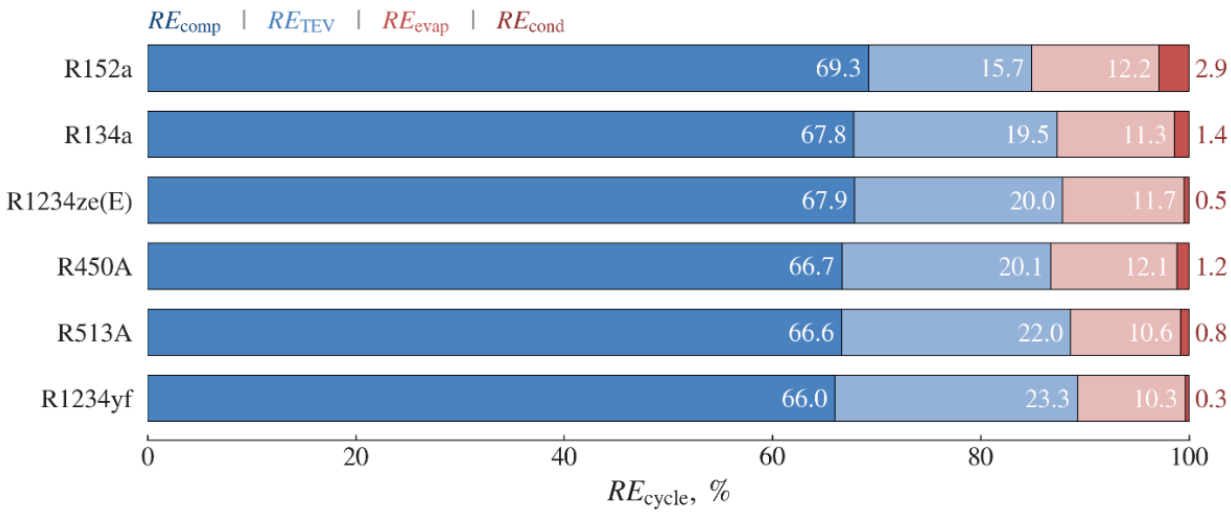

Figure 25 – Relative exergy destruction shares of components for different refrigerants

Figure 26 illustrates the influence of the discharge temperature T_4 on the condenser exergy efficiency η_{cond}^{ex}. The highest η_{cond}^{ex} is obtained for refrigerant R1234yf at the lowest T_4, whereas the lowest η_{cond}^{ex} corresponds to R152a at the highest T_4. A nearly linear correlation is observed between T_4 and η_{cond}^{ex}, indicating that, in this operating mode, an increase in discharge temperature leads to a reduction in condenser exergy efficiency. For the refrigerants considered, η_{cond}^{ex} lies in the range 94.9-99.3%. The exergy efficiencies of the remaining components are summarized in Table 6: the evaporator, compressor, and expansion valve exhibit exergy efficiencies of 50.4-53.6%, 58.3-58.8%, and 79.9-85.7%, respectively [11,13].

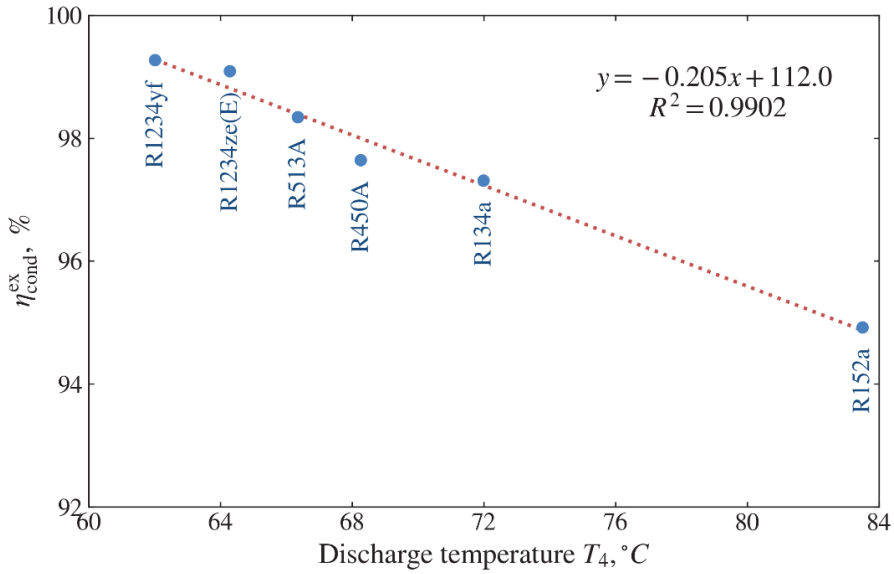

Figure 26 – Condenser exergy efficiency vs discharge temperature for different refrigerants

Table 6 – Efficiencies of the heat pump cycle and its individual components

Refrigerant	COP_{cycle}	COP_{system}	η_{2nd}, %	η_{cycle}^{ex}, %	η_{system}^{ex}, %	η_{evap}^{ex}, %	η_{comp}^{ex}, %	η_{cond}^{ex}, %	η_{TEV}^{ex}, %
R152a	3.09	2.91	35.3	32.1	30.2	53.6	58.8	94.9	85.7
R134a	2.97	2.80	34.0	30.9	29.1	53.6	58.5	97.3	83.5
R1234ze(E)	2.96	2.79	33.8	30.7	29.0	52.5	58.3	99.1	79.7
R450A	2.89	2.73	33.1	30.0	28.4	50.4	58.4	97.6	81.3
R513A	2.88	2.72	32.9	29.9	28.3	53.6	58.4	98.3	83.1
R1234yf	2.83	2.67	32.3	29.4	27.8	53.2	58.3	99.3	82.1

The second law efficiency η_{2nd}, the cycle exergy efficiency η_{cycle}^{ex}, and the overall system exergy efficiency η_{system}^{ex} are evaluated using Equations (52)-(54), and the results are presented in Figure 27. For all refrigerants, these three indicators show similar behaviour, falling in the intervals 32.3-35.3%, 29.4-32.1%, and 27.8-30.2%, respectively. As reported in Table 6, the maximum values of these efficiencies are achieved with R152a, while the minimum values are associated with R1234yf. Within

the set of candidate refrigerants, only R152a outperforms R134a, whereas R1234ze(E) yields efficiency values closest to those of R134a. The trends of COP_{cycle} and COP_{system} follow a similar pattern.

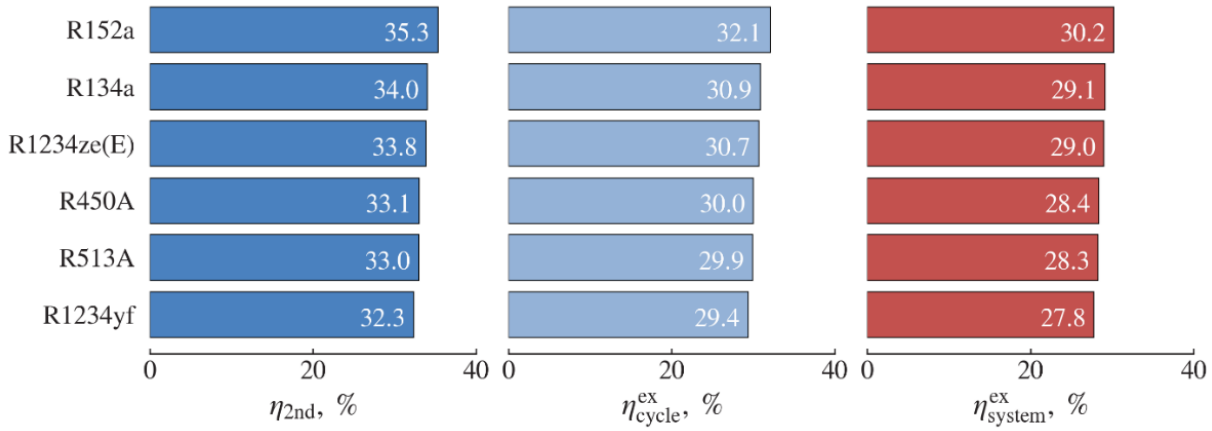

Figure 27 – Second law, cycle, and overall system exergy efficiencies for different refrigerants

Figure 28 compares the total equivalent warming impact (TEWI) of the water-to-water heat pump operating with R134a and the environmentally friendlier alternative refrigerants. TEWI accounts for both direct and indirect greenhouse gas emissions, the former being determined by the GWP of the refrigerant. Because of its high GWP, R134a produces the largest direct emissions, followed by R513A, R450A, and R152a, with direct impacts of 1.14, 0.84, and 0.12 tons of CO_2 equivalent, respectively. The smallest direct emissions are obtained for the HFO refrigerants R1234yf and R1234ze(E), each contributing only 0.01 tons of CO_2 equivalent.

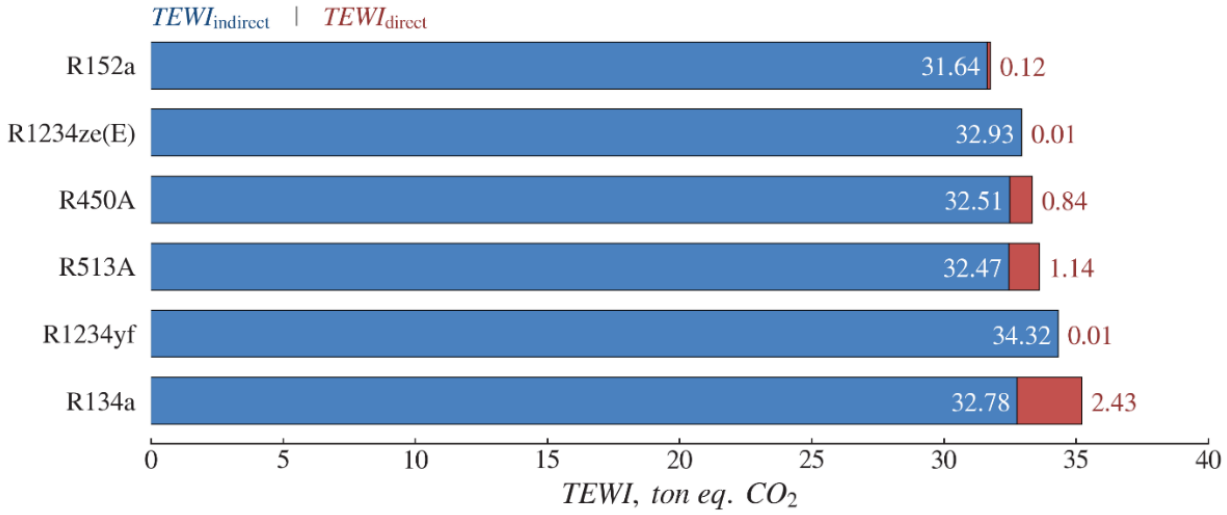

Figure 28 – Total equivalent warming impact of the heat pump for different refrigerants

The lowest indirect emissions are associated with R152a, at 31.64 tons of CO_2 equivalent, whereas the highest value of 34.32 tons of CO_2 equivalent is found for R1234yf due to its higher compressor power demand. In these calculations, the carbon dioxide emission factor β is taken as 0.8 kg of CO_2 per kWh for a coal-based electric power generation system [13,87].

Figure 29 presents the normalized relationships between key performance indicators for the different refrigerants: $\mathrm{COP}_{\mathrm{cycle}}$ versus TEWI and $\eta^{\mathrm{ex}}_{\mathrm{cycle}}$ versus $\dot{E}^{\mathrm{dest}}_{\mathrm{cycle}}$. In these diagrams, R134a serves as the reference fluid (all normalized values equal to unity), while the remaining working fluids are treated as low-GWP alternatives in line with the planned phase-down of HFCs such as R134a under the 2016 Paris Protocol (Kigali Amendment) [3].

In both Figure 29a and Figure 29b, the most favourable operating region corresponds to the second quadrant: a normalized TEWI below 1 combined with $\mathrm{COP}_{\mathrm{cycle}} > 1$, and, analogously, $\eta^{\mathrm{ex}}_{\mathrm{cycle}} > 1$ together with $\dot{E}^{\mathrm{dest}}_{\mathrm{cycle}} < 1$. Refrigerants located in this quadrant simultaneously improve efficiency and reduce environmental impact relative to R134a.

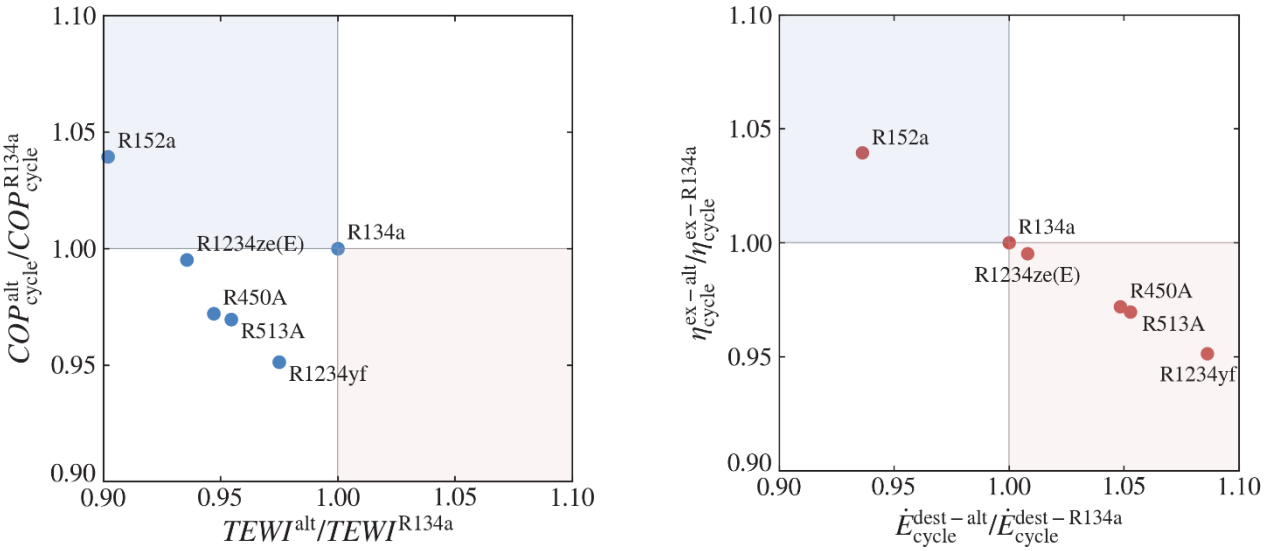

a) b)

Figure 29 – Normalized variations of key cycle parameters for different refrigerants: a) COP vs. TEW; b) Cycle efficiency vs. exergy destruction.

According to Figure 29, R152a clearly emerges as the best candidate: it provides higher $\mathrm{COP}_{\mathrm{cycle}}$ and $\eta^{\mathrm{ex}}_{\mathrm{cycle}}$ than R134a, while also exhibiting the lowest TEWI and exergy destruction rate $\dot{E}^{\mathrm{dest}}_{\mathrm{cycle}}$. The next most attractive option in terms of TEWI reduction is R1234ze(E), whose other performance metrics remain close to those of R134a. By contrast, R1234yf yields the lowest efficiencies and the highest exergy destruction, despite achieving a lower TEWI than R134a. The blend refrigerants R450A and R513A show similar behaviour: although they offer reduced TEWI, their efficiency indicators are inferior to those of R134a [13].

Among the candidate fluids, R152a appears to be a strong replacement for R134a from a thermodynamic standpoint; however, its flammability limits the allowable refrigerant charge in practical systems [13,86]. Hydrofluoroolefin (HFO) refrigerants such as R1234yf and R1234ze(E) are often promoted as key long-term substitutes for HFCs because of their very low global warming potential. Despite this advantage, their thermophysical properties are generally inferior to those of R134a, which leads to poorer thermodynamic performance. In addition, the rapid atmospheric degradation of HFOs results in the formation of trifluoroacetate (TFA) [21]; for R1234yf, the expected TFA load is nearly five times higher than that associated with R134a [21], and the subsequent deposition of TFA can pollute aquatic ecosystems [18,19].

To balance safety, environmental impact, and performance, HFC/HFO blends such as R450A and R513A have been proposed. These mixtures are non-flammable and have GWPs approximately 60% lower than that of R134a, while offering acceptable thermodynamic behaviour. For these reasons, R450A and R513A can be regarded as practical alternative refrigerants.

2.5 Chapter summary

This chapter has applied a combined experimental and 3E (energy-exergy-environmental) analysis to a ground source heat pump (GSHP) installation in Almaty and used the results to validate the thermodynamic framework developed earlier. A prototype of a GSHP heating system was developed and installed in the Koksai Mosque in the Almaty region of Kazakhstan. Experiments were performed for refrigerant R134a, and the energy and exergy efficiencies of the system under local weather conditions were evaluated. The thermodynamic model was then validated by comparison with experimental data. On the basis of the verified model, calculations of energy and exergy efficiencies were extended to a set of environmentally friendlier refrigerants considered as alternatives to R134a, and the environmental impact of the heating system using different refrigerants was estimated using the TEWI parameter. In this way, the chapter links measured performance, model predictions, and environmental indicators for a representative GSHP in a continental climate.

The following major conclusions can be drawn from this study [13]:

- The experimental values of cycle COP (COP_{cycle}) vary in the range of 2.24-2.97, while system COP (COP_{system}) varies in the range of 2.11-2.76 for the investigated operating conditions.
- The predicted and experimental results are found to be in good agreement, with deviations not exceeding 6.2%, which confirms the adequacy of the thermodynamic model for both energy and exergy indicators.
- The thermodynamic model therefore describes the energy and exergy efficiencies of the system with sufficient accuracy to support extrapolation to alternative refrigerants and operating regimes.
- For low-GWP refrigerants considered as replacements for R134a, the 3E analysis shows that environmentally friendlier working fluids can reduce TEWI while maintaining comparable or only moderately reduced COP, providing a basis for selecting suitable refrigerants for GSHP applications in continental climates.
- Refrigerant R152a emerges as a promising alternative to R134a, providing higher COP_{cycle}, COP_{system}, and lower TEWI, with estimated values of 3.09, 2.91, and 31.76-ton eq., respectively.
- Refrigerants R450A and R513A are identified as safer non-flammable substitutes, offering TEWI values and COP_{cycle}, COP_{system} only about 3% lower than those of R134a.
- Refrigerants R1234yf and R1234ze can be regarded as interim replacements for R134a, given their low GWP but potential environmental concerns associated with trifluoroacetic acid formation.

Overall, the validated 3E framework and the Almaty case study supply system-level benchmarks that complement the finite-time thermodynamic optimization of Chapter 1 and support practical design and refrigerant-selection guidelines for GSHPs in Kazakhstan and similar cold regions.

CONCLUSION

This dissertation develops and validates an integrated methodology for the thermodynamic optimization of ground source heat pump (GSHP) systems operating in cold, continental climates. The proposed approach combines a finite-time thermodynamics (FTT) framework – where finite heat-transfer rates, entropy production, and cycle-reservoir irreversibilities are explicitly represented – with a validated 3E (energy-exergy-environmental) analysis based on data from a GSHP installation in Almaty. Taken together, these elements translate classical thermodynamic limits into quantitative design and operating rules and show, on a real system, how GSHP efficiency can be improved while lowering the associated environmental impact under long heating seasons.

The thesis begins by formulating the main idea, aim, and objectives. The central aim is to construct a systematic optimization methodology for GSHPs modeled as a four-heat-exchanger (four-reservoir) system – ground/BHE, evaporator-side loop, condenser-side loop, and user-side heat exchanger – and to allocate limited thermal and geometric resources (heat exchanger effectiveness and capacity rate distribution) where they provide the greatest improvement in system-level performance. The specific objectives are to (i) formulate multi-variable optimization problems under imposed ground heat extraction and imposed heat delivery, with compressor-power minimization or COP-maximization criteria; (ii) perform parametric analyses that clarify how temperature ratios, irreversibility levels, and total exchanger resources shape optimal solutions; and (iii) validate these theoretical insights using a calibrated 3E assessment based on experimental GSHP data from the Almaty installation.

The scientific novelty of the work is summarized in three main contributions. First, the thesis proposes a comprehensive FTT-based framework for GSHPs treated as a four-reservoir problem, replacing component-wise or ad-hoc sizing with cycle-reservoir co-optimization under realistic finite-rate constraints. Second, it introduces and compares optimization criteria under different imposed conditions – specifically, imposed heat extraction and imposed heat production – while representing irreversibilities either through an irreversibility ratio or through entropy-production-based formulations. Third, it integrates these FTT models with a measured-data-driven 3E methodology, so that energy, exergy, and environmental indicators are evaluated consistently within the same framework. Together, these contributions yield generalizable rules for exchanger-area and capacity-rate allocation, working fluid selection, and operating temperature ranges in severe winter climates.

Chapter 1 provides the theoretical FTT optimization backbone. Modeling the GSHP as four coupled exchangers connected to finite-capacitance reservoirs reveals how entropy generation concentrates when exchanger resources are poorly distributed, and leads to allocation rules that minimize compressor power input or maximize COP under imposed operating conditions. The results show, for example, that increasing system irreversibility can reduce the maximum COP by up to about 62% and raise compressor power by more than a factor of 3.4 compared to reversible conditions, whereas improving the delivery-side capacity rate from 0.4 to 0.8 and increasing heat exchanger effectiveness in the mid-range can cut power demand by roughly 25-30%.

These trends highlight the dominant influence of sink-side allocation and temperature lift on GSHP performance and provide a theoretical basis for sizing guidelines.

Chapter 2 extends the analysis to a real installation and establishes experimental and 3E validation. A prototype water-to-water GSHP system at the Koksai Mosque (Almaty region) is designed, instrumented, and tested using R134a as the working fluid. The corresponding thermodynamic model is calibrated against measured temperatures, heat fluxes, and COP values, with deviations between measured and predicted cycle and system COP generally within about 6.2%. The experimental COP_{cycle} is found to lie between 2.24 and 2.97, while COP_{system} ranges from 2.11 to 2.76, confirming that the model captures energy and exergy efficiencies with engineering accuracy and can be used for refrigerant and operating-regime comparisons.

On this basis, the 3E analysis evaluates several low-GWP refrigerants as alternatives to R134a. The results show that R152a offers higher COP_{cycle}, and a lower TEWI than R134a, but its flammability constrains allowable charge and practical use. Non-flammable blends R450A and R513A reduce TEWI while keeping COP penalties to about 3% compared with R134a, making them attractive near-term replacements.. Overall, the validated 3E framework links thermodynamic performance to environmental impact and supports refrigerant selection for GSHPs in continental climates.

From a practical standpoint, the combined FTT and 3E results provide actionable guidance for GSHP design and operation in cold regions. The optimization framework indicates that priority should be given to enhancing sink-side heat exchangers and narrowing the source-sink temperature gap, rather than uniformly increasing all exchanger areas. The experimental and TEWI-based analyses, in turn, help identify refrigerants and operating conditions that balance efficiency, environmental impact, and safety, thereby supporting decarbonization strategies for space-heating systems in Kazakhstan and similar climates.

At the same time, the findings are subject to several limitations that motivate future research. The FTT model is formulated at system level and does not yet resolve fully dynamic borefield behavior or long-term seasonal ground temperature drift; the experimental validation focuses on a single installation and building type; and economic criteria and advanced control strategies (e.g., variable-speed operation, hybridization with solar or thermal storage) are treated only implicitly. Future work should therefore extend the framework to (i) coupled FTT-borefield models with seasonal ground regeneration, (ii) multi-objective thermoeconomic and environmental optimization, and (iii) dynamic control and real-time optimization of GSHPs, including hybrid high-temperature and cascade configurations.

In conclusion, the thesis delivers a unified theoretical and experimental basis for the thermodynamic optimization of GSHP systems with four thermal reservoirs, and demonstrates its applicability to real installations in continental climates. The results support more efficient and environmentally responsible deployment of GSHPs and provide a platform for further methodological developments and broader adoption in building-sector decarbonization.

REFERENCES

1. Calvin K., Dasgupta D., Krinner G., Mukherji A., et al. IPCC, 2023: Climate Change 2023: Synthesis Report. Contribution of Working Groups I, II and III to the Sixth Assessment Report of the Intergovernmental Panel on Climate Change [Core Writing Team, H. Lee and J. Romero (eds.)]. IPCC, Geneva, Switzerland. First. Intergovernmental Panel on Climate Change (IPCC), 2023.

2. Haehnlein S., Bayer P., Blum P. International legal status of the use of shallow geothermal energy // Renewable and Sustainable Energy Reviews. 2010. Vol. 14, No. 9. P. 2611–2625.

3. International Energy Agency. The Future of Heat Pumps. OECD, 2022.

4. Lund J. W., Freeston D. H., Boyd T. L. Direct utilization of geothermal energy 2010 worldwide review // Geothermics. 2011. Vol. 40, No. 3. P. 159–180.

5. Adebayo P., Beragama Jathunge C., Darbandi A., Fry N., Shor R., Mohamad A., Wemhöner C., Mwesigye A. Development, modeling, and optimization of ground source heat pump systems for cold climates: A comprehensive review // Energy and Buildings. 2024. Vol. 320. P. 114646.

6. Sanner B. Ground Source Heat Pumps – history, development, current status, and future prospects. 2017.

7. Baimbetov D., Karlina Ye., Yerdesh Ye., Syrlybekkyzy S., Toleukhanov A., Mohanraj M., Belyayev Ye. Thermal analysis of a compression heat pump-assisted solar still for Caspian regions of Kazakhstan // J Therm Anal Calorim. 2024. Vol. 149, No. 19. P. 11269–11291.

8. Karlina Y., Yerdesh Y., Toleukhanov A., Belyayev Y., Wang H. S., Botella O. Numerical Simulation Study of Thermal Performance in Hot Water Storage Tanks with External and Internal Heat Exchangers // Energies. 2024. Vol. 17, No. 22. P. 5623.

9. Olympios A. V., Sapin P., Mersch M., Maghrabi A. M., Markides C. N. A review of recent progress in the design and integration of domestic heat pumps // Next Energy. 2024. Vol. 5. P. 100163.

10. Arpagaus C., Bless F., Uhlmann M., Schiffmann J., Bertsch S. S. High temperature heat pumps: Market overview, state of the art, research status, refrigerants, and application potentials // Energy. 2018. Vol. 152. P. 985–1010.

11. Belyayev Y., Toleukhanov A., Yerdesh Y., Seitov A., Amanzholov T., Wang H. S. Energy and exergy performance study of ground source heat pump in continental climate conditions. Dalešice, Czech Republic: AIP Conference Proceedings, 2024. Vol. 3126.

12. Mosaffa A. H., Farshi L. G., Infante Ferreira C. A., Rosen M. A. Exergoeconomic and environmental analyses of CO2/NH3 cascade refrigeration systems equipped with different types of flash tank intercoolers // Energy Conversion and Management. 2016. Vol. 117. P. 442–453.

13. Yerdesh Y., Amanzholov T., Aliuly A., Seitov A., Toleukhanov A., Murugesan M., Botella O., Feidt M., Wang H. S., Tsoy A., Belyayev Y. Experimental and Theoretical Investigations of a Ground Source Heat Pump System for Water and Space Heating Applications in Kazakhstan // Energies. 2022. Vol. 15, No. 22. P. 8336.

14. Yerdesh Ye., Abdulina Z., Aliuly A., Belyayev Ye., Mohanraj M., Kaltayev A. Numerical simulation on solar collector and cascade heat pump combi water heating systems in Kazakhstan climates // Renewable Energy. 2020. Vol. 145. P. 1222–1234.

15. Yerdesh Ye., Toleukhanov A., Mohanraj M., Wang H. S., Botella O., Feidt M., Belyayev Ye. Air-to-Water Cascade Heat Pump Thermal Performance Modelling for Continental Climate Regions // Entropie Thermodynamique. 2022. Vol. 3.

16. Cheng C.-Y., Chen C.-K. Ecological optimization of an endoreversible Brayton cycle // Energy Conversion and Management. 1998. Vol. 39, No. 1–2. P. 33–44.

17. Durmayaz A. Optimization of thermal systems based on finite-time thermodynamics and thermoeconomics // Progress in Energy and Combustion Science. 2004. Vol. 30, No. 2. P. 175–217.

18. Mohanraj M., Belyayev Ye., Jayaraj S., Kaltayev A. Research and developments on solar assisted compression heat pump systems – A comprehensive review (Part A: Modeling and modifications) // Renewable and Sustainable Energy Reviews. 2018. Vol. 83. P. 90–123.

19. Mohanraj M., Belyayev Ye., Jayaraj S., Kaltayev A. Research and developments on solar assisted compression heat pump systems – A comprehensive review (Part-B: Applications) // Renewable and Sustainable Energy Reviews. 2018. Vol. 83. P. 124–155.

20. Bobbo S., Fedele L., Curcio M., Bet A., De Carli M., Emmi G., Poletto F., Tarabotti A., Mendrinos D., Mezzasalma G., Bernardi A. Energetic and Exergetic Analysis of Low Global Warming Potential Refrigerants as Substitutes for R410A in Ground Source Heat Pumps // Energies. 2019. Vol. 12, No. 18. P. 3538.

21. Holland R., Khan M. A. H., Driscoll I., Chhantyal-Pun R., Derwent R. G., Taatjes C. A., Orr-Ewing A. J., Percival C. J., Shallcross D. E. Investigation of the Production of Trifluoroacetic Acid from Two Halocarbons, HFC-134a and HFO-1234yf and Its Fates Using a Global Three-Dimensional Chemical Transport Model // ACS Earth Space Chem. 2021. Vol. 5, No. 4. P. 849–857.

22. Amanzholov T., Seitov A., Aliuly A., Yerdesh Y., Murugesan M., Botella O., Feidt M., Wang H. S., Belyayev Y., Toleukhanov A. Thermal Response Measurement and Performance Evaluation of Borehole Heat Exchangers: A Case Study in Kazakhstan // Energies. 2022. Vol. 15, No. 22. P. 8490.

23. Gehlin S. Thermal response test : method development and evaluation. Lulea, Sweden: Lulea University of Technology, 2002. 191 P.

24. Cunha R. P., Bourne-Webb P. J. A critical review on the current knowledge of geothermal energy piles to sustainably climatize buildings // Renewable and Sustainable Energy Reviews. 2022. Vol. 158. P. 112072.

25. Reuss M. The use of borehole thermal energy storage (BTES) systems // Advances in Thermal Energy Storage Systems / ed. Cabeza L. F. Woodhead Publishing, 2015. P. 117–147.

26. Boon D. P., Farr G. J., Abesser C., Patton A. M., James D. R., Schofield D. I., Tucker D. G. Groundwater heat pump feasibility in shallow urban aquifers: Experience from Cardiff, UK // Science of The Total Environment. 2019. Vol. 697. P. 133847.

27. Ndiaye D., Bernier M. Transient model of a geothermal heat pump in cycling conditions – Part A: The model // International Journal of Refrigeration. 2012. Vol. 35, No. 8. P. 2110–2123.

28. Warner J., Liu X., Shi L., Qu M., Zhang M. A novel shallow bore ground heat exchanger for ground source heat pump applications – Model development and validation // Applied Thermal Engineering. 2020. Vol. 164. P. 114460.

29. Yang L. W., Xu R. J., Hua N., Xia Y., Zhou W. B., Yang T., Belyayev Y., Wang H. S. Review of the advances in solar-assisted air source heat pumps for the domestic sector // Energy Conversion and Management. 2021. Vol. 247. P. 114710.

30. Yang W., Xu R., Wang F., Chen S. Experimental and numerical investigations on the thermal performance of a horizontal spiral-coil ground heat exchanger // Renewable Energy. 2020. Vol. 147. P. 979–995.

31. Nikitin A., Deymi-Dashtebayaz M., Muraveinikov S., Nikitina V., Nazeri R., Farahnak M. Comparative study of air source and ground source heat pumps in 10 coldest Russian cities based on energy-exergy-economic-environmental analysis // Journal of Cleaner Production. 2021. Vol. 321. P. 128979.

32. Toleukhanov A., Belyayev Y., Botella O., Yerdesh Y., Amanzholov T. Simulation-based mathematical modeling of borehole heat exchanger thermal performance for ground source heat pumps // Journal of Mathematical Sciences. 2025. Vol. 291, No. 2.

33. Arat H., Arslan O. Exergoeconomic analysis of district heating system boosted by the geothermal heat pump // Energy. 2017. Vol. 119. P. 1159–1170.

34. Belliardi M., Cereghetti N., Caputo P., Ferrari S. A Method to Analyze the Performance of Geocooling Systems with Borehole Heat Exchangers. Results in a Monitored Residential Building in Southern Alps // Energies. 2021. Vol. 14, No. 21. P. 7407.

35. Bejan A. Entropy generation minimization: the method of thermodynamic optimization of finite-size systems and finite-time processes. Boca Raton: CRC Press, 1996. 362 P.

36. Feidt M. Finite Physical Dimensions Optimal Thermodynamics 2: Complex Systems. Amsterdam, The Netherlands: ISTE Press - Elsevier, 2018. 218 P.

37. Feidt M. Finite Physical Dimensions Optimal Thermodynamics 1: Fundamentals. 1st ed. Amsterdam, The Netherlands: ISTE Press - Elsevier, 2017. 274 P.

38. Qin X., Chen L., Ge Y., Sun F. Thermodynamic modeling and performance analysis of the variable-temperature heat reservoir absorption heat pump cycle // Physica A: Statistical Mechanics and its Applications. 2015. Vol. 436. P. 788–797.

39. Ye Z., Holubec V. Maximum efficiency of low-dissipation heat pumps at given heating load // Phys. Rev. E. 2022. Vol. 105, No. 2. P. 024139.

40. Roy R., Mandal B. K. Thermo-economic analysis and multi-objective optimization of vapour cascade refrigeration system using different refrigerant combinations: A comparative study // J Therm Anal Calorim. 2020. Vol. 139, No. 5. P. 3247–3261.

41. Velasco F. J. S., Haddouche M. R., Illán-Gómez F., García-Cascales J. R. Experimental characterization of the coupling and heating performance of a CO2

water-to-water heat pump and a water storage tank for domestic hot water production system // Energy and Buildings. 2022. Vol. 265. P. 112085.

42. Arz A., Minghini A., Feidt M., Costea M., Moyne C. Influence of boundary conditions on the optimization of a geothermal heat pump studied using a thermodynamic model // IOP Conf. Ser.: Earth Environ. Sci. 2022. Vol. 960, No. 1. P. 012003.

43. Novikov I. I. The efficiency of atomic power stations (a review) // Journal of Nuclear Energy (1954). 1958. Vol. 7, No. 1–2. P. 125–128.

44. Chambadal P. Les centrales nucléaires. Paris, France: Armand Colin, 1957. Vol. 321. 188 P.

45. Curzon F. L., Ahlborn B. Efficiency of a Carnot engine at maximum power output // American Journal of Physics. 1975. Vol. 43, No. 1. P. 22–24.

46. Bejan A. Entropy Generation Minimization: The Method of Thermodynamic Optimization of Finite-Size Systems and Finite-Time Processes. 1st ed. Boca Raton: CRC Press, 2013. 400 P.

47. Sahin B., Kodal A. Finite time thermoeconomic optimization for endoreversible refrigerators and heat pumps // Energy Conversion and Management. 1999. Vol. 40, No. 9. P. 951–960.

48. Salah El-Din M. M. Performance analysis of heat pumps and refrigerators with variable reservoir temperatures // Energy Conversion and Management. 2001. Vol. 42, No. 2. P. 201–216.

49. Sarkar J., Bhattacharyya S., Ram Gopal M. Analytical minimization of overall conductance and heat transfer area in refrigeration and heat pump systems and its numerical confirmation // Energy Conversion and Management. 2007. Vol. 48, No. 4. P. 1245–1250.

50. Chen L., Xiaoqin Z., Sun F., Wu C. Exergy-based ecological optimization for a generalized irreversible Carnot heat-pump // Applied Energy. 2007. Vol. 84, No. 1. P. 78–88.

51. Bi Y., Chen L., Sun F. Ecological, exergetic efficiency and heating load optimizations for endoreversible variable-temperature heat reservoir simple air heat pump cycles // International Journal of Low-Carbon Technologies. 2010. Vol. 5, No. 1. P. 7–17.

52. Huleihil M., Andresen B. Generalized Performance Characteristics of Refrigeration and Heat Pump Systems // Physics Research International. 2010. Vol. 2010. P. 1–10.

53. Chen L., Feng H., Sun F. Exergoeconomic performance optimization for a combined cooling, heating and power generation plant with an endoreversible closed Brayton cycle // Mathematical and Computer Modelling. 2011. Vol. 54, No. 11–12. P. 2785–2801.

54. Ahmadi M. H., Ahmadi M.-A., Pourfayaz F., Bidi M. Thermodynamic analysis and optimization for an irreversible heat pump working on reversed Brayton cycle // Energy Conversion and Management. 2016. Vol. 110. P. 260–267.

55. Feidt M., Costea M. Une nouvelle approche d'optimisation de pompe à chaleur tenant compte du couplage entre les réservoirs thermiques et le cycle // International Journal of Refrigeration. 2021. Vol. 132. P. 322–329.

56. Rachedi M., Feidt M., Amirat M., Merzouk M. Optimal operating conditions of a transcritical endoreversible cycle using a low enthalpy heat source // Applied Thermal Engineering. 2016. Vol. 107. P. 379–385.

57. Virtanen P., Gommers R., Oliphant T. E., Haberland M., et al. SciPy 1.0: fundamental algorithms for scientific computing in Python // Nat Methods. 2020. Vol. 17, No. 3. P. 261–272.

58. Esen H., Inalli M., Esen M., Pihtili K. Energy and exergy analysis of a ground-coupled heat pump system with two horizontal ground heat exchangers // Building and Environment. 2007. Vol. 42, No. 10. P. 3606–3615.

59. Verda V., Cosentino S., Russo S. L., Sciacovelli A. Second law analysis of horizontal geothermal heat pump systems // Energy and Buildings. 2016. Vol. 124. P. 236–240.

60. Ally M. R., Munk J. D., Baxter V. D., Gehl A. C. Data, exergy, and energy analyses of a vertical-bore, ground-source heat pump for domestic water heating under simulated occupancy conditions // Applied Thermal Engineering. 2015. Vol. 89. P. 192–203.

61. Ozcan O., Ozgener O. Energetic and exergetic performance analysis of Bethe-Zeldovich-Thompson (BZT) fluids in geothermal heat pumps // International Journal of Refrigeration. 2011. Vol. 34, No. 8. P. 1943–1952.

62. Li C., Mao J., Peng X., Mao W., Xing Z., Wang B. Influence of ground surface boundary conditions on horizontal ground source heat pump systems // Applied Thermal Engineering. 2019. Vol. 152. P. 160–168.

63. Welsch B., Rühaak W., Schulte D. O., Bär K., Sass I. Characteristics of medium deep borehole thermal energy storage: Characteristics of medium deep borehole thermal energy storage // Int. J. Energy Res. 2016. Vol. 40, No. 13. P. 1855–1868.

64. Hu R., Li X., Liang J., Wang H., Liu G. Field study on cooling performance of a heat recovery ground source heat pump system coupled with thermally activated building systems (TABSs) // Energy Conversion and Management. 2022. Vol. 262. P. 115678.

65. Ren Y., Lu X., Zhang W., Zhang J., Liu J., Ma F., Cui Z., Yu H., Zhu T., Zhang Y. Preliminary Study on Optimization of a Geothermal Heating System Coupled with Energy Storage for Office Building Heating in North China // Energies. 2022. Vol. 15, No. 23. P. 8947.

66. Wang Z., Wang L., Ma A., Liang K., Song Z., Feng L. Performance evaluation of ground water-source heat pump system with a fresh air pre-conditioner using ground water // Energy Conversion and Management. 2019. Vol. 188. P. 250–261.

67. Lee K. C. Classification of Geothermal Resources - An engineering approach: SGP-TR-151-13. United States: Geothermal Institute, The University of Auckland, Auckland, NZ, 1996. P. 85–92.

68. Amanzholov T., Akhmetov B., Georgiev A., Kaltayev A., Popov R., Dzhonova D., Tungatarova M. Numerical modelling as a supplementary tool for Thermal Response Test // Bulgarian Chemical Communications. 2016. Vol. 48, No. Special Issue E. P. 109–114.

69. Sang J., Liu X., Liang C., Feng G., Li Z., Wu X., Song M. Differences between design expectations and actual operation of ground source heat pumps for green buildings in the cold region of northern China // Energy. 2022. Vol. 252. P. 124077.

70. Shamoushaki M., Aliehyaei M., Taghizadeh-Hesary F. Energy, Exergy, Exergoeconomic, and Exergoenvironmental Assessment of Flash-Binary Geothermal Combined Cooling, Heating and Power Cycle // Energies. 2021. Vol. 14, No. 15. P. 4464.

71. Stanek W., Simla T., Gazda W. Exergetic and thermo-ecological assessment of heat pump supported by electricity from renewable sources // Renewable Energy. 2019. Vol. 131. P. 404–412.

72. Ceglia F., Marrasso E., Roselli C., Sasso M., Tzscheutschler P. Exergetic and exergoeconomic analysis of an experimental ground source heat pump system coupled with a thermal storage based on Hardware in Loop // Applied Thermal Engineering. 2022. Vol. 212. P. 118559.

73. Aminyavari M., Najafi B., Shirazi A., Rinaldi F. Exergetic, economic and environmental (3E) analyses, and multi-objective optimization of a CO2/NH3 cascade refrigeration system // Applied Thermal Engineering. 2014. Vol. 65, No. 1–2. P. 42–50.

74. Qureshi B. A., Zubair S. M. Thermoeconomic considerations in the allocation of heat transfer inventory for irreversible refrigeration and heat pump systems // International Journal of Refrigeration. 2015. Vol. 54. P. 67–75.

75. Akbari Kordlar M., Mahmoudi S. M. S., Talati F., Yari M., Mosaffa A. H. A new flexible geothermal based cogeneration system producing power and refrigeration, part two: The influence of ambient temperature // Renewable Energy. 2019. Vol. 134. P. 875–887.

76. Renaldi R., Friedrich D. Techno-economic analysis of a solar district heating system with seasonal thermal storage in the UK // Applied Energy. 2019. Vol. 236. P. 388–400.

77. Tempesti D., Fiaschi D. Thermo-economic assessment of a micro CHP system fuelled by geothermal and solar energy // Energy. 2013. Vol. 58. P. 45–51.

78. Bae S., Nam Y., Choi J., Lee K., Choi J. Analysis on Thermal Performance of Ground Heat Exchanger According to Design Type Based on Thermal Response Test // Energies. 2019. Vol. 12, No. 4. P. 651.

79. Kim J., Nam Y. Development of the Performance Prediction Equation for a Modular Ground Heat Exchanger // Energies. 2020. Vol. 13, No. 22. P. 6005.

80. Zhang M., Liu X., Biswas K., Warner J. A three-dimensional numerical investigation of a novel shallow bore ground heat exchanger integrated with phase change material // Applied Thermal Engineering. 2019. Vol. 162. P. 114297.

81. Tang F., Nowamooz H. Outlet temperatures of a slinky-type Horizontal Ground Heat Exchanger with the atmosphere-soil interaction // Renewable Energy. 2020. Vol. 146. P. 705–718.

82. Ndiaye D., Bernier M. Transient model of a geothermal heat pump in cycling conditions – Part B: Experimental validation and results // International Journal of Refrigeration. 2012. Vol. 35, No. 8. P. 2124–2137.

83. Colombo L. P. M., Lucchini A., Molinaroli L. Experimental analysis of the use of R1234yf and R1234ze(E) as drop-in alternatives of R134a in a water-to-water heat pump // International Journal of Refrigeration. 2020. Vol. 115. P. 18–27.

84. Molinaroli L., Lucchini A., Colombo L. P. M. Drop-in analysis of R450A and R513A as low-GWP alternatives to R134a in a water-to-water heat pump // International Journal of Refrigeration. 2022. Vol. 135. P. 139–147.

85. Koshkin N. N., Sakun I. A., Bambushek Y. M., Buharin N. N., Gerasimov Y. D., Ilyin A. Y., Pekarev V. I., Stukalenko A. K., Timofyevskyi L. S. Refrigeration Machines and Installations, Textbook for Technical Colleges. Saint Petersburg: Mechanical Engineering Publisher, 1985. 510 P.

86. Islam Md. A., Mitra S., Thu K., Saha B. B. Study on thermodynamic and environmental effects of vapor compression refrigeration system employing first to next-generation popular refrigerants // International Journal of Refrigeration. 2021. Vol. 131. P. 568–580.

87. Grof T. Greening of Industry under the Montreal Protocol: Background Paper. Vienna, Austria: United Nations Industrial Development Organization, 2009. P. 1–30.